Robustly Hyperbolic 1D Closures for Classical and Quantum Hydrodynamics

William Morin

Thesis submitted to the University of Ottawa
in partial fulfillment of the requirements for the
Ph.D. in Mechanical Engineering

Mechanical Engineering
University of Ottawa

Abstract

The use of moment-closure methods for the prediction of non-equilibrium gas flows offers many modelling and numerical advantages over traditional methods. In particular, the maximum-entropy family of moment closures has been found to be very successful, offering models described by hyperbolic systems of balance laws. Unfortunately, most maximum-entropy closures cannot be expressed in closed form. The only affordable option is to propose approximations which are presently only available for a limited number of moments. Other Grad-based moment closures have been proposed. However, almost all of them suffer from questionable modelling assumption or numerical difficulties. Fortunately quadrature-based moment methods have been shown to produce accurate, globally hyperbolic models. The resulting moment systems maintain balance-law form and can be constructed to be Galilean invariant for arbitrarily large number of moments, making them an excellent alternative.

The present work starts by reviewing key concepts of kinetic theory and moment closure, followed by a non-exhaustive litterature review of the main ideas developped in the last decades. Then three journal articles, constituting this thesis by contribution, are included. The first article shows the potential of moment closures to produce reliable quantum hydrodynamic models. As an initial investigation, a maximum-entropy approximation was used to predict the time evolution of a Gaussian wave packet in phase space, allowing for a better understanding of the advantages and drawbacks of the method for situation where quantum effects are significant. The second paper investigates a new technique for the construction of globally hyperbolic closures. A new orthogonal-polynomial-based moment closure hierarchy (OPMC) covering the even-order closures is also presented. The accuracy of the new hierarchy is accessed using numerical solutions of Riemann problems along with strong shock-wave calculations. Finally, the applicability of this novel hierarchy to plasma physics is investigated in the third paper. Discretized solutions of the Vlasov-Poisson-BGK system of equations are compared against solutions of the moment systems for two canonical plasma problems featuring both the collisional and collisionless regimes.

Acknowledgements

First and foremost, I sincerely thank my research supervisor, Prof. James G. M^{c}Donald. By welcoming me into his group over eight years ago, he provided me with the opportunity to grow in a uniquely inspiring and rewarding research atmosphere. The many challenging research topics he proposed offered me a wide range of intellectually stimulating avenues to explore. His deep insights into gaskinetic theory and moment closures provided me with enlightening answers to many complex problems. I am also grateful to him for his patience, constant encouragement, and the confidence he placed in me.

I would also like to thank Prof. Matei Radulescu for all the insightful discussions we've had over the years, which helped me gain a deeper understanding, not only of my work but also of various related physical problems.

I would like to express my gratitude to my fellow students and friends at the university for many collaborations and very interesting discussions, which undoubtedly contributed positively to the success of this work.

Finally, I wish to thank my family and friends for their unconditional support and constant encouragement.

Contents

Chapter 1

Introduction

In many engineering applications, during the design process, approximate solutions of complex physical problems are required in order to optimize performance and evaluate design criteria. Theoretical analysis, while being considered as a strong method owing to its universality, has limited applicability to real engineering problems because of the generally simple assumptions involved. Conversely, obtaining solutions through experiments is highly expensive and requires extensive time and resources, especially if an iterative design strategy is used. The use of computational methods to solve complex physical problems through discretization of governing equations allows for reliable solutions that, in turn, can be used in the design process. The efficiency and performance of computational methods depend on many factors such as the computational mesh, the numerical discretization and the choice of the physical models. Even if rigorous selection of numerical methods is of great importance, this work focuses primarily on the accurate construction of governing equations. When dealing with hydrodynamic systems, depending on the flow characteristics and scale of the problem, different physical phenomena need to be considered in order to provide an accurate description.

Hydrodynamic models based on moment methods have gained in popularity over the past decades, finding interest in many areas of physics and engineering. For example, gas flows in the transition or rarefied regime are relatively common. Microscale flows, high-altitude flight and space capsule re-entry are all examples of applications occurring in these regimes. Particle-based models, such as Direct Simulation Monte-Carlo (DSMC) [1], and models based on directly solving the Boltzmann equation, such as discrete-velocity methods [2], have had success predicting non-equilibrium flows in strongly rarefied regimes. Unfortunately, these methods often carry a prohibitively expensive computational cost especially when aiming for

time accurate calculations. On another note, the rapid advancement in the field of microfluidics and nanotechnology is another driving factors of this growing interest [3, 4, 5, 6, 7]. The derivation of reliable and affordable many-particle quantum models is thought to be key for the development of a new generation of efficient technologies. Unfortunately, few models successfully predict the time evolution of such quantum systems. Direct numerical solutions of the Schrödinger or the Wigner equation can be computationally expensive, especially for many-body systems.

Fortunately, moment-closures offer potential advantages for both classical and quantum-mechanical systems, as compared to existing methods [8, 9, 10, 11]. Moment closures are usually based on an assumed form of the velocity distribution function (VDF) describing the phase-space probability distribution of particles. The set of partial differential equations (PDEs) associated with moment-closure methods are significantly less expensive to solve than particle-based and direct-discretization methods. Moment-closures offer a set of first-order hyperbolic balance laws that can accurately predict states far from local thermodynamic equilibrium. Their first-order nature promises numerical advantages, such as a decreased sensitivity to mesh quality [12]. This is advantageous when dealing with complex geometries that are typical of practical problems. The requirement for the evaluation of only first derivatives also offers the possibility for an extra order of spacial accuracy for a given stencil.

The two most popular families of traditional moment-closure methods are the Grad hierarchy [8] and the maximum-entropy hierarchy [13, 9, 10]. The Grad closures, unfortunately, have a very restricted region of hyperbolicity and are not sufficiently robust, even for moderate departure from equilibrium. The Grad closures are also not guaranteed to yield strictly positive velocity distribution function due to the polynomial nature of the assumed VDF. The maximum-entropy closures hierarchy, on the other hand, can more robustly give flow predictions for states that are far from equilibrium. They also guarantee a strictly positive distribution function. However, due to the specific form of the VDF, the closing flux cannot be integrated in closed form thus requiring approximations that are currently only available for a limited number of moments. Moreover, it was found that there are physically realizable moment states for which the entropy-maximization problem does not have a solution. In those regions, closing fluxes are singular [14, 15]. More recently, a number of new families inspired by either the Grad or maximum-entropy closures have been introduced. Almost all suffering from questionable modeling assumptions, limiting their applicability. For example, Struchtrup and Torrilhon have proposed regularized extensions for the thirteen-moment Grad closure [16]. These closures aim to extend the physical validity of the Grad closures through the addition of higher-order derivatives at the cost of the hyperbolic, first-order

structure. Alternatively, Cai *et al.* have proposed a hyperbolization technique that leads to robustly hyperbolic Grad-style closures at the expense of balance-law form [17, 18]. As more recently demonstrated by Fox and Laurent, quadrature-based methods, on the other hand, offer more flexibility in producing stable globally hyperbolic moment equations while yielding a system in balance-law form [19, 20].

1.1 Thesis Goals

The goal of this thesis was originally to investigate the potential of moment closures as robust and accurate quantum hydrodynamic models. This led to the publication of the first journal article outlining the need for higher-order hyperbolic moment closures. The observations made from this paper coupled with the growing interest in quadrature-based closure led to the second journal article. In this paper, a new technique for the construction of hyperbolic moment systems in balance-law form is presented. New closures are shown along with a novel hierarchy covering the even-order moments, effectively filling the gap between the previously discovered quadrature-based hierarchies. Finally, the third paper included in this work studies the applicability of this new hierarchy for the prediction of low-temperature plasma flows. This investigation is done using two canonical plasma-physics problems. First, ions in a stationary electric potential are considered, allowing for a better understanding of the underlying behavior of the new closures along with their limitations. Linear Landau damping is also studied in both the collisional and collisionless regimes identifying the advantages and drawbacks of the moment methods for plasma flows.

1.2 Structure and Scope of the Current Study

This thesis is structured as follows. First, a brief overview of kinetic theory and moment closures is presented in Chapter 2. This is followed by the first journal publication included in Chapter 3. The original contribution of this paper is mainly the use of an approximate maximum-entropy moment closure to the Wigner equations. This study allows for a better understanding of the capacities and limitations of moment methods as accurate models for quantum systems. The second journal article, presented in Chapter 4, investigates the global hyperbolicity conditions of one-dimensional quadrature-based closures. The original contributions of this work include the development of a novel technique for the construction of 1D globally hyperbolic moment closures along with a new hierarchy of closures covering the even-order moment systems. The accuracy of the new hierarchy is assessed by comparing numerical results of Riemann problems and strong shock-wave calculations to discretized

solutions of the Boltzmann's equation. Finally, Chapter 5 contains the last published article of this thesis. The original contribution consists of an investigation of the applicability of the new hierarchy, introduced in Chapter 4, to low-temperature plasma problems. Finally, in Chapter 5, conclusions are summarized and possible avenues for future work are identified.

Chapter 2

Kinetic Theory and Moment Closure

On a macroscopic scale, gases are huge collections of interacting particles. These particles are usually separated by distances considerably larger than their own range of interaction. For classical gases, knowledge of the particle positions and velocities, assuming spherical particles with no internal degrees of freedom, is sufficient to determine the gas state. Further information is needed when dealing with polyatomic gases. Nonetheless, the particles trajectories can be calculated using Newtonian mechanics. For gases at atmospheric conditions, one cubic meter contains on the order of 10^{25} particles, rendering the tracking of each individual particles prohibitively expensive. One alternative, proposed by Liouville in 1838 [21], was to use a probability density function, $\mathcal{P}$, to describe the state of the gas. The time evolution of this probability density function is governed by Liouville's equation. Unfortunately, when considering a system with N particles, the function, $\mathcal{P}$, describes the state in $6N$ dimensional phase-space, making direct discretization of Liouville's equation unfeasible for most practical cases. Luckily, the detailed description of Liouville's equation is not necessary if only macroscopic properties are of interest.

In 1872, Boltzmann published an evolution equation for the so-called one-particle (or reduced) distribution function [22], denoted $\mathcal{F}$ in this work, where the phase-space of the gas is reduced from $6N$ to only 6 independent dimensions. Boltzmann's new formalism was based on several assumptions. First, only binary collisions are considered, assuming that the gas is sufficiently diluted. Secondly, the mean free path, λ, characterizing the average distance between inter-particle collisions is much larger than the effective range of inter-molecular forces. Finally, the positions and velocities of particles before collision are uncorrelated; which is called the molecular chaos assumption. Originally introduced by Maxwell [23], this assumption is directly related to Boltzmann's H-theorem [22]. Without going into extensive

details, the H-theorem states that the entropy of any Boltzmann gas will increase with time before reaching a state of maximum-entropy, which is described by the Maxwell-Boltzmann distribution (Maxwellian), denoted $\mathcal{M}$. For further information references are available here, [24, 25, 26]. However, for most gas processes, even Boltzmann's description is too detailed. Direct discretization of his evolution equation is still very computationally involved. Another level of abstraction is therefore needed. Moment methods are a promising approach for the description of non-equilibrium and moderately rarefied gas flows. Moments equations are derived directly from the Boltzmann equation, integrating over all velocity space, effectively reducing the phase-space to three dimensions. The resulting system only describes the evolution of the gas macroscopic properties instead of the distribution function. Figure 2.1, depicts different available mathematical models along with their respective solution method. Starting from molecular dynamics, effectively solving Newton's law for each individual particles, hierarchical assumptions are listed leading all the way to the Euler equations.

In classical fluid mechanics, the microscopic structure of the fluid is relatively unimportant, due to the fact that the molecular nature of fluids exist on scales which are much smaller than the characteristic scale of the studied problem. This large separation of scales leads to microscopic fluctuations that "average out" over the scale of the problem. In this situation, knowledge of the smallest scale structure is not necessary to provide accurate solutions. However, if the dimensions of molecular processes become larger in comparison to the problem characteristic length scales, this averaging process may not be possible and the microscopic behavior of the gas becomes important. This is typically characterized using flow regimes. The different flow regimes are controlled by inter-particle collisions. This collisional effect is quantified by the Knudsen number,

$$\mathrm{Kn} = \frac{\lambda}{L}\,, \tag{2.1}$$

which is defined as the ratio between the mean free path and a representative length, L. As shown in Figure 2.2, for very low Knudsen number, the scale associated with molecular processes are much smaller than the problem characteristic lengths. This is known as the continuum regime. In this regime traditional fluid-mechanic techniques, such as the Navier-Stokes-Fourier equations, are valid. In the limit where, $\mathrm{Kn} \to 0$, the velocity distribution function can be shown to be Maxwellian, and the Boltzmann equation reduces to the Euler system. On the other hand, for much larger Knudsen numbers, collisional effects are negligible and the details of gas-particles dynamics become paramount. This so-called free-molecular regime is typically well approximated by particles methods such as DSMC. For flows in the transition regime, traditional equations are invalid and particle based methods

Physical description	**Mathematical model**	**Solution method**
Deterministic molecular	Newton's Law $f = ma$	Molecular dynamics
	$\Updownarrow$	
Probabilistic molecular	Liouville equation $\mathcal{P}(x_{ij}, v_{ij}, t),\ j \in [1, N]$	DSMC
	binary collisions $\Downarrow$ *molecular chaos*	
	Boltzmann's equation $\mathcal{F}(x_i, v_i, t)$	Direct solution
	$\Downarrow$ *thermodynamics*	
Hydrodynamic continuum	Extended hydrodynamics	Direct solution
	moment methods $\Downarrow$ $\Downarrow$ *Champan-Enskog expansion*	
	Moment equations Burnett equations	Direct solution
	small deviation $\Downarrow$ *from LTE*	
	Navier-Stokes-Fourier equations $\partial_t \boldsymbol{U} + \nabla \cdot \boldsymbol{F} = \nabla \cdot (\boldsymbol{D} \nabla \boldsymbol{U})$	Direct solution
	$\Downarrow$ *local equilibrium*	
	Euler equations $\partial_t \boldsymbol{U} + \nabla \cdot \boldsymbol{F} = 0$	Direct solution

Figure 2.1: The hierarchical assumptions starting from molecular dynamics leading all the way to the Euler equations.

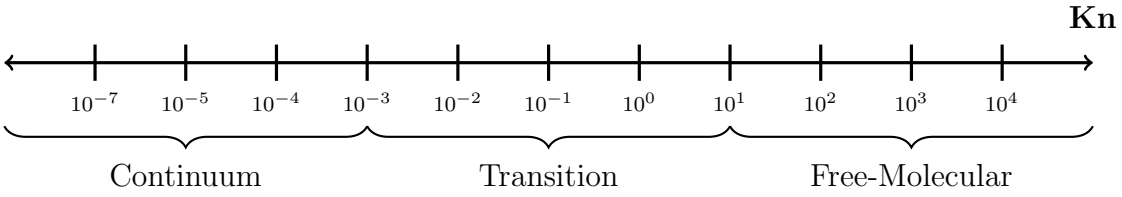

Figure 2.2: Flow regimes with respect to the Knudsen number

are often prohibitively expensive. Moment methods have been shown to be particularly well suited to tackle problems in this regime.

2.1 The Distribution Function

The classical kinetic theory of gases relies on a statistical representation of the gas particle velocities. Instead of tracking every single particle, a velocity distribution function, $\mathcal{F}(x_i, v_i, t)$, is used. This function lives in 6-dimensional phase-space and describes the density of particles in the neighborhood of a position, x_i, with a velocity, v_i, at a time, t. The exact form of this distribution varies vastly depending on the gas state. The most well-known distribution function is the Maxwell-Boltzmann distribution,

$$\mathcal{M} = \frac{\rho}{m}\left(\frac{\rho}{2\pi p}\right)^{\frac{3}{2}} \exp\left(-\frac{\rho}{2p}(v_i - u_i)(v_i - u_i)\right), \tag{2.2}$$

where ρ is the mass density of the gas, p is the pressure, m is the particle mass, u_i is the flow bulk velocity and v_i is the particle velocity. The random velocity, $c_i = v_i - u_i$, is defined as the difference between the particle velocity and the flow bulk velocity. As mentioned above the Maxwell-Boltzmann distribution statistically represent gases that are in local thermodynamic equilibrium. For non-equilibrium gases, the exact form of the associated distribution function is generally not known.

In order to determine the macroscopic properties of a gas defined by a particular distribution function, velocity moments must be taken. This involves multiplying the distribution function by a velocity weight and integrating over all velocity space. For example, the mass density, ρ, is found by taking m, the molecular mass as weighting function,

$$\rho = \iiint_{\infty} m\mathcal{F}(x_i, v_i, t)\mathrm{d}^3 v_i = \langle m\mathcal{F} \rangle \tag{2.3}$$

Other examples of commonly used moments include

$$\begin{aligned} \rho u_i &= \langle m v_i \mathcal{F} \rangle \ , \\ P_{ij} &= \langle m c_i c_j \mathcal{F} \rangle \ , \\ Q_{ijk} &= \langle m c_i c_j c_k \mathcal{F} \rangle \ , \\ R_{ijkl} &= \langle m c_i c_j c_k c_l \mathcal{F} \rangle \ , \\ S_{ijklm} &= \langle m c_i c_j c_k c_l c_m \mathcal{F} \rangle \ . , \end{aligned} \tag{2.4}$$

where, $P_{ij} = p\delta_{ij} - \tau_{ij}$ represents the anisotropic pressure tensor, defined as the difference between the thermodynamic pressure, p, and the deviatoric stresses, τ_{ij}. The third-order tensor, Q_{ijk}, is the generalized heat-flux tensor. The heat-transfer in a given direction is equivalent to half of the corresponding trace of the heat-flux tensor, $q_i = \frac{1}{2} Q_{ijj}$. For monatomic gases, the thermodynamic pressure is obtained by averaging the diagonal entries of the anisotropic pressure tensor, $p = P_{ii}/3$. The notation, $\langle \cdot \rangle$, is used to represent integration over all velocity space. Moments of the full particle velocity or convective moments are denoted, $U_n = \langle m v_i v_j \cdots v_n \mathcal{F} \rangle$ while random-velocity moments are denoted $V_n = \langle m c_i c_j \cdots c_n \mathcal{F} \rangle$. Higher-order moments, such as R_{ijkl} and S_{ijklm} represent high-order statistics of particles velocities. In this way, moments of any arbitrary order can be defined. However, traditional macroscopic properties tend to be associated to low-order moments. The physical significance of higher order moments are less obvious.

2.2 The Boltzmann Equation

The time evolution of the distribution function, $\mathcal{F}(x_i, v_i, t)$, is governed by the Boltzmann equation,

$$\frac{\partial \mathcal{F}}{\partial t} + v_i \frac{\partial \mathcal{F}}{\partial x_i} + \frac{\partial \left(a_i \mathcal{F} \right)}{\partial v_i} = \frac{\delta \mathcal{F}}{\delta t} \, . \tag{2.5}$$

Here, a_i is the particle acceleration due to external forces. These forces can include gravity, electromagnetic fields, and others. The term on the right-hand side of Eq. (2.5) is the collision operator, which models the effect of inter-particles interaction on the distribution function. Following the assumptions that only binary collisions of identical particles occurring on a scale that is much smaller than the mean free path, that a single collision does not noticeably affect the distribution function, and that the particles velocities are statistically independent

(molecular chaos), it is possible to express the collision term as,

$$\frac{\delta \mathcal{F}}{\delta t} = \left\langle \int_0^{2\pi} \int_0^{\pi} \left(\mathcal{F}' \mathcal{F}_1' - \mathcal{F}\mathcal{F}_1\right) g\sigma \sin\chi d\chi d\epsilon \right\rangle_{v_i'} , \tag{2.6}$$

where $\mathcal{F}$ and $\mathcal{F}_1$ are the distribution functions of the two particles undergoing a collision at particle velocities v_i and v_{1i}, while $\mathcal{F}'$ and $\mathcal{F}_1'$ are the distribution functions of the two particles post collision with particle velocities v_i' and v_{1i}'. The particles' relative speed pre-collision is expressed as $g = |v_i - v_{1i}|$, σ is the differential collision cross-section, χ is the deflection angle and finally ϵ is a solid angle integrated around a particle undergoing collisions [26, 27].

This particular operator possesses many interesting properties. It can be shown to conserve mass, momentum and energy, and to increase the entropy monotonically until the distribution function becomes a Maxwellian. More importantly, it can be shown to satisfy the second law of thermodynamics. This can be easily shown by taking moments of the Boltzmann equation using the velocity weight

$$\mathcal{W} = -k \ln \frac{\mathcal{F}}{y} , \tag{2.7}$$

where y is a normalizing constant, leading to,

$$\frac{\partial}{\partial t}\left\langle -k \ln \frac{\mathcal{F}}{y}\mathcal{F} \right\rangle + \frac{\partial}{\partial x_i}\left\langle -k \ln \frac{\mathcal{F}}{y} v_i \mathcal{F} \right\rangle + \frac{\partial}{\partial v_i}\left\langle -k \ln \frac{\mathcal{F}}{y} a_i \mathcal{F} \right\rangle = \left\langle -k \ln \frac{\mathcal{F}}{y} \frac{\delta \mathcal{F}}{\delta t} \right\rangle . \tag{2.8}$$

Neglecting any acceleration and further defining the variable $S = \left\langle -k \ln \frac{\mathcal{F}}{y}\mathcal{F} \right\rangle$, as well as its flux, $\Psi_i = \left\langle -k \ln \frac{\mathcal{F}}{y} v_i \mathcal{F} \right\rangle$ and its production term $\Phi = \left\langle -k \ln \frac{\mathcal{F}}{y} \frac{\delta \mathcal{F}}{\delta t} \right\rangle$, the expression can be simplified to a transport equation,

$$\frac{\partial S}{\partial t} + \frac{\partial \Psi_i}{\partial x_i} = \Phi . \tag{2.9}$$

By further assuming an isolated system where the boundary flux of S is zero, the rate of change of S can be expressed as,

$$\frac{\partial S}{\partial t} = \Phi . \tag{2.10}$$

By observation of the production term, Φ, after substituting Eq. (2.6) into the right-hand side of Eq. (2.8) and performing some classical manipulations [27], it can be seen that it is

always greater than zero,

$$\Phi = \frac{k}{4}\left\langle\left\langle\int_0^{2\pi}\int_0^{\pi}\ln\frac{\mathcal{F}'\mathcal{F}_1'}{\mathcal{F}\mathcal{F}_1}\left(\mathcal{F}'\mathcal{F}_1'-\mathcal{F}\mathcal{F}_1\right)g\sigma\sin\chi d\chi d\epsilon\right\rangle_{v_i'}\right\rangle_{v_i}\geq 0\,, \tag{2.11}$$

since g and σ are always greater than zero, χ is positive for the integration interval $0 \leq \chi \leq \pi$ and the terms $\ln\frac{\mathcal{F}'\mathcal{F}_1'}{\mathcal{F}\mathcal{F}_1}$ and $(\mathcal{F}'\mathcal{F}_1' - \mathcal{F}\mathcal{F}_1)$ are only negative at the same time. In fact, S represents an entropy and the production term, Φ is always greater than zero in Eq. (2.10). In this case, entropy is always generated and the second law of thermodynamics is satisfied [22].

As one can see, the collision operator contains high-dimensional integrals which generally cannot be evaluated in closed form. For many applications, however, it is possible to use simplifying collision models, such as the relaxation-time BGK model, first proposed by Bhatnagar *et al.* [28],

$$\frac{\delta\mathcal{F}}{\delta t} = -\frac{\mathcal{F}-\mathcal{M}}{\tau}\,, \tag{2.12}$$

where τ is a characteristic relaxation time and $\mathcal{M}$ is the Maxwellian with the same mass, momentum, and energy densities. The BGK model moves the distribution function, $\mathcal{F}$, towards equilibrium at finite time scale, τ. This time scale, defined as the inverse of the collision frequency, is very small when dealing with gases in the continuum regime as inter-particle collisions dominate. On the other hand, τ goes to infinity in the free-molecular regime when collisions can be neglected. One of the major drawbacks associated with the BGK collision operator is the incorrect Prandtl number, which can be shown to be 1, whereas experimental values for monatomic gases are close to $\mathrm{Pr} = 3/2$. More sophisticated collision operators, such as ES-BGK [29], are necessary to recover a correct Prandtl number. A study comparing the accuracy of different collision operators is readily available [30].

2.3 Maxwell's Equation of Change

The Boltzmann equation is high-dimensional, with three dimensions in physical space, three dimensions in velocity, and one time dimension. Directly solving this equation requires numerical discretization in both physical and velocity space, resulting in a method that is prohibitively expensive. Fortunately, for most practical problems, all the information obtained by solving the Boltzmann equation is not necessary. In most cases, it is sufficient to only solve for a desired set of macroscopic properties. A system of equations controlling the evolution of these macroscopic properties (moments of interest) can be derived by taking velocity

moments of the Boltzmann equation. A vector, $\boldsymbol{\mathcal{W}} = [1, v_i, v_i v_j, v_i v_j v_k, \cdots, v_i v_j v_{k \cdots} v_p]^{\mathrm{T}}$, is defined containing the velocity weights associated with each moment such that the solution vector, $\boldsymbol{U}$, is defined as,

$$\boldsymbol{U} = \langle m \boldsymbol{\mathcal{W}} \mathcal{F} \rangle \ .$$

A system of equations for the moments evolution can be derived as,

$$\left\langle m \boldsymbol{\mathcal{W}} \left(\frac{\partial \mathcal{F}}{\partial t} + v_i \frac{\partial \mathcal{F}}{\partial x_i} + \frac{\partial \left(a_i \mathcal{F} \right)}{\partial v_i} \right) \right\rangle = \left\langle m \boldsymbol{\mathcal{W}} \frac{\delta \mathcal{F}}{\delta t} \right\rangle \ .$$

For the purpose of this derivation, the collision operator is replaced by the BGK model (Eq. 2.12),

$$\left\langle m \boldsymbol{\mathcal{W}} \left(\frac{\partial \mathcal{F}}{\partial t} + v_i \frac{\partial \mathcal{F}}{\partial x_i} + \frac{\partial \left(a_i \mathcal{F} \right)}{\partial v_i} \right) \right\rangle = \left\langle -m \boldsymbol{\mathcal{W}} \frac{\mathcal{F} - \mathcal{M}}{\tau} \right\rangle \ .$$

Since the position, x_i, and velocity, v_i are independent, the velocity space integrals can be moved inside the space and time partial derivatives allowing for further simplifications,

$$\frac{\partial}{\partial t} \langle m \boldsymbol{\mathcal{W}} \mathcal{F} \rangle + \frac{\partial}{\partial x_i} \langle m v_i \boldsymbol{\mathcal{W}} \mathcal{F} \rangle + \left\langle m \boldsymbol{\mathcal{W}} \frac{\partial \left(a_i \mathcal{F} \right)}{\partial v_i} \right\rangle = -\frac{1}{\tau} \left[\langle m \boldsymbol{\mathcal{W}} \mathcal{F} \rangle - \langle m \boldsymbol{\mathcal{W}} \mathcal{M} \rangle \right] \ . \tag{2.13}$$

By using a simple chain rule and assuming that the acceleration, a_i, is not function of the particle velocities, one can derive the form of Maxwell's equation of change that is used in this work,

$$\frac{\partial}{\partial t} \langle m \boldsymbol{\mathcal{W}} \mathcal{F} \rangle + \frac{\partial}{\partial x_i} \langle m v_i \boldsymbol{\mathcal{W}} \mathcal{F} \rangle = -a_i \left\langle m \mathcal{F} \frac{\partial \boldsymbol{\mathcal{W}}}{\partial v_i} \right\rangle - \frac{1}{\tau} \left[\langle m \boldsymbol{\mathcal{W}} \mathcal{F} \rangle - \langle \boldsymbol{\mathcal{W}} \mathcal{M} \rangle \right] \ . \tag{2.14}$$

The resulting number of equations in the system is the same as the size of the velocity weight vector. For simplicity, Eq. (2.14) is often written as,

$$\frac{\partial \boldsymbol{U}}{\partial t} + \frac{\partial \boldsymbol{F_i}}{\partial x_i} = \boldsymbol{S} + \boldsymbol{C} \, , \tag{2.15}$$

where $\boldsymbol{U}$ is the solution vector, $\boldsymbol{F_i}$ is the flux, $\boldsymbol{S}$ is a source term taking into account the particle accelerations and $\boldsymbol{C}$ is the collision source term. By using the chain rule, Eq. (2.15) is often written,

$$\frac{\partial \boldsymbol{U}}{\partial t} + \frac{\mathrm{d} \boldsymbol{F_i}}{\mathrm{d} \boldsymbol{U}} \frac{\partial \boldsymbol{U}}{\partial x_i} = \boldsymbol{S} + \boldsymbol{C} \, , \tag{2.16}$$

where $\frac{\mathrm{d} \boldsymbol{F_i}}{\mathrm{d} \boldsymbol{U}}$ is the flux Jacobian. The eigenvalues of the flux Jacobian correspond to the wave speeds of the system, denoted $\boldsymbol{\lambda}$. If the eigenvalues of the Jacobian are strictly real and distinct, then the system is said to be strongly hyperbolic and information propagates at

finite speeds. When dealing with first-order balance laws, hyperbolicity is paramount to ensure the well-posedness of the system. This criteria is discussed extensively in Chapter 5.

Unfortunately, only taking velocity-moment of the Boltzmann equation cannot naturally lead to a closed system of equations. This is because the time evolution of a given moment always depends on the spacial divergence of a moment that is one order higher in velocity; such that at least one member of the flux vector is unknown. An infinite number of moment equations would therefore be needed to have a closed system. Techniques to artificially truncate this infinite set of moment equations are called moment closures.

2.4 Moment Closure

Many moment closures have been introduced over the past decades. The strategy used to close the system has a huge impact on the resulting moment equations. In this section, a non-exhaustive list of the main ideas is presented. One traditional idea, first introduced by Grad, assumes the form of the distribution functions to be a polynomial expansion around a Maxwellian. Alternatively, the maximum-entropy technique relies on using the distribution function that maximizes the Boltzmann entropy, a measure of likelihood, of the distribution. Some more recent techniques, such as the ϕ-divergences closures are based around an approximation of the original maximum-entropy idea. Finally, the quadrature-based closures use weighted quadrature methods to approximate the distribution function. The work presented in this thesis only treats one-dimensional systems. However, for completeness, the following section favors a full three-dimensional description.

As mentioned in the previous section, only taking velocity moments of the Boltzmann equation cannot lead to a closed system of equations. One method used to obtain a closed system of equation is to assume the form of the distribution function. This allows one to relate the higher-order moments to the lower order moment of interest. This assumed distribution function must have the same number of free parameters, $\boldsymbol{\alpha}$, as there are moments in the solution vector (macroscopic properties of interest). The free parameters are chosen so that they are in agreement with the known moments, as given by Eq. (2.4). It then becomes possible to directly integrate the closing fluxes, using the assumed distribution function. The obtained closing fluxes naturally become a function of the known moments. However, as is demonstrated in the second journal article, assuming the form of the distribution function is not always needed. The construction of quadrature-based closure only relies on a set of restrictions forcing the resulting moment system to be hyperbolic and maintain balance-law form.

2.4.1 The Euler Equations

As a first example, the well-known compressible Euler equations describing inviscid, adiabatic gas flows are presented. They are described here as a set of five moment equations. For which the associated velocity weight vector is, $\boldsymbol{\mathcal{W}} = [1, v_i, v_i v_i]$. Note that the number of velocity weights is always equal to the number of unknowns in the Maxwellian which are ρ, u_i and p.

$$\frac{\partial}{\partial t}\left\langle m\mathcal{F}\right\rangle + \frac{\partial}{\partial x_i}\left\langle mv_i\mathcal{F}\right\rangle = -\frac{1}{\tau}\left(\left\langle m\mathcal{F}\right\rangle - \left\langle m\mathcal{M}\right\rangle\right) \tag{2.17}$$

$$\frac{\partial}{\partial t}\left\langle mv_i\mathcal{F}\right\rangle + \frac{\partial}{\partial x_j}\left\langle mv_iv_j\mathcal{F}\right\rangle = -\frac{1}{\tau}\left(\left\langle mv_i\mathcal{F}\right\rangle - \left\langle mv_i\mathcal{M}\right\rangle\right) \tag{2.18}$$

$$\frac{\partial}{\partial t}\left\langle mv_iv_i\mathcal{F}\right\rangle + \frac{\partial}{\partial x_j}\left\langle mv_iv_iv_j\mathcal{F}\right\rangle = -\frac{1}{\tau}\left(\left\langle mv_iv_i\mathcal{F}\right\rangle - \left\langle mv_iv_i\mathcal{M}\right\rangle\right)\,. \tag{2.19}$$

As explained previously, the spacial divergence term in Eqs. (2.18) and (2.19) contains moments that are not part of the known moments of interest and therefore the system is not closed. Closure is obtained by choosing a form for the distribution function, relating the closing fluxes to the known lower-order moments. If one chooses the Maxwellian as distribution function, $\mathcal{F} = \mathcal{M}$, the Euler equations are recovered,

$$\frac{\partial}{\partial t}\left(\rho\right) + \frac{\partial}{\partial x_i}\left(\rho u_i\right) = 0 \tag{2.20}$$

$$\frac{\partial}{\partial t}\left(\rho u_i\right) + \frac{\partial}{\partial x_j}\left(\rho u_iu_j + p\delta_{ij}\right) = 0 \tag{2.21}$$

$$\frac{\partial}{\partial t}\left(\rho u_iu_i + 3p\right) + \frac{\partial}{\partial x_j}\left(\rho u_iu_iu_j + 5pu_j\right) = 0\,. \tag{2.22}$$

Since the distribution function can be integrated directly, the closing flux can be determined,

$$\left\langle mv_iv_iv_j\mathcal{M}\right\rangle = \rho u_iu_iu_j + 5pu_j\,. \tag{2.23}$$

Here, it is important to note that Eq. (2.22) is double the traditional energy equation. It is written this way for consistency with other closures shown in this work. As already well known, the Euler equations are only valid for inviscid flows with no heat-transfer. This demonstrates the need of a more complex distribution function with a larger velocity weight vector allowing to model a larger set of macroscopic properties.

2.4.2 The Grad Hierarchy

Perhaps the most well-known moment closure technique is the original hierarchy developed in 1949 by Grad [8]. The assumed form of the distribution function consists of a Hermite polynomial expansion around the equilibrium distribution,

$$\mathcal{F} = (\alpha_0 H_0 + \alpha_i H_i + \alpha_{ij} H_{ij} + \cdots)\,\mathcal{M}\,, \tag{2.24}$$

where the Maxwellian is a function of the local density, bulk velocity, and pressure. In Eq. (2.24), the $\alpha_{i_1,i_2,\cdots,i_N}$ are the closure coefficients depending on lower-order moments, while the $H_{i_0,i_1,\cdots,i_N}$ are Hermite polynomials. These polynomials are defined as,

$$H_{i_0,i_1,\cdots,i_N} = \frac{1}{\mathcal{M}} \frac{\partial^N}{\partial c_{i_0} \partial c_{i_1} \cdots \partial c_{i_N}} \mathcal{M}\,. \tag{2.25}$$

where N is the order of the polynomial. These polynomials form an orthogonal basis with respect to the Maxwellian distribution function, that is

$$\iiint\limits_{\infty} H_{i_0,i_1,\cdots,i_N} H_{j_0,j_1,\cdots,j_M} \mathcal{M}\, dc_x dc_y dc_z = 0 \quad \text{for} \quad i_0, i_1, \cdots, i_N \neq j_0, j_1, \cdots, j_M\,. \tag{2.26}$$

The coefficients multiplying the Hermite polynomials, $\boldsymbol{\alpha}$, are consistant with the moments of interest. The number of coefficient must be equal to the number of moments in the solution vector. In the original work of Grad [8], both the 13- and 20-moment closures were considered. These moment systems include a treatment for the heat-flux vector Q_i and the generalized heat-flux tensor Q_{ijk} respectively. Extensions to more moments have been considered [31, 26], since their inclusion is generally assumed to yield better approximations.

As an example, the Grad 13-moment closure is constructed. This closure has the ability to model both the viscous stresses and heat-transfer. The associated distribution takes the general form,

$$\mathcal{F}_{G13} = (\alpha_0 + \alpha_i H_i + \alpha_{ij} H_{ij} + \alpha_{ijj} H_{ijj})\,\mathcal{M}\,, \tag{2.27}$$

where the system of equations is generated using the velocity weight vector $\boldsymbol{\mathcal{W}} = [1, v_i, v_i v_j, v_i v_j v_j]$. The corresponding random-velocity moments of interest are $\boldsymbol{V} = [\rho, u_i, P_{ij}, Q_{ijj}]$. The first four Hermite polynomials can be calculated as,

$$\begin{aligned} H_0 &= 1\,, \\ H_i &= -\frac{\rho}{p} c_i\,, \end{aligned}$$

$$H_{ij} = \frac{\rho^2}{p^2} c_i c_j - \frac{\rho}{p} \delta_{ij} \,,$$
$$H_{ijj} = -\frac{\rho^3}{p^3} c_i c_j c_j + 5 \frac{\rho^2}{p^2} c_i \,.$$

By taking moments of the distribution, one can show that the coefficients need to be

$$\begin{aligned}
\alpha_0 &= 1 \,, \\
\alpha_i &= 0 \,, \\
\alpha_{ij} &= \frac{P_{ij} - p\delta_{ij}}{2\rho} \,, \\
\alpha_{ijj} &= -\frac{Q_{ijj}}{10\rho} \,,
\end{aligned}$$

in order to agree with the known moments. The resulting distribution function can now be inserted into Maxwell's equation of change (Eq. 2.14), assuming no particle acceleration. This leads to a set of thirteen PDEs,

$$\frac{\partial}{\partial t}(\rho) + \frac{\partial}{\partial x_i}(\rho u_i) = 0 \tag{2.28}$$

$$\frac{\partial}{\partial t}(\rho u_i) + \frac{\partial}{\partial x_j}(\rho u_i u_j + P_{ij}) = 0 \tag{2.29}$$

$$\begin{aligned}
&\frac{\partial}{\partial t}(\rho u_i u_j + P_{ij}) \\
&+ \frac{\partial}{\partial x_k}(\rho u_i u_j u_k + u_i P_{jk} + u_j P_{ik} + u_k P_{ij} \\
&\qquad + \frac{1}{5}(Q_{ill}\delta_{jk} + Q_{jll}\delta_{ik} + Q_{kll}\delta_{ij})) = -\frac{3P_{ij} - P_{kk}\delta_{ij}}{3\tau}
\end{aligned} \tag{2.30}$$

$$\begin{aligned}
&\frac{\partial}{\partial t}(\rho u_i u_j u_j + u_i P_{jj} + 2u_j P_{ij} + Q_{ijj}) \\
&+ \frac{\partial}{\partial x_k}\Bigg(\rho u_i u_j u_j u_k + 2u_i u_j P_{jk} + u_i u_k P_{jj} + u_j u_j P_{ik} + 2u_j u_k P_{ij} \\
&\qquad + u_i Q_{kjj} + u_k Q_{ijj} + 2u_j \frac{1}{5}(Q_{ill}\delta_{jk} + Q_{jll}\delta_{ik} + Q_{kll}\delta_{ij}) + \left(7\frac{p}{\rho}P_{ik} - 2\frac{p^2}{\rho}\delta_{ik}\right)\Bigg) \\
&\qquad = -\frac{3Q_{ijj} + 2(3P_{ik}u_k - P_{kk}u_i)}{3\tau}
\end{aligned} \tag{2.31}$$

The first equation is the conservation of mass, the following three are the conservation of momentum. The next six describe the conservation of energy decomposed into modes associated with different directions. Finally, the last three describe the evolution of the energy flux, including the heat transfer vector, Q_i.

However, if one is only interested in the evolution of the following moments $\boldsymbol{V} = [\rho, u_i, p]$, the associated Grad distribution function with the Hermite polynomial H_0, H_i and H_{ii} is,

$$\mathcal{F} = \left(\alpha_0 - \alpha_i \frac{\rho}{p} c_i + \alpha_{ii} \left(\frac{\rho^2}{p^2} c_i c_i - 3\frac{\rho}{p}\right)\right) \mathcal{M}\,. \tag{2.32}$$

By computing the coefficients α_0, α_i and α_{ii} so that they are in agreement with the moment of the solution vector,

$$\alpha_0 = 1\,, \qquad \alpha_i = 0\,, \qquad \alpha_{ii} = 0\,, \tag{2.33}$$

one can see that the resulting distribution function is simply the Maxwellian. This shows that the Euler equations are the lowest-order member of the Grad hierarchy.

Although Grad-type expansions result in a closed set of transport equations for a given set of moments, the assumed distribution function can, in many cases, be non-physical. Due to the polynomial nature of the distribution, it can yield negative probabilities for some values of the particle velocity; leading in some cases to negative mass densities. More significantly, there are realizable moments arbitrarily close to equilibrium for which the resulting moment equations are not hyperbolic [18]. This lost of hyperbolicity happens when the eigenvalues of the corresponding flux Jacobian are complex valued. As a consequence, the moment equations become ill-posed for initial value problems. Researchers have proposed a regularization to extend the mathematical robustness of the closures, consequently adding non-conservative terms into the moment system [17, 18].

2.4.3 The Maximum-Entropy Hierarchy

Instead of a polynomial, series-expansion technique as proposed by Grad [8], the maximum-entropy hierarchy selects the form of the distribution function that maximizes the Boltzmann entropy while remaining consistent with the macroscopic moments of the solution vector [13, 9, 10]. This closure technique is equivalent to choosing the most likely distribution function that corresponds to a given set of moments. It has been shown that such choice leads to closures that have many desirable mathematical properties. Mathematically this optimization problem is expressed as,

$$\max_{\mathcal{F}} \langle -(\mathcal{F}\ln\mathcal{F} - \mathcal{F})\rangle \qquad \text{such that} \qquad \boldsymbol{U} = \langle \boldsymbol{\mathcal{W}}\mathcal{F}\rangle\,, \tag{2.34}$$

where, $\langle -(\mathcal{F}\ln\mathcal{F} - \mathcal{F})\rangle$ is the Boltzmann entropy. This optimization problem is usually solved using the method of Lagrange multipliers. A vector of Lagrange multipliers, $\boldsymbol{\alpha}$, is

defined and the constrained maximization is recast as an expanded unconstrained problem, where one searches for a critical point of,

$$\mathcal{L} = \langle -\left((\mathcal{F}\ln\mathcal{F} - \mathcal{F})\right)\rangle - \boldsymbol{\alpha}^T\left(\boldsymbol{U} - \langle\boldsymbol{\mathcal{W}}\mathcal{F}\rangle\right) . \tag{2.35}$$

The critical point of the Lagrangian function is defined as the point where $\frac{\partial\mathcal{L}}{\partial\mathcal{F}} = 0$,

$$\begin{aligned}\frac{\partial\mathcal{L}}{\partial\mathcal{F}} &= \langle -\ln\mathcal{F}\rangle + \boldsymbol{\alpha}^T\langle\boldsymbol{\mathcal{W}}\rangle = 0\,,\\ \left\langle\ln\mathcal{F} - \boldsymbol{\alpha}^T\boldsymbol{\mathcal{W}}\right\rangle &= 0\,.\end{aligned} \tag{2.36}$$

By observation, Eq. (2.36) is satisfied by distribution functions of the form

$$\mathcal{F}_{\text{M.E.}} = e^{\boldsymbol{\alpha}^T\boldsymbol{\mathcal{W}}} \quad , \tag{2.37}$$

where $\boldsymbol{\alpha}$ is the vector of free-parameters, which are also the Lagrange multipliers, and $\boldsymbol{\mathcal{W}}$ is the associated velocity weights vector.

The distribution function associated with this technique ensures a positive number density for all velocity space. Closures of this type also have an elegant proof of hyperbolicity for the resulting PDEs [32]. However, as shown by Junk [14], there exists state for which a maximum-entropy distribution function cannot be constructed. Moreover, due to the specific form of distribution function, the closing flux cannot be integrated in closed form, thus requiring approximations, which are currently only available for a limited number of moments.

The first two members of the maximum-entropy hierarchy are the 5-moment and 10-moment closures. In both cases the distribution function is an exponential of a second-order polynomial in velocity. The 5-moment closure leads to the compressible Euler equations. The 10-moment distribution function can be obtained using the velocity weights, $\boldsymbol{\mathcal{W}} = [1, v_i, v_iv_j]$, resulting in,

$$\mathcal{F} = \frac{\rho}{m\left(2\pi\right)^{3/2}\left(\det\Theta\right)^{1/2}}\exp\left(-\frac{1}{2}\Theta_{ij}^{-1}c_ic_j\right) , \qquad \text{where} \qquad \Theta_{ij} = \frac{P_{ij}}{\rho}\,. \tag{2.38}$$

When the distribution function is used in Maxwell's equation of change (Eq. 2.14) it results in a system of ten hyperbolic equations describing the transport of the macroscopic quantities

ρ, u_i and P_{ij},

$$\frac{\partial}{\partial t}(\rho) + \frac{\partial}{\partial x_k}(\rho u_k) = 0 \tag{2.39}$$

$$\frac{\partial}{\partial t}(\rho u_i) + \frac{\partial}{\partial x_k}(\rho u_i u_k + P_{ik}) = 0 \tag{2.40}$$

$$\frac{\partial}{\partial t}(\rho u_i u_j + P_{ij}) + \frac{\partial}{\partial x_k}(\rho u_i u_j u_k + u_i P_{jk} + u_j P_{ik} + u_k P_{ij}) = 0\,. \tag{2.41}$$

It is important to note that the third-order random-velocity moments are zero, $\langle m c_i c_j c_k \mathcal{F} \rangle = 0$ rendering the model unable to account for the effects of thermal diffusion (i.e. the transport of translational particle energy by random particle motion). This closure has been proven to be very accurate and successful for flow prediction in both the continuum and transition regimes [33, 34, 35, 36, 37]. However, its inability to model heat transfer greatly limits its applicability.

The next two members of this family are the 14-moment and 21-moment closures. The distribution functions associated with these two closures are an exponential of a fourth-order polynomial, allowing for some skewness or asymmetry in the distribution function and therefore granting the closure the ability to predict non-zero heat-flux. Unfortunately, due to the fourth-order nature of the polynomial, $\boldsymbol{\alpha}^{\boldsymbol{T}}\boldsymbol{\mathcal{W}}$, the closing fluxes are impossible to integrate in closed form. To obtain the closing fluxes at each flux calculation, one needs to use an iterative procedure that requires repeated numerical integration over all velocity space. This iterative procedure consists of solving the entropy-maximization problem numerically in order to solve for the coefficients, $\boldsymbol{\alpha}$, contained in the distribution function and then numerically integrate the closing fluxes. Commonly, a Newton search is used to solve this problem, for which convergence appears to be challenging in some instances. This procedure is prohibitively expensive and cannot practically be used as it requires many 3D numerical integrations on infinite domains whenever a flux is needed.

Approximations for the closing fluxes of both the 14- and 21-moment closures were proposed by M$^{\text{c}}$Donald and Torrilhon [32] and Giroux and M$^{\text{c}}$Donald [38]. The approximation is robust and hyperbolic for a one-dimensional gas. However, both extensions to three-dimensions, while being accurate, are not as robust and lose hyperbolicity for some physically realizable states.

2.4.4 The φ-Divergences Closure

A more recent closure, inspired from the maximum-entropy hierarchy, has been proposed by Abdelmalik and van Brummelen [39]. The φ-divergences closure is based on an approximation of the exponential function allowing direct integration. The standard limit definition of the exponential states that

$$\exp(f) = \lim_{n\to\infty}\left(1+\frac{f}{n}\right)^n \approx \left(1+\frac{f}{N}\right)^N , \tag{2.42}$$

where f is an arbitrary function. Unfortunately, the resulting function is not well-behaved, in the limit where $v \to \pm\infty$, the truncated exponential and its derivatives do not decay to zero. This is essential in order to obtain finite macroscopic properties. Furthermore, for odd values of N, the resulting function allows for negative regions, which can result in negative mass densities. To preserve the properties mentioned above, a modified approximation of the exponential is required. One such approximation is the q-exponential [40],

$$\widetilde{\exp}_q(f) = [1+(1-q)f]_+^{1/(1-q)} , \tag{2.43}$$

where $q \neq 1$ and $[f]_+ = \frac{1}{2}f + \frac{1}{2}|f|$ represent non-negative part of the function f. The q-exponential and the truncated limit definition of the exponential are related when $1-q = \frac{1}{N}$,

$$\widetilde{\exp}_q(f) = \left[1+\frac{f}{N}\right]_+^N . \tag{2.44}$$

The proposed distribution function for the φ-divergences closure is

$$\mathcal{F}_N = \mathcal{M}\ \widetilde{\exp}_q(\boldsymbol{\alpha}^{\boldsymbol{T}}\boldsymbol{\mathcal{W}}) = \mathcal{M}\left(1+\frac{\boldsymbol{\alpha}^{\boldsymbol{T}}\boldsymbol{\mathcal{W}}}{N}\right)_+^N , \tag{2.45}$$

where $\boldsymbol{\alpha}$ and $\boldsymbol{\mathcal{W}}$ are the free parameters and the velocity weights respectively and $\mathcal{M}$ is a Maxwellian distribution that pre-factors the q-exponential approximation. Pre-factoring by a Maxwellian ensures a decay to zero as $v \to \pm\infty$. The values for the free-coefficients, $\boldsymbol{\alpha}$, are found by performing a Newton search using the moments. This closure leads to a hyperbolic set of equations with a strictly positive distribution function. When a value of $N = 1$ is chosen, a Grad distribution is recovered. Conversely, when a value of $N \to \infty$ is chosen, the resulting distribution function corresponds to the one that maximizes entropy. However, the major drawback of this method is that the Maxwellian used in this description needs to be constant in space and time to conserve hyperbolicity, greatly limiting the applicability of

this method.

2.4.5 Quadrature-Based Moment Closures

Quadrature-based moment closures have gained in popularity in recent years. They are known to produce robust and globally hyperbolic closures. First introduced by McGraw [41] in the context of aerosol dynamics description, Fox later developed the QMOM [42] closures covering the even-order moment systems, then with Laurent, the HyQMOM hierarchy [20] covering the odd-order moment systems. This method is central to the work presented in this thesis and will be discussed in great length in Chapter 4. Consequently, a brief overview is presented here. In general, for a one dimensional gas, quadrature-based moment closures approximate the velocity distribution function as a weighted sum of Dirac deltas,

$$\mathcal{F} = \sum_{i=0}^{i=n} \mathfrak{W}_i \delta(v - \zeta_i) \tag{2.46}$$

where, ζ_i, is the position of each quadrature point and $\mathfrak{W}_i$ is the associated weight. The weights are linked to the known moments through,

$$\boldsymbol{V}\boldsymbol{\mathfrak{W}} = \boldsymbol{U}\,, \tag{2.47}$$

while the flux is computed as,

$$\boldsymbol{F} = \boldsymbol{V}\boldsymbol{\Omega}\boldsymbol{\mathfrak{W}} = \boldsymbol{V}\boldsymbol{\Omega}\boldsymbol{V}^{-1}\boldsymbol{U}\,, \tag{2.48}$$

$$\boldsymbol{V} = \begin{bmatrix} 1 & 1 & 1 & \cdots & 1 \\ \zeta_0 & \zeta_1 & \zeta_2 & \cdots & \zeta_n \\ \zeta_0^2 & \zeta_1^2 & \zeta_2^2 & \cdots & \zeta_n^2 \\ \vdots & & \cdots & & \vdots \\ \zeta_0^n & \zeta_1^n & \zeta_2^n & \cdots & \zeta_n^n \end{bmatrix}, \qquad \boldsymbol{\Omega} = \begin{bmatrix} \zeta_0 & 0 & 0 & \cdots & 0 \\ 0 & \zeta_1 & 0 & \cdots & 0 \\ \vdots & 0 & \ddots & 0 & \vdots \\ 0 & \cdots & 0 & \zeta_{n-1} & 0 \\ 0 & \cdots & 0 & 0 & \zeta_n \end{bmatrix}. \tag{2.49}$$

However, simply choosing the quadrature points in terms of the known moments, $\boldsymbol{U}$, such that they are real valued, does not necessarily produce a hyperbolic set of moment equations. For most cases, the quadrature points will not agree with the system wave speeds found through the eigenvalues of the flux Jacobian. For hyperbolicity to occur the system wave speeds denoted, λ, are required to be the quadrature points, that is $\boldsymbol{\zeta} = \boldsymbol{\lambda}$, allowing the flux

Jacobian to be written as,

$$\frac{d\boldsymbol{F}}{d\boldsymbol{U}} = \boldsymbol{V}\,\boldsymbol{\Omega}\,\boldsymbol{V}^{-1}\,. \tag{2.50}$$

Satisfying this requirement for any number of moments has proven difficult. Chapter 4 introduces a novel technique for the construction of globally hyperbolic one-dimensional quadrature-based moment closures along with a new hierarchy of even-order moment systems.

Multi-Dimensional Quadrature-Based Distribution Function

In the case of multi-dimensional distribution functions, the quadrature points cannot be obtained through a direct method, as is possible for one-dimensional distribution functions. When the distribution function spans multiple dimensions, a choice of quadrature points with strictly positive weights appears to be challenging. Furthermore, the resulting model is not guaranteed to be hyperbolic. A method must be used to solve for the quadrature points while insuring positive weights, realizability, and hyperbolicity. Such methods have been proposed by Fox [43], the most successful ones being the conditional quadrature method of moments (CQMOM) [44] and the extended quadrature method of moments (EQMOM) [45]. These methods preserve all previously mentioned desired properties in a way that is not too extensively expensive to compute.

2.5 The Chapman-Enskog Method

Another popular strategy to simplify the Boltzmann equation into fluid models is to use a Chapman-Enskog expansion. This method was developed independently by Chapman [46] and Enskog [47], where it is assumed that the distribution function can be expressed as an expansion around the equilibrium state, allowing some deviation from the Maxwellian,

$$\mathcal{F} = \mathcal{M}(f_0 + \epsilon f_1 + \epsilon^2 f_2 + \epsilon^3 f_2 + \cdots)\,, \tag{2.51}$$

where ϵ is a "smallness" parameter and the functions, f_i, are of the same order. This assumed form of the distribution can then be substituted into the Boltzmann equation (Eq. 2.5), assuming no acceleration field is affecting the particles,

$$\begin{aligned}\frac{\partial}{\partial t}\left(\mathcal{M}(f_0 + \epsilon f_1 + \epsilon^2 f_2 + \epsilon^3 f_2 + \cdots)\right) + v_i\frac{\partial}{\partial x_i}\left(\mathcal{M}(f_0 + \epsilon f_1 + \epsilon^2 f_2 + \epsilon^3 f_2 + \cdots)\right) \\ = -\frac{1}{\epsilon\hat{\tau}}\left(\mathcal{M}(f_0 + \epsilon f_1 + \epsilon^2 f_2 + \epsilon^3 f_2 + \cdots) - \mathcal{M}\right)\,.\end{aligned} \tag{2.52}$$

Note that $\tau = \epsilon\hat{\tau}$ has been defined since τ, the mean free collision time, is also assumed to be small. One can then multiply Eq. (2.52) by ϵ and collect terms of the same order,

$$\frac{\mathcal{M}f_0 - \mathcal{M}}{\hat{\tau}} + \epsilon\left[\frac{\partial}{\partial t}\left(f_0\mathcal{M}\right) + v_i\frac{\partial}{\partial x_i}\left(f_0\mathcal{M}\right) + \frac{f_1\mathcal{M}}{\hat{\tau}}\right] \tag{2.53}$$
$$+\epsilon^2\left[\frac{\partial}{\partial t}\left(f_1\mathcal{M}\right) + v_i\frac{\partial}{\partial x_i}\left(f_1\mathcal{M}\right) + \frac{f_2\mathcal{M}}{\hat{\tau}}\right] + \epsilon^3\left[\frac{\partial}{\partial t}\left(f_2\mathcal{M}\right) + v_i\frac{\partial}{\partial x_i}\left(f_2\mathcal{M}\right) + \frac{f_3\mathcal{M}}{\hat{\tau}}\right] + \cdots = 0\,.$$

The first member of this hierarchy is obtained by only considering the zeroth-order term,

$$\frac{\mathcal{M}f_0 - \mathcal{M}}{\hat{\tau}} = 0\,, \tag{2.54}$$

leading to $f_0 = 1$ and $\mathcal{F} = \mathcal{M}$. As shown previously, this distribution function leads to the compressible Euler equations.

The first-order expansion is more involved. For the second member of this hierarchy, the terms of order ϵ are considered,

$$\epsilon\left[\frac{\partial}{\partial t}\left(f_0\mathcal{M}\right) + v_i\frac{\partial}{\partial x_i}\left(f_0\mathcal{M}\right) + \frac{f_1\mathcal{M}}{\hat{\tau}}\right] = 0\,. \tag{2.55}$$

This provides an expression for the first-order correction, f_1, where $f_0 = 1$,

$$f_1 = -\frac{\hat{\tau}}{\mathcal{M}}\left[\frac{\partial\mathcal{M}}{\partial t} + v_i\frac{\partial\mathcal{M}}{\partial x_i}\right]\,. \tag{2.56}$$

Substituting into Eq. (2.51) and keeping the first-order terms allows the kinetic equation to be expressed as,

$$\frac{\partial}{\partial t}\left(\mathcal{M}(1+f_1)\right) + v_i\frac{\partial}{\partial x_i}\left(\mathcal{M}(1+f_1)\right) = -\frac{1}{\tau}\left(\mathcal{M}(1+f_1) - \mathcal{M}\right)\,. \tag{2.57}$$

A fluid model can be obtained using the Maxwell's equation of change (Eq. 2.14) assuming no particle acceleration,

$$\frac{\partial}{\partial t}\left\langle m\boldsymbol{\mathcal{W}}\mathcal{M}(1+f_1)\right\rangle + \frac{\partial}{\partial x_i}\left\langle mv_i\boldsymbol{\mathcal{W}}\mathcal{M}(1+f_1)\right\rangle = -\frac{1}{\tau}\left[\left\langle m\boldsymbol{\mathcal{W}}\mathcal{M}(1+f_1)\right\rangle - \left\langle\boldsymbol{\mathcal{W}}\mathcal{M}\right\rangle\right]\,. \tag{2.58}$$

The velocity related weights are taken as $\boldsymbol{\mathcal{W}} = [1, v_i, v_iv_j]^{\mathrm{T}}$ generating balance laws for mass, momentum and energy,

$$\frac{\partial}{\partial t}\left(\rho\right) + \frac{\partial}{\partial x_i}\left(\rho u_i\right) = 0 \tag{2.59}$$

$$\frac{\partial}{\partial t}\left(\rho u_i\right) + \frac{\partial}{\partial x_i}\left(\rho u_i u_j + P_{ij}\right) + \frac{\partial}{\partial x_i}\left\langle m c_i c_j f_1 \mathcal{M}\right\rangle = 0 \tag{2.60}$$

$$\frac{\partial}{\partial t}\left(\frac{1}{2}\rho u_i u_j + \frac{3}{2}p\right) + \frac{\partial}{\partial x_i}\left(u_i\left[\frac{1}{2}\rho u_j u_j + \frac{5}{2}p\right]\right) + u_j\frac{\partial}{\partial x_i}\left\langle m c_i c_j f_1 \mathcal{M}\right\rangle + \frac{\partial}{\partial x_i}\left\langle \frac{1}{2} m c_i c_j c_j f_1 \mathcal{M}\right\rangle = 0\,. \tag{2.61}$$

One can see that there is no correction of the continuity equation. However, both the momentum and energy equations display first-order corrections. Using Eq. (2.56), the moments can be evaluated,

$$-\left\langle m c_i c_j f_1 \mathcal{M}\right\rangle = \tau_{ij} = \tau p\left(\frac{\partial u_i}{\partial x_j} + \frac{\partial u_j}{\partial x_i}\right) - \frac{2}{3}\tau p \delta_{ij}\frac{\partial u_k}{\partial x_k}\,, \tag{2.62}$$

$$\left\langle \frac{1}{2} m c_i c_j c_j f_1 \mathcal{M}\right\rangle = q_i = -\frac{5}{2}\frac{\tau p k}{m}\frac{\partial T}{\partial x_i}\,, \tag{2.63}$$

where k is the Boltzmann's constant and $T = \frac{mp}{k\rho}$ is the temperature. The heat-flux agrees with Fourier's law if the thermal conductivity is defined as, $\kappa = \frac{5}{2}\frac{\tau p k}{m}$. These equations are exactly the Navier-Stokes-Fourier equations provided that the viscosity $\mu = \tau p$.

The Navier-Stokes-Fourier system of equations are accurate for situations in the continuum regime and moderately close to thermodynamic equilibrium. However, when dealing with problems where the non-equilibrium effects are important, higher-order expansions are needed. The second- and third-order expansions lead to the Burnett and Super-Burnett system of equations respectively. Unfortunately, these equations have many drawbacks. The equilibrium state was shown to be linearly unstable under longitudinal perturbations and are also frame dependent in rotating coordinates [48, 49]. Furthermore, appropriate boundary conditions are in general, unknown[50].

2.6 The Wigner Formalism

Departing from classical gases, this section briefly covers the Wigner formalism of quantum mechanics, since it is central to the first presented publication in Chapter 3. The Wigner formalism finds use in many engineering fields, such as modeling electron transport in quantum electronics, calculating the static and dynamical properties of many-body quantum systems in quantum chemistry, and investigating waves passing through different media in signal processing [51]. These many-particle situations are often modeled as a one-particle system in a statistical mixture of N different states. Each state is described by a wave function, $\psi_k = \psi_k(x,t)$ and is associated with a probability, $P_k \geq 0$, satisfying $\sum_{k=1}^{k=N} P_k = 1$. In

the standard wave-function formulation, the evolution of each state needs to be computed, often leading to a prohibitive computational cost. However, the Wigner formalism allows the derivation of a single equivalent Wigner function,

$$W(x,p,t) = \frac{1}{(2\pi\hbar)^3}\sum_{k=1}^{N} P_k \int d^3y\, \psi_k^*(x+y,t)\psi_k(x-y,t)e^{2ipy/\hbar}\,. \tag{2.64}$$

The advantage of the Wigner formalism for many-body situations then becomes apparent, since the difficulty of solving the equivalent Wigner function does not scale with the number of different states, as it would for a classical wave-function formulation. However, numerical solutions of the Wigner function can also be computationally taxing. The high-dimensional nature of this equation makes the accurate resolution of this equation often prohibitively expensive for practical applications. The time evolution of the Wigner function is given by the Wigner equation,

$$\frac{\partial W}{\partial t} + \frac{p}{m}\frac{\partial W}{\partial x} - \frac{dV(x)}{dx}\frac{\partial W}{\partial p} = \sum_{s=1}^{\infty}(-\hbar)^s \frac{1}{(2s+1)!}\left(\frac{1}{2}\right)^{2s} \frac{\partial^{2s+1}V(x)}{\partial x^{2s+1}}\frac{\partial^{2s+1}W}{\partial p^{2s+1}}\,, \tag{2.65}$$

with m being the particle mass and $\hbar$ the normalized Plank constant. One can observe that Eq. (2.65) is very similar to the classical collisionless Boltzmann equation. The third term on the left-hand side is the traditional acceleration term for a force that acts against the gradient of a potential. The series on the right-hand side contains quantum corrections, with the size of each successive terms each proportional to $\hbar^s$. These terms are therefore only relevant at very small scales when spacial gradients can become sufficiently large. Fortunately, due to these similarities, moment of this equation can be taken, hopefully leading to the development of accurate moment-closures based approximations.

Chapter 3

First Journal Publication: Application of Approximate Maximum-Entropy Moment Closure to the Wigner Equation

This journal article contains a detailed review of quantum mechanics starting from the familiar Schrödinger formalism and leading up to the Wigner formulation. The advantages of the Wigner formulation for the construction of moment equations are shown along with some preliminary results displaying the advantages and drawbacks of the chosen closure as a quantum-hydrodynamics model. This paper was the first step of the presented Ph.D work, allowing better understanding of the challenges posed by accurately describing systems where quantum effects are important, effectively steering the research topic towards the development of higher moment hyperbolic methods rather than direct application of already existing models. The contribution of the co-author, Fabien Giroux, was the implementation of a Newton search algorithm for the numerical solution of the maximum-entropy distribution function which was used in Section 4. The code had already been implemented and tested in the scope of a previous research project, making it a useful and time-saving tool.

JOURNAL OF COMPUTATIONAL AND THEORETICAL TRANSPORT
2023, VOL. 52, NO. 5, 374–398
https://doi.org/10.1080/23324309.2023.2283469

Taylor & Francis
Taylor & Francis Group

Application of Approximate Maximum-Entropy Moment Closure to the Wigner Equation

William Morin, Fabien Giroux, and James G. McDonald

Department of Mechanical Engineering, University of Ottawa, Ottawa, Canada

ABSTRACT

This paper investigates the potential of moment closures as a possible path to future quantum hydrodynamics models. Moment closures are known to produce accurate predictions of continuum and non-equilibrium classical gas flows while offering modeling and numerical advantages over other commonly used methods. The maximum-entropy hierarchy of moment closures holds the promise of robustly hyperbolic stable moment equations, however, the predicted distribution function in phase space is positive by design, which is in disagreement with the quasi-distribution function described by the Wigner equation. In this paper, predictions made by an interpolative one-dimensional five-moment system are compared to direct numerical solutions of the Wigner equation for a simple low-energy quantum state in unbounded double-well potentials. Numerical solutions for a particle in various potentials described by quartic polynomials are presented. The capacity of moment methods to provide accurate and efficient models for quantum systems is explored.

KEYWORDS

Hyperbolic moment closures; maximum-entropy moment closure; Wigner equation; quantum hydrodynamics

1. Introduction

The aim of this study is to present an initial investigation into a new approach to quantum hydrodynamics based on an approximate maximum-entropy moment closure from the kinetic theory of gases. Research regarding the development of affordable and robust hydrodynamic models for classical non-equilibrium gases has increased in popularity in recent years (Abdelmalik and van Brummelen 2016; Cai, Fan, and Li 2013; Fox and Laurent 2022; Torrilhon 2016). The rapid advancement in the field of microfluidics and nanotechnology is one of the driving factors of this growing interest (Cai et al. 2012; Degond and Ringhofer 2003; Ferry and Grubin 1996; Frommlet, Markowich, and Ringhofer 1999; Gardner 1994). The derivation of reliable and affordable many-particle quantum models is the key to the development of a new generation of efficient technologies.

CONTACT James G. McDonald james.mcdonald@uottawa.ca Department of Mechanical Engineering, University of Ottawa, Ottawa, Ontario, Canada.

Unfortunately, few models successfully predict the time evolution of such quantum systems, especially when subjected to unbounded potentials. Directly solving the Schrödinger equation can be computationally expensive, especially for complicated many-body systems. Numerical solutions of the Wigner equation can be even worse. The high-dimensional nature of this equation makes the accurate resolution of this equation often prohibitively expensive for practical applications. Other continuum models also exist, however, they all suffer from *ad-hoc* modeling assumptions, which greatly limits their reliability. Moment methods present a possible path toward affordable and efficient methods.

Moment-based closures applied to the Wigner equation are not new. Considerable attempts have been made in the past decades toward approximating carrier transport in semiconductors using maximum-entropy closures (Allegretto et al. 2003; Anile and Muscato 1995; Anile and Romano 1999; Anile and Trovato 1997). In these works, due to issues related to integrating the distribution in closed form, polynomial expansions around equilibrium are used. The closures used in these previous works are, therefore, equivalent to Grad-type closures from classical kinetic theory (Grad 1949). Such closures are known to lack robustness due to the flux Jacobian developing complex eigenvalues arbitrarily close to equilibrium for three dimensional situations (Cai, Fan, and Li 2014). Alternatively, this current paper investigates the approximate maximum-entropy closure proposed by McDonald and Torrilhon (2013), which was shown to produce better predictions of highly non-equilibrium situations. The goal of this paper is not to present this maximum-entropy moment closures as a new gold standard in quantum hydrodynamics, but rather to demonstrate the solution fidelity of a classical moment method applied to quantum systems and motivate future development of new methods that are more tailored to problems where quantum effects are significant.

1.1. Scope of the current study

Unbounded potentials are omnipresent in the modeling of many quantum mechanical systems. This specific subset of potentials is especially relevant in simulating quantum tunneling phenomena with applications in many areas of physics, chemistry, and nanotechnology (Chen, Xiong, and Shao 2019; Cordes and Das 2001; Weiner and Tse 1981). Among these potentials, the double-well potential, which consists of two minima separated by a barrier, has been important in studying quantum state transitions as well as the potential energy surface of many hydrogen bonds (Somorjai and Hornig 2004). Though such potentials are used exclusively in the present work, the method can be applied to any potentials, provided that the

potential is described by a differentiable function. A double-well potential was used in this study, as it was found to be suitably numerically challenging while remaining relevant in many physical problems.

The observables related to the time evolution of a given non-relativistic quantum system are usually calculated through the Schrödinger equation. However, in this paper, the Wigner formalism is adopted due to its structural similarity to the Boltzmann equation. Directly solving the Wigner function is often not a trivial task. The presence of a non-local and highly oscillating pseudo-differential operator coupled with an unbounded potential often poses challenges even for well-established solvers (Chen, Xiong, and Shao 2019).

This paper begins with a brief overview of the Wigner formalism followed by a review of the maximum-entropy moment closure hierarchy with emphasis on the five-moment system adapted to this study. Numerical solutions of the Wigner equation for a simple low-energy quantum state in various unbounded double-well potentials are presented and compared with numerical solutions obtained by the five-moment maximum-entropy closure. The probability density, $P(x)$, in position space as well as the expected values for the position and momentum are plotted to investigate the accuracy of this moment method, as well as to demonstrate the major challenges that arise when these moment models are used as the base of a quantum hydrodynamic model.

2. Wigner equation and quantum mechanics in phase space

In this section, the Wigner formalism of quantum mechanics for a one-dimensional system is presented. Various similarities with the Boltzmann equation are also discussed to motivate the use of the maximum-entropy hierarchy of moment closures, which is presented in section 3.

In the standard formulation of quantum mechanics, the probability density, $P(x)$, describing the likelihood of finding a particle at a particular position at a given time, is given by $P(x) = |\psi(x)|^2$, where $\psi(x)$ is the wave function of the system expressed in the position basis. The time evolution of the wave function is given by the Schrödinger equation,

$$i\hbar \frac{\partial \psi(x,t)}{\partial t} = -\frac{\hbar^2}{2m}\frac{\partial^2 \psi(x,t)}{\partial^2 x} + V(x,t)\psi(x,t),$$

where $V(x, t)$ is the potential. Knowing $\psi(x)$, the wave function in momentum space, $\phi(p)$, can be simply computed through a Fourier Transform as,

$$\phi(p) = \frac{1}{\sqrt{\hbar}} \int_{-\infty}^{\infty} \mathrm{d}x \; e^{-ixp/\hbar} \; \psi(x). \tag{1}$$

All integrals in this work are understood to cover the entire space of the relevant independent variable.

The probability density in momentum space is defined as, $P(p) = |\phi(p)|^2$. However, using this formulation, visualizing both probability densities simultaneously is inconvenient. It would be desirable to be able to visualize both distributions at the same time. Using the Wigner function, $W(x,p,t)$, one can visualize these probabilities simultaneously in phase space (Wigner 1932). In general, it is not possible to find a strictly positive probability distribution function in phase space for any arbitrary quantum state. The Wigner function is thus not a probability distribution function, but it is often called a quasi-distribution function due to the fact that it allows for negative regions. More importantly, this quasi-distribution can be conveniently used to study quantum corrections to classical statistical mechanics by linking the wave function to a probability distribution in phase space, which is of interest in this work.

The Wigner function is related to the wave function through the transform,

$$W(x,p,t) = \frac{1}{\pi\hbar}\int \mathrm{d}y \quad \psi^*(x+y)\psi(x-y)e^{2ipy/\hbar}. \tag{2}$$

Obviously, one of the main goals of quantum mechanics is to calculate expectation values associated with physical observables. For the Wigner formalism to be a complete formulation of quantum mechanics, and not just a clever visual tool to better understand quantum states, it must allow for the reliable calculation of these physical quantities. Operators acting on the Wigner function are obtained through the Weyl transform. The Weyl transform, $\tilde{A}(x,p)$ of an operator, $\hat{A}$, is defined as,

$$\tilde{A}(x,p) = \int \mathrm{d}y \ \langle x+y|\hat{A}|x-y\rangle \ e^{-2ipy/\hbar}, \tag{3}$$

where $\hat{A}$ is expressed in position space. The associated expectation value, $\langle A\rangle$, is then given by

$$\langle A\rangle = \int\int \mathrm{d}x\mathrm{d}p \ W(x,p) \ \tilde{A}(x,p). \tag{4}$$

As one can see, the expectation value, $\langle A\rangle$, is simply the weighted average of the Wigner function with the associated operator as the weight. Interestingly, if the Wigner function is integrated over momentum space alone,

$$\int \mathrm{d}p \ W(x,p) = \psi^*(x)\psi(x), \tag{5}$$

one recovers the probability distribution in position space. Similarly, if integrated over x instead, the expression

$$\int \mathrm{d}x \;\; W(x,p) = \phi^*(p)\phi(p), \tag{6}$$

gives the probability distribution in momentum space. The expected values of the position and momentum can be calculated using Equation (3), where the position and momentum operators are taken as $\tilde{A} = x$ or $\tilde{A} = p$, respectively. That is,

$$\langle x \rangle = \int\int \mathrm{d}x\mathrm{d}p \;\; W(x,p) \;\; x, \tag{7}$$

$$\langle p \rangle = \int\int \mathrm{d}x\mathrm{d}p \;\; W(x,p) \;\; p. \tag{8}$$

Many other operators, such as the energy and angular momentum, can be defined in the same way.

The equation that describes the time evolution of the Wigner function can be derived as follows. First, one takes the time derivative of Equation (2),

$$\frac{\partial W}{\partial t} = \frac{\partial}{\partial t}\left(\frac{1}{\hbar\pi}\int dy \quad \psi^*(x+y)\psi(x-y)e^{2ipy/\hbar}\right). \tag{9}$$

After swapping the order of differentiation and integration, it is possible to replace the derivatives of the wave function using the Schrödinger equation,

$$\frac{\partial \psi}{\partial t} = \frac{i\hbar}{2m}\frac{\partial^2 \psi}{\partial x^2} - \frac{i}{\hbar}V(x)\psi. \tag{10}$$

In the resulting expression, a kinetic and a potential term can be identified,

$$\frac{\partial W}{\partial t} = \frac{\partial W_T}{\partial t} + \frac{\partial W_V}{\partial t}. \tag{11}$$

The kinetic term eventually takes the form,

$$\frac{\partial W_T}{\partial t} = -\frac{p}{m}\frac{\partial W}{\partial x}, \tag{12}$$

with m being the particle mass. The potential term can be expanded as a Taylor series, provided that $V(x)$ can be expressed as a power series in x,

$$\frac{\partial W_V}{\partial t} = \sum_{s=0}^{\infty}(-\hbar)^s \frac{1}{(2s+1)!}\left(\frac{1}{2}\right)^{2s} \frac{\partial^{2s+1}V(x)}{\partial x^{2s+1}} \;\; \frac{\partial^{2s+1}W}{\partial p^{2s+1}}. \tag{13}$$

The literature on Wigner functions is extensive, the complete derivation of the previous relations is available in several review articles and book

chapters. For example, a good detailed review of the above derivation is given by Case (2008).

The Wigner formalism finds use in many engineering fields, such as modeling electron transport in quantum electronics, calculating the static and dynamical properties of many-body quantum systems in quantum chemistry, and investigating waves passing through different media in signal processing (Weinbub and Ferry 2018). These many-particle situations are often modeled as a one-particle system in a statistical mixture of N different states. Each state is described by a wave function, $\psi_k = \psi_k(x_i, t)$ and is associated with a probability, $P_k \geq 0$, satisfying $\sum_{k=1}^{k=N} P_k = 1$. In the standard wave-function formulation, the evolution of each state needs to be computed, often leading to a prohibitive computational cost. However, the Wigner formalism allows the derivation of a single equivalent Wigner function,

$$W(x_i, p_i, t) = \frac{1}{(2\pi\hbar)^3} \sum_{k=1}^{N} P_k \int d^3 y_i \ \psi_k^*(x_i + y_i, t)\psi_k(x_i - y_i, t) e^{2ip_i y_i/\hbar}.$$

The advantage of the Wigner formalism for many-body situations then becomes apparent, since the difficulty of solving the equivalent Wigner function does not scale with the number of different states, as it would for a classical wave-function formulation.

2.1. The Wigner equation for quartic double-well potentials

The scope of this paper is the numerical approximation of the Wigner function for low-energy, one-dimensional quantum states in an unbounded double-well potential. The Wigner equation can therefore be simplified by restricting the potential to those described by quartic polynomials.

The quartic potentials studied in this paper all have the form,

$$V(x) = \frac{1}{2}\left(v_2 x^2 + v_3 x^3 + v_4 x^4\right), \tag{14}$$

where the parameters v_2, v_3 and v_4 are specified real numbers. These potentials have a local maximum at $x = 0$ and have two minima when $v2$ is negative and $v4$ is positive. It is important to note that if $v3 = 0$, the potential function is symmetric. The three independent coefficients can be adjusted to fit three characteristic geometrical quantities of the potential denoted V_{max}, V^*, and g, as illustrated in Figure 1. Five specific potentials, chosen for the current study, have been adopted from Chen, Xiong, and Shao (2019) and Somorjai and Hornig (2004).

Since this paper is restricted to only quartic potentials, it is possible to evaluate the Taylor expansion shown in Equation (13) as,

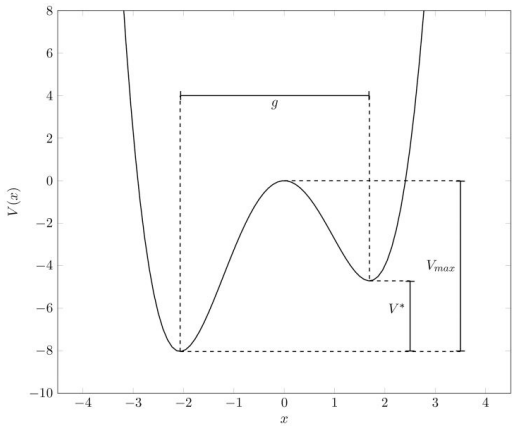

	V_1	V_2	V_3	V_4	V_5
v_2	-1.24	-0.4	-1.6	-5.26	-1.24
v_3	0.0	0.0	0.0	0.0	0.04
v_4	0.02	0.05	0.2	0.6575	0.022
V_{max}	1.24	0.4	1.6	5.26	12.39
V^*	0.0	0.0	0.0	0.0	6.13
g	11.13	4.0	4.0	4.0	10.7

Figure 1. Illustration of a generic quartic, double-well potential, and the coefficients from five quartic double-well potentials used in this work.

$$\frac{\partial W_V}{\partial t} = \frac{dV(x)}{dx}\frac{\partial W}{\partial p} - \frac{\hbar^2}{24}\frac{d^3V(x)}{dx^3}\frac{\partial^3 W}{\partial p^3}, \tag{15}$$

where all higher-order terms of the Taylor series are zero. The final form of the time-dependent Wigner equation for quartic potentials, as used in this work, is

$$\frac{\partial W}{\partial t} + \frac{p}{m}\frac{\partial W}{\partial x} - \frac{dV(x)}{dx}\frac{\partial W}{\partial p} = -\frac{\hbar^2}{24}\frac{d^3V(x)}{dx^3}\frac{\partial^3 W}{\partial p^3}. \tag{16}$$

One can observe that Equation (16), is very similar to the classical Liouville (or collisionless Boltzmann) equation. The third term on the left-hand side is the traditional acceleration term for a force that acts against the gradient of a potential. The term on the right-hand side is a quantum correction with size proportional to $\hbar^2$. It will therefore only be relevant at very small scales when $\frac{d^3V(x)}{dx^3}$ can be large. For general non-quartic potentials, other higher-order corrections will exist, but they will be proportional to even higher powers of $\hbar$. The similarity of the Wigner equation to the Boltzmann equation gives hope that moment models, which have proven accurate for classical gases, can also be effectively applied to quantum systems described by the Wigner equation.

3. Moment-closure and the five-moment model of the maximum-entropy hierarchy

The method of moment-closure descends from the traditional kinetic theory of gases, in which a probability distribution function is used to statistically described a gas. Instead of tracking every gas particle individually, kinetic theory suggests a distribution function, $\mathcal{F}(x, v, t)$, describing the phase-space density of particles. In contrast with the Wigner function, $\mathcal{F}$,

traditionally uses the velocity as an independent variable in place of the momentum. These variables are obviously related through $p = mv$. In most cases, only some macroscopic properties are of interest, and not all the information contained in the distribution function is necessary. It is possible to obtain these macroscopic properties by multiplying the distribution function by a monomial velocity weight and integrating over all velocity space. This process is commonly known as taking moments of the distribution function. For a one-dimensional treatment, the following are examples of moments of the distribution function yielding macroscopic properties of classical interest:

$$\begin{aligned} \rho &= \int m\mathcal{F}\,\mathrm{d}v = \langle m\mathcal{F}\rangle_v, \\ \rho u &= \langle mv\mathcal{F}\rangle_v, \\ \rho\theta &= \langle mc^2\mathcal{F}\rangle_v, \\ q &= \langle mc^3\mathcal{F}\rangle_v, \\ r &= \langle mc^4\mathcal{F}\rangle_v, \\ s &= \langle mc^5\mathcal{F}\rangle_v. \end{aligned}$$

The notation, $\langle\cdot\rangle_v$, is used to denote the integral over velocity space. This should not to be confused with $\langle x\rangle$ and $\langle p\rangle$, which are the expectation values of the position and momentum, respectively.

For a classical gas, the bulk velocity is given by u, while c represents the deviatoric velocity, which is defined as $c = v - u$. The variables ρ and θ are the mass density and the temperature. The variable q is double the heat flux. The moments denoted by r and s are higher-order moments for which there is currently no familiar physical interpretation. For a quantum system, ρ, is analogous to the probability density, $P(x)$, while ρu give the density current, which is often denoted as j. In this framework, the variable θ refers to the second-order moment of the distribution and is associated with the energy. It is not related to the random motion of many particles (or the temperature), as it would be for a classical gas. All higher-order moments give statistical information regarding the system state, even when their interpretation is not familiar.

For a classical gas, the time evolution of the distribution function is described by the Boltzmann equation,

$$\frac{\partial\mathcal{F}}{\partial t} + v\frac{\partial\mathcal{F}}{\partial x} + \frac{\partial\ (a\mathcal{F})}{\partial v} = \frac{\delta\mathcal{F}}{\delta t}\,. \tag{17}$$

The second term of Equation (17) represents the convective contribution to the time evolution, while the third term describes the accelerating effects on the particles due to external fields. The right-hand side of the equation represents the effects of inter-particle collisions on the distribution function. For the present work, collisions are neglected.

While it is possible to numerically solve the Boltzmann equation, it is high dimensional. This translates into a large computation cost. Fortunately, the number of dimensions can be reduced, since only some macroscopic properties are typically of interest. It is possible to take velocity moments of the Boltzmann equation to obtain a set of equations describing these properties of interest,

$$\frac{\partial}{\partial t}\langle \mathcal{W}\mathcal{F}\rangle_v + \frac{\partial}{\partial x}\langle v\mathcal{W}\mathcal{F}\rangle_v + \frac{\partial}{\partial v}\left\langle a\mathcal{W}\frac{\partial \mathcal{F}}{\partial v}\right\rangle_v = 0, \tag{18}$$

where $\mathcal{W}$ is a vector containing velocity weights corresponding to the moments of interest. The same approach can be used to obtain evolution laws for statistical information regarding a quantum system. Similarly, one can take moments of the Wigner equation, Equation (16),

$$\frac{\partial}{\partial t}\langle \mathcal{W}W\rangle_p + \frac{\partial}{\partial x}\langle v\mathcal{W}W\rangle_p + \frac{\partial}{\partial v}\left\langle -\frac{1}{m}\frac{dV(x)}{dx}\mathcal{W}\frac{\partial W}{\partial v}\right\rangle_p = \left\langle \frac{1}{m^3}\frac{\hbar^2}{24}\frac{d^3V(x)}{dx^3}\mathcal{W}\frac{\partial^3 W}{\partial v^3}\right\rangle_p. \tag{19}$$

Here, the moments, $\langle\cdot\rangle_p$, are taken in momentum space. Also, in this description, the vector $\mathcal{W}$, contains momentum weights. Unfortunately, this method does not lead to a closed set of equations. This is because the time evolution of a given moment always depends on the spacial divergence of a moment that is one order higher in velocity (or momentum).

One method to close the system of equations is to assume a form for $\mathcal{F}$ or W. The assumed distribution function should contain the same number of free parameters as there are moments of interest. The free parameters are chosen to be in agreement with the macroscopic properties (moments) of interest. It then becomes possible to express the closing moment as a function of the known moments by integrating the now-known distribution function. The system of equation is then closed.

A promising technique is to select the distribution function that maximizes the classical entropy while still being in agreement with the known moments (Dreyer 1987; Levermore 1996; Müller and Ruggeri 1993). For a monatomic perfect gas, the classical entropy density is expressed as $\langle -\mathcal{F}\ln\mathcal{F}\rangle_v$. Maximizing this quantity subject to the moment constraints leads to the assumed form of the distribution function being

$$\mathcal{F}_{\text{M.E.}} = e^{\boldsymbol{\alpha}^T\mathcal{W}}, \tag{20}$$

where $\boldsymbol{\alpha}$ is a vector of free parameters and $\mathcal{W}$ is the vector of weights related to the moments of interest. Although the current work is concerned with quantum systems, the entropy for a classical monatomic perfect gas is

used as a first step. The distribution function of the form shown in Equation (20) ensures positive number density over the entire velocity domain, which is far from ideal since the Wigner function allows for negative regions in the distribution. Systems of partial differential equations (PDEs) resulting from this closure are also guaranteed to be hyperbolic whenever a function of the form given in Equation (20) exists that is consistent with the known moments.

The first member of the maximum-entropy hierarchy for one-dimensional physics is the three-moment model. This model is associated with a distribution function that is the exponential of a second-order polynomial, which leads to the compressible Euler equations. This distribution function is often referred to as the Maxwell-Boltzmann distribution or Maxwellian. The next member of this hierarchy is the five-moment model. Its associated distribution function is an exponential of a fourth-order polynomial. This allows for some skewness, or asymmetry, in the distribution function. For classical gases, such skewness is related to heat transfer. Unfortunately, because of the fourth-order nature of the polynomial, it is impossible to integrate the distribution function analytically in closed form. A closed-form expression for the closing fluxes is therefore unattainable. If one wishes to use the true five-moment maximum-entropy closure, an expensive and ill-conditioned procedure must be used whenever a flux is required. Fortunately, for the case of the five-moment closure, a robust and hyperbolic approximation has been proposed by McDonald and Torrilhon (2013).

The PDEs describing the time evolution of the five-moment state applied to the specified quantum system are

$$\frac{\partial}{\partial t}[\rho] + \frac{\partial}{\partial x}[\rho u] = 0, \tag{21}$$

$$\frac{\partial}{\partial t}[\rho u] + \frac{\partial}{\partial x}\left[\rho u^2 + \rho\theta\right] = -\rho\frac{dV(x)}{dx}, \tag{22}$$

$$\frac{\partial}{\partial t}\left[\rho u^2 + \rho\theta\right] + \frac{\partial}{\partial x}\left[\rho u^3 + 3\rho u\theta + q\right] = -2\rho u\frac{dV(x)}{dx}, \tag{23}$$

$$\begin{aligned}\frac{\partial}{\partial t}\left[\rho u^3 + 3\rho u\theta + q\right] + \frac{\partial}{\partial x}\left[\rho u^4 + 6\rho u^2\theta + 4uq + r\right] \\ = -3(\rho u^2 + \rho\theta)\frac{dV(x)}{dx} + 6\rho\left(\frac{-\hbar^2}{24}\right)\frac{d^3V(x)}{dx^3},\end{aligned} \tag{24}$$

$$\begin{aligned}\frac{\partial}{\partial t}\left[\rho u^4 + 6\rho u^2\theta + 4uq + r\right] + \frac{\partial}{\partial x}\left[\rho u^5 + 10\rho u^3\theta + 10u^2q + 5ur + s\right] \\ = -4(\rho u^3 + 3\rho u\theta + q)\frac{dV(x)}{dx} + 24\rho u\left(\frac{-\hbar^2}{24}\right)\frac{d^3V(x)}{dx^3}.\end{aligned} \tag{25}$$

In this presentation, the classical acceleration term and quantum correction are on the right-hand side.

Because of the fourth-order polynomial in the exponential describing the distribution function, the closing flux, the variable s shown in red in Equation (25), needs to be approximated. Due to the requirement for Galilean invariance, this flux can only be a function of ρ, θ, q, and r. By non-dimensionalizing the moments as

$$\rho_\star = 1, \quad \theta_\star = 1, \quad q_\star = \frac{1}{\rho}\left(\frac{1}{\theta}\right)^{3/2} q, \quad r_\star = \frac{1}{\rho}\left(\frac{1}{\theta}\right)^{2} r, \quad s_\star = \frac{1}{\rho}\left(\frac{1}{\theta}\right)^{5/2} s, \tag{26}$$

the non-dimensional $s_\star$ becomes a function of only $q_\star$ and $r_\star$.

The set of physically realizable moment states that can be reached by a positive distribution function is illustrated in Figure 2, where the boundary of physical realizability is obtained by solving the Hamburger moment problem (Hamburger 1944). Only states for which $r_\star > q_\star^2 + 1$ are attainable by a positive distribution (and all these states are possible). Unfortunately, Junk has shown that the region of physical realizability contains a half line that cannot be reached by maximum-entropy distribution functions of the form given in Equation (20) (Junk 1998). In other words, if the third-order moment is zero, a maximum-entropy distribution function cannot have a non-dimensional fourth moment that is higher than it is for an equilibrium Maxwellian. As this line is approached, closing fluxes become singular.

As stated, a closed-form expression for $s_\star$ is unavailable. an approximation is used instead. To ease the development of this approximation for the closing flux, a parabolic mapping parameter is defined,

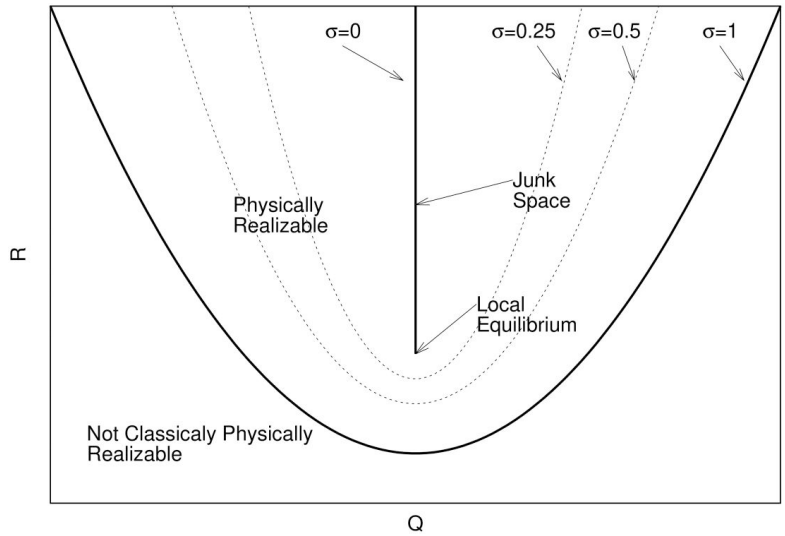

Figure 2. States attainable by positive distributions.

$$\sigma = \frac{3 - r_* + \sqrt{(3 - r_*)^2 + 8q_*^2}}{4}. \tag{27}$$

This parameter maps moment space from the Junk region to the realizability boundary as it varies between 0 and 1. Using the mapping parameter, σ, a non-dimensional approximation is proposed for the closing flux, $s_\star$,

$$s_\star = \frac{q_\star^3}{\sigma^2} + (10 - 8\sigma^{1/2})q_\star. \tag{28}$$

This approximation provides a closed hyperbolic system of five PDEs predicting the time evolution of the system that is a good approximation for the true maximum-entropy closure.

4. Numerical results

To investigate the ability of the moment model to describe simple quantum states, a numerical investigation of the time evolution of a low-energy Gaussian wave packet subjected to different double-well potential geometries is shown. The initial conditions are all of the form

$$W_0(x, p, 0) = \frac{1}{\pi}\exp\left((x - x_0)^2 + p^2\right). \tag{29}$$

All potentials described in Figure 1 are used. Comparisons are made between the five-moment approximations and the direct numerical solution of the Wigner equation. It is important to note that, for all calculations, $\hbar$ and m have been set to unity.

A first-order Gudunov-type finite-volume scheme with HLL flux function is used for the numerical solution of the moment equations. The wave speeds are numerically computed as the eigenvalues of the analytic flux Jacobian. A first-order accurate explicit time marching scheme is used to treat the hyperbolic left-hand side while the right-hand side is treated implicitly. Position space is discretized into 1000 cells for all calculations.

For comparison, the numerical solutions of the Wigner equation are obtained by directly discretizing position and momentum spaces. First-order upwind fluxes are used for the first-order space and momentum-space derivatives on the left-hand side of Equation (16). A second-order centered finite-difference rule is used to approximate the third-order momentum derivative on the right-hand side. First-order fully implicit time marching is used with the generalized minimal residual method (GMRES) used to solve the resulting linear system. All cases are run using a grid of 1000×1000 cells in phase space.

For the first part of this investigation, $P(x) = \rho$, the zeroth order moment, is plotted against the probability density obtained by Wigner for different non-dimensional times. In Figure 3, the wave-packet is initially located at the center of the V_1 double-well potential, $x_0 = 0$. Even if the five-moment system cannot recover all the oscillations displayed by the Wigner distribution, a good agreement is observed throughout the calculation. The general shape of the position-space probability is remarkably well recovered using only five moments.

Figures 4–6 show the time evolution of $P(x)$ for increasingly steep symmetric double-well potentials. In all three calculations, the initial Gaussian bump was positioned one non-dimensional length unit to the left of the first well center. This initial condition was chosen to give a positive initial acceleration to the Gaussian wave-packet, thus allowing $P(x)$, to extend to the adjacent well, consequently producing more complex structures. One can observe good agreement with the Wigner results for the V_2 and V_3 quartic potentials. However, even if good predictions are achieved at early times, the greater steepness of the V_4 potential was found to be harder for the five-moment system to model accurately.

Figure 7 shows the behavior of the moment system when subjected to the V_5 asymmetric potential. The initial wave-packet is again initially place at $x_0 = 0.0$. Again, one can observe good initial agreement with the exact solution. However, the accuracy of the solution obtained by the moment system deteriorates over time. Finally, in Figure 8 the initial Gaussian bump is located one non-dimensional unit to the right of the first well center, to give a negative initial acceleration. Again, good agreement was noted at early times, but deviations are eventually observed between the moment solution and the direct solution of the Wigner equation.

As observed, the accuracy of the five-moment model varies over time. This seems to be mostly due to the fact that the maximum-entropy distribution does not allow negative density regions. However, it could also be attributed to the fact that the number of moments in this closure is too low to capture all the structure displayed by the Wigner function. To further investigate these results, a side-by-side comparison of the Wigner quasi-probability distribution and the distribution predicted by the five-moment system is presented. The maximum-entropy distribution functions, $\mathcal{F}$, are obtained by numerically solving the maximum entropy problem, from the known moments, $\boldsymbol{U}$, provided by the Wigner solver using a Newton search algorithm following a procedure introduced by Levermore (1996). Figures 9–12 show the distribution functions of the case presented in Figure 7 (V_5 potential with $x_0 = 0.0$) at four different times, $t = 1$, $t = 4$, $t = 7$, and $t = 10$. As expected, at time $t = 1$, both distributions are almost identical. As shown in Figure 10, as soon as a significant negative region of

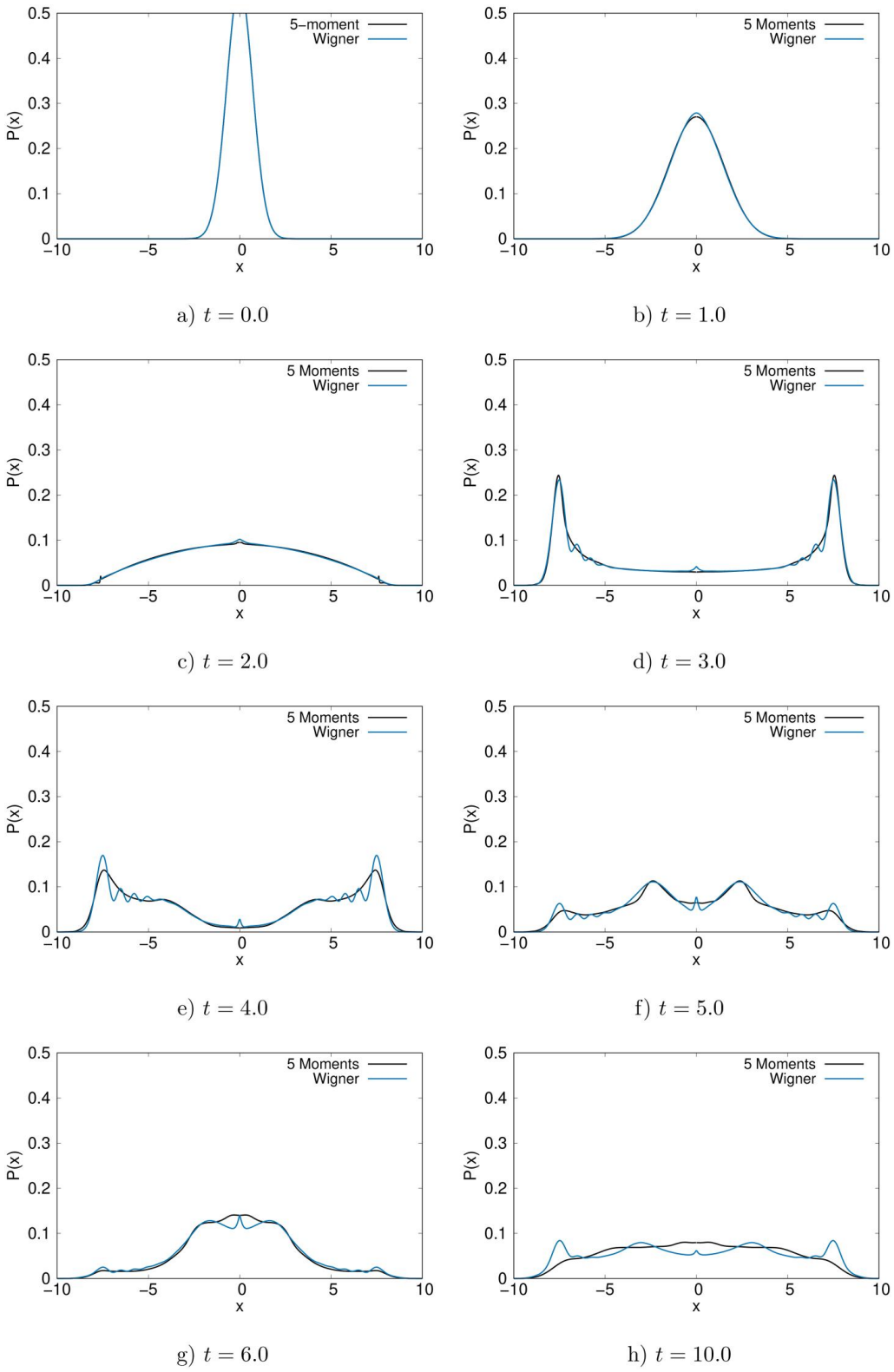

Figure 3. Time evolution of $P(x)$ for a Gaussian wave-packet initially centered at $x = 0.0$ with potential V_1.

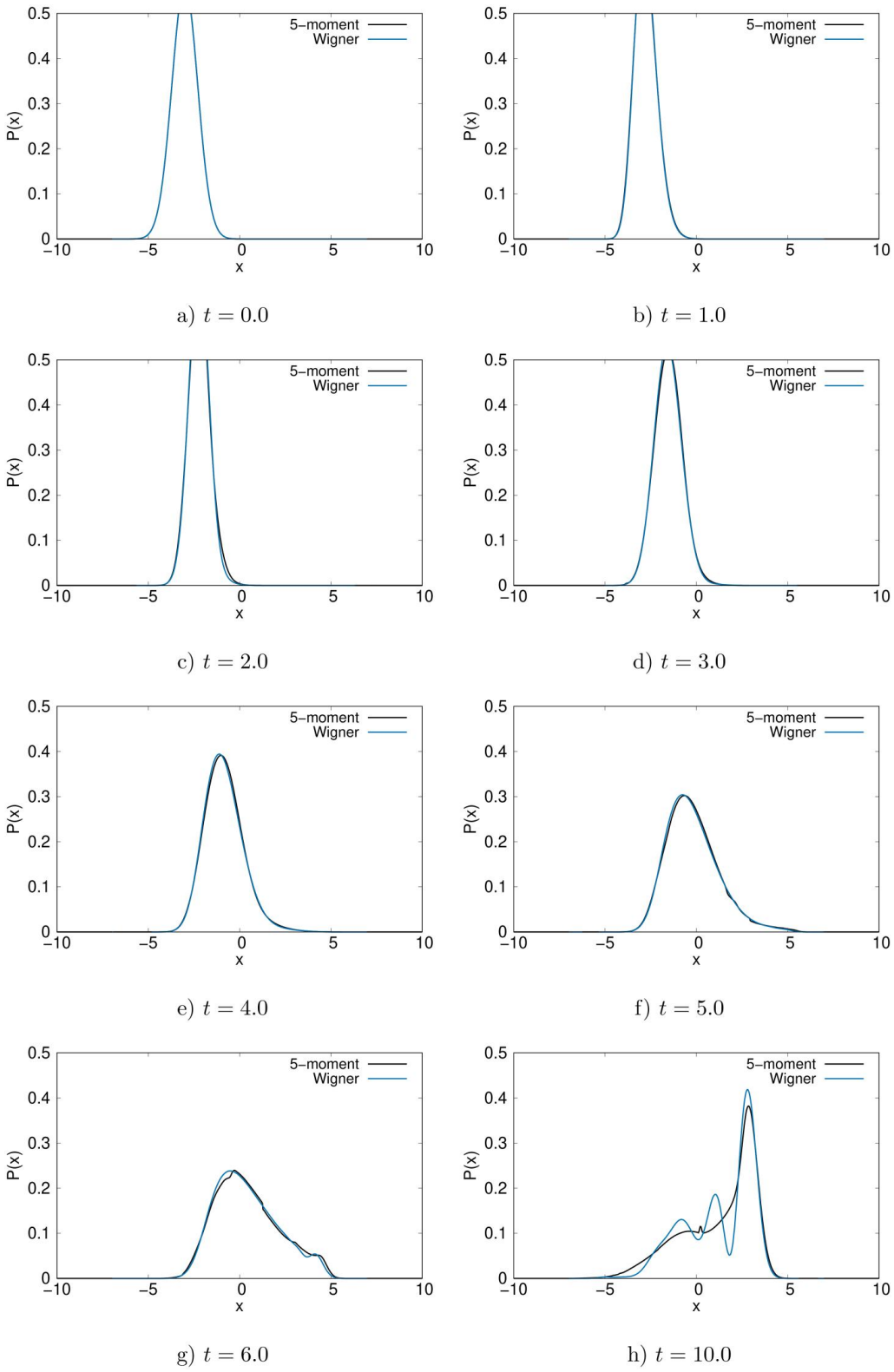

Figure 4. Time evolution of $P(x)$ for a Gaussian wave-packet initially located at $x = -3.0$ (one unit of the left of the first well) with potential V_2.

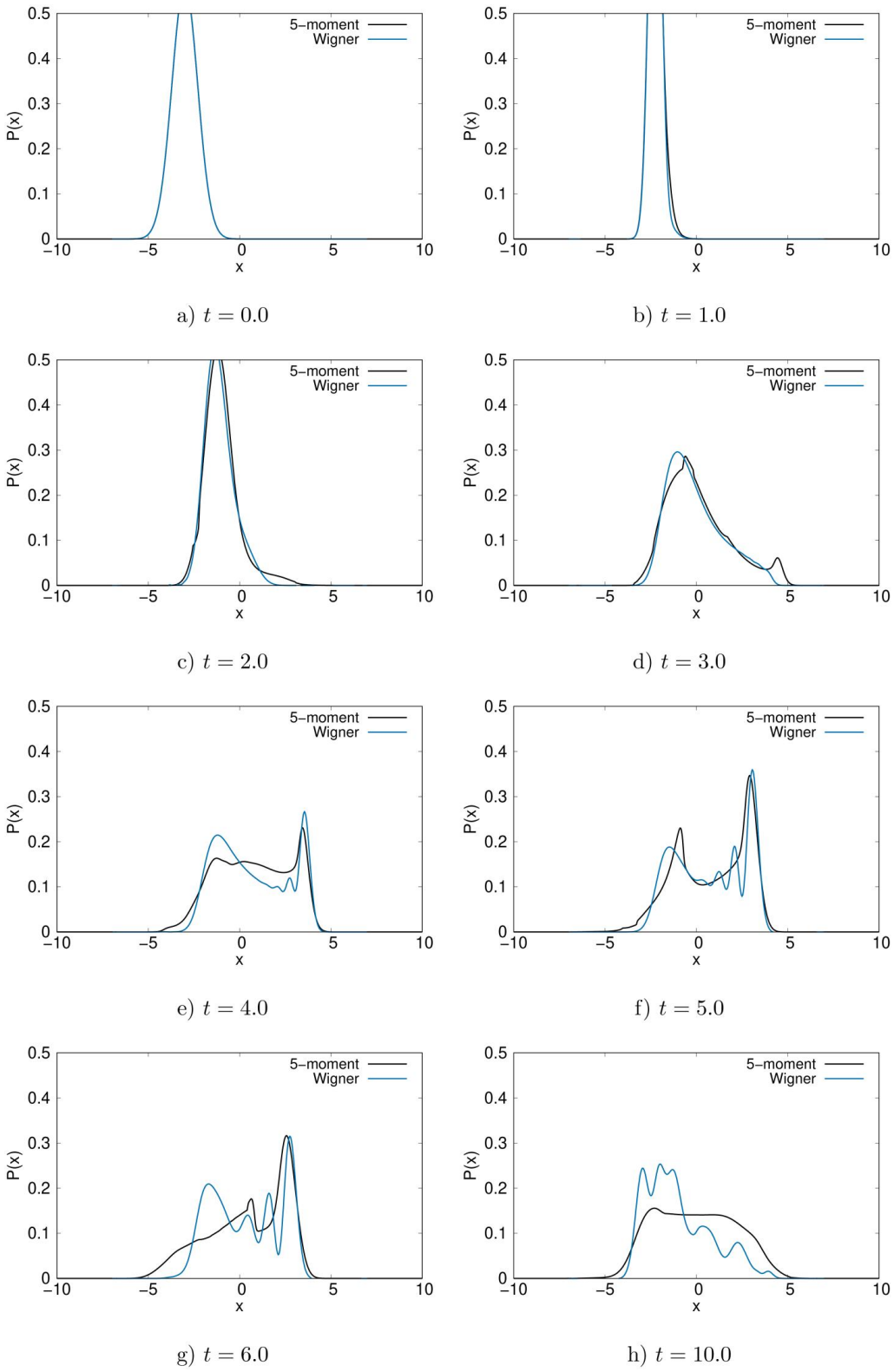

Figure 5. Time evolution of $P(x)$ for a Gaussian wave-packet initially located at $x = -3.0$ (one unit of the left of the first well) with potential V_3.

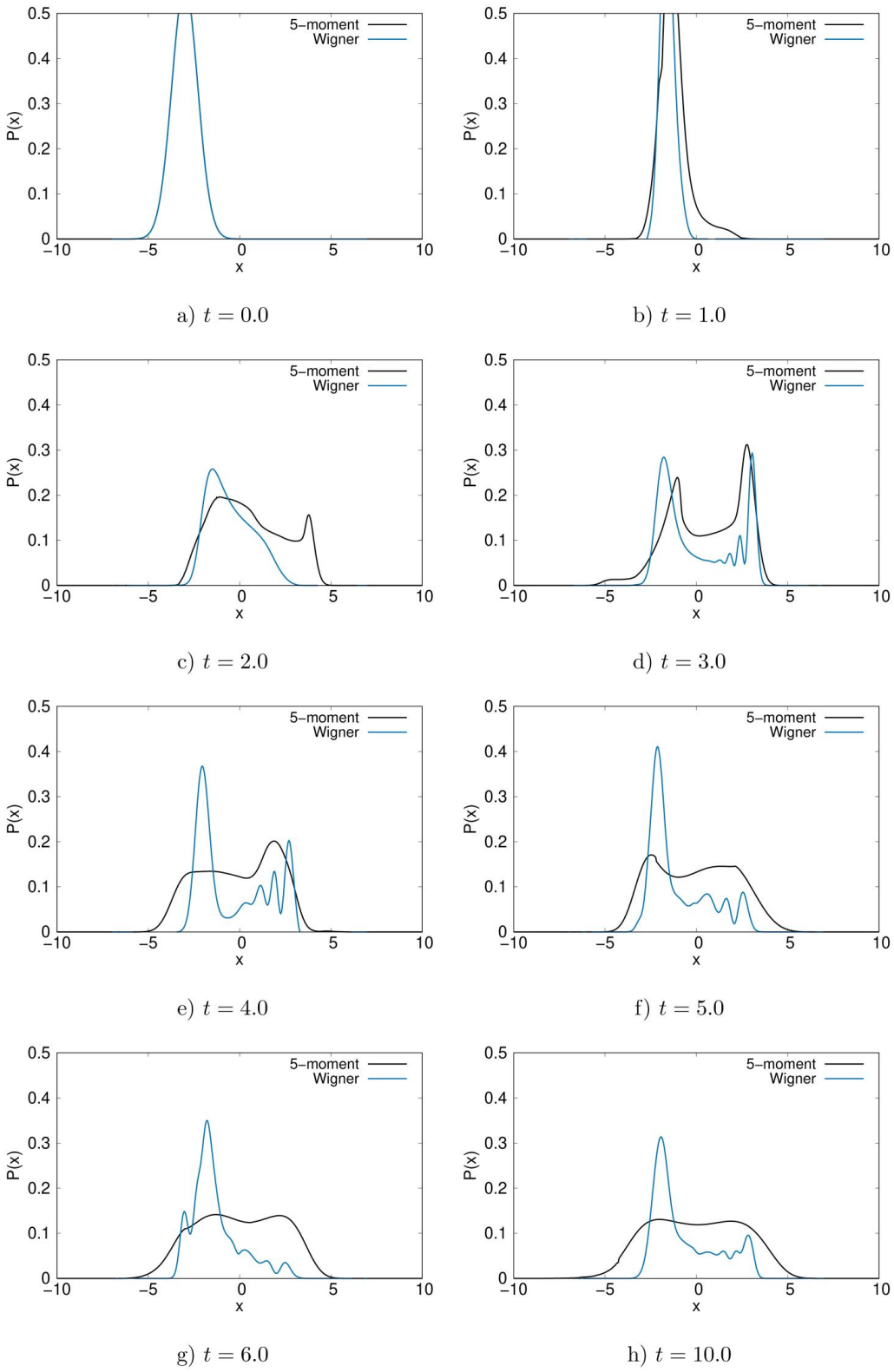

Figure 6. Time evolution of $P(x)$ for a Gaussian wave-packet initially located at $x = -3.0$ (one unit of the left of the first well) with potential V_4.

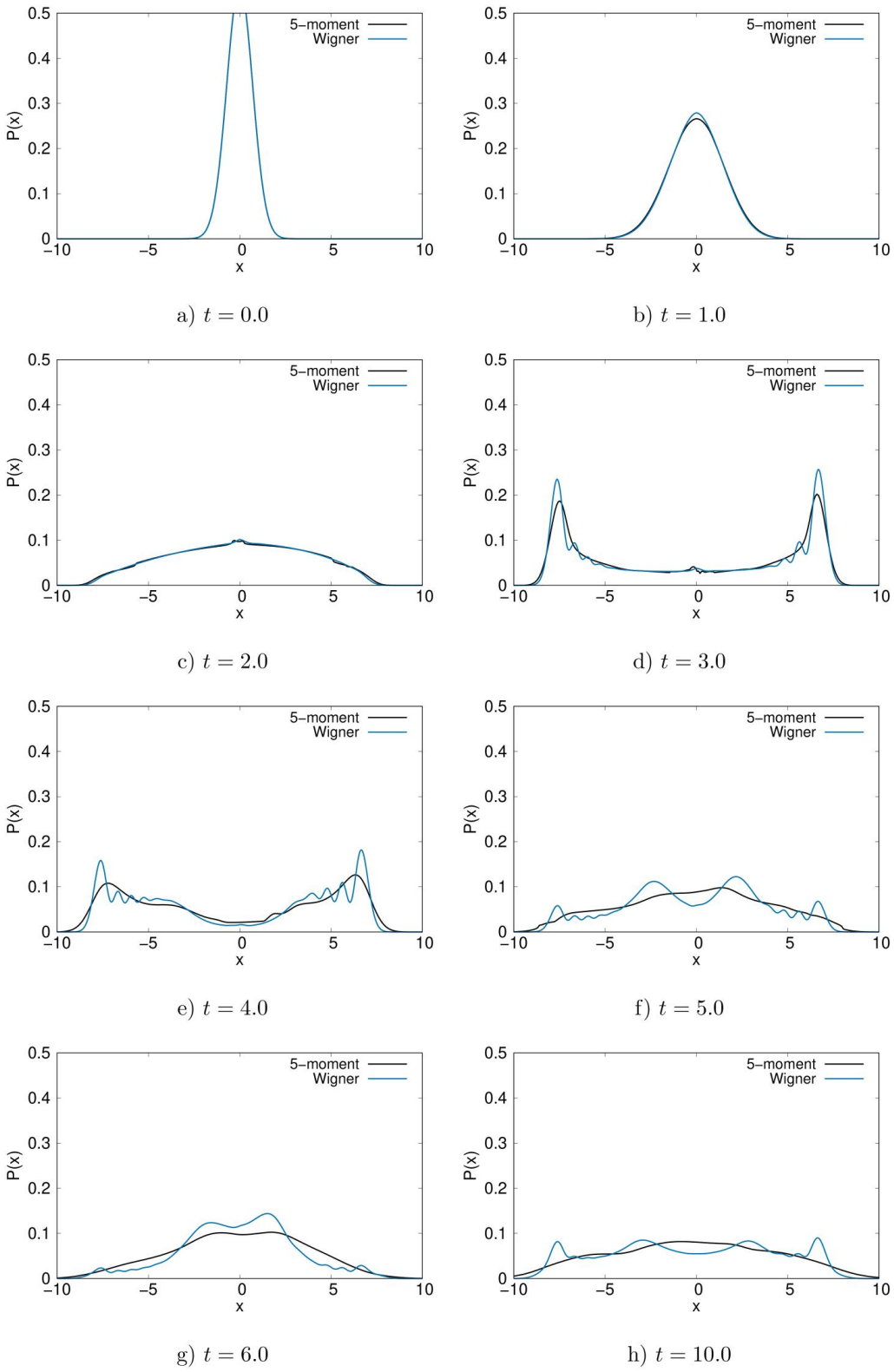

Figure 7. Time evolution of $P(x)$ for a Gaussian wave-packet initially centered at $x = 0.0$ with potential V_5.

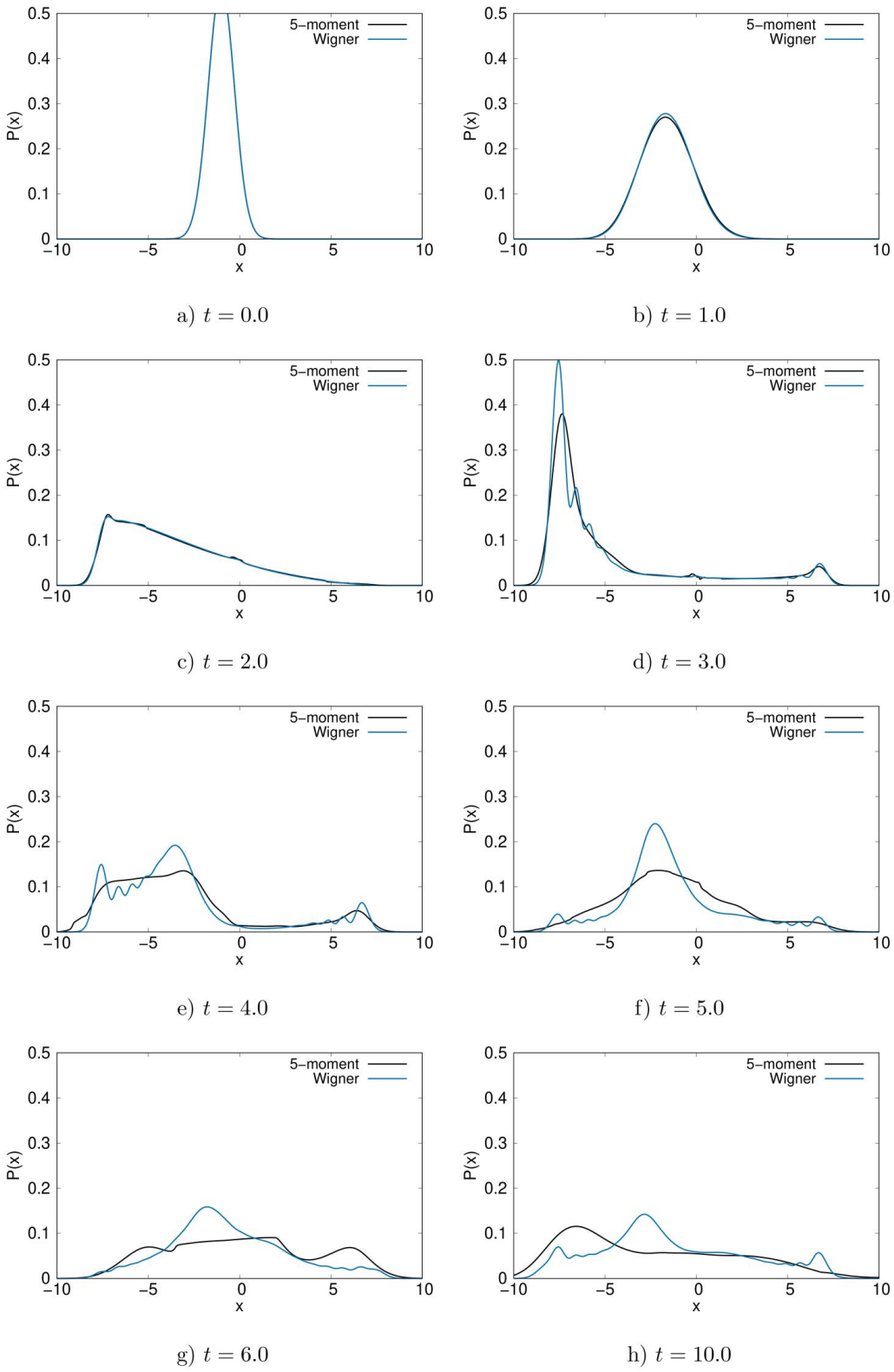

Figure 8. Time evolution of $P(x)$ for a Gaussian wave-packet initially located at $x = -3.67$ (one unit of the right of the first well) with potential V_5.

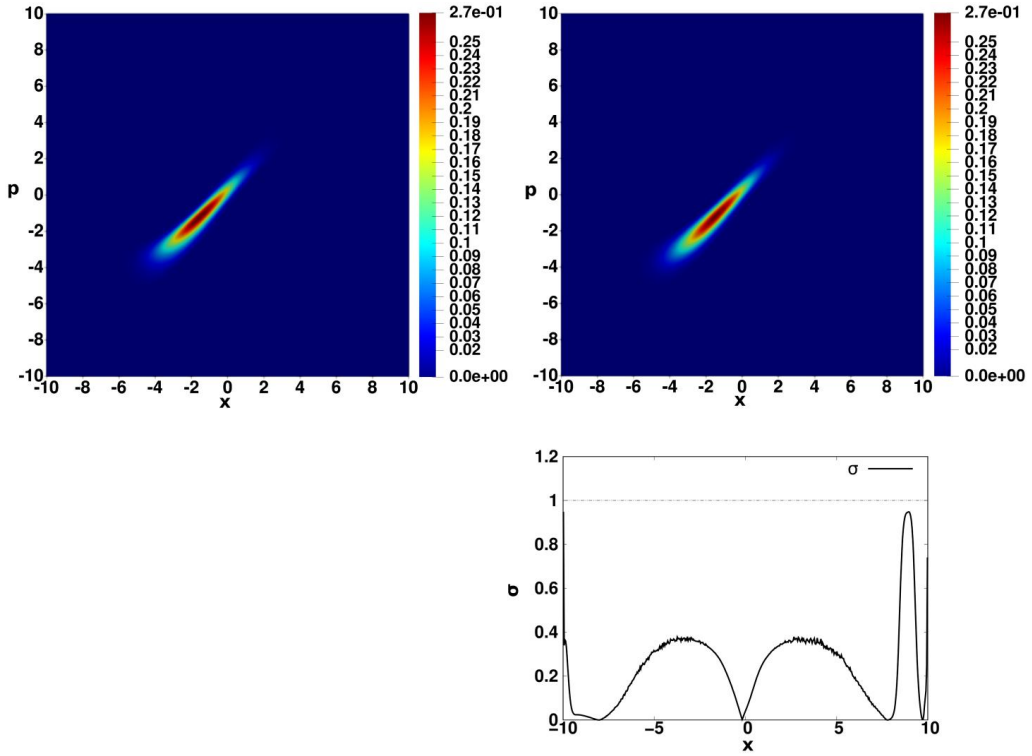

Figure 9. Wigner distribution in phase space (on the right), five-moments distribution in phase space (on the left) with associated x-σ plot at a non-dimensional time $t = 1.0$.

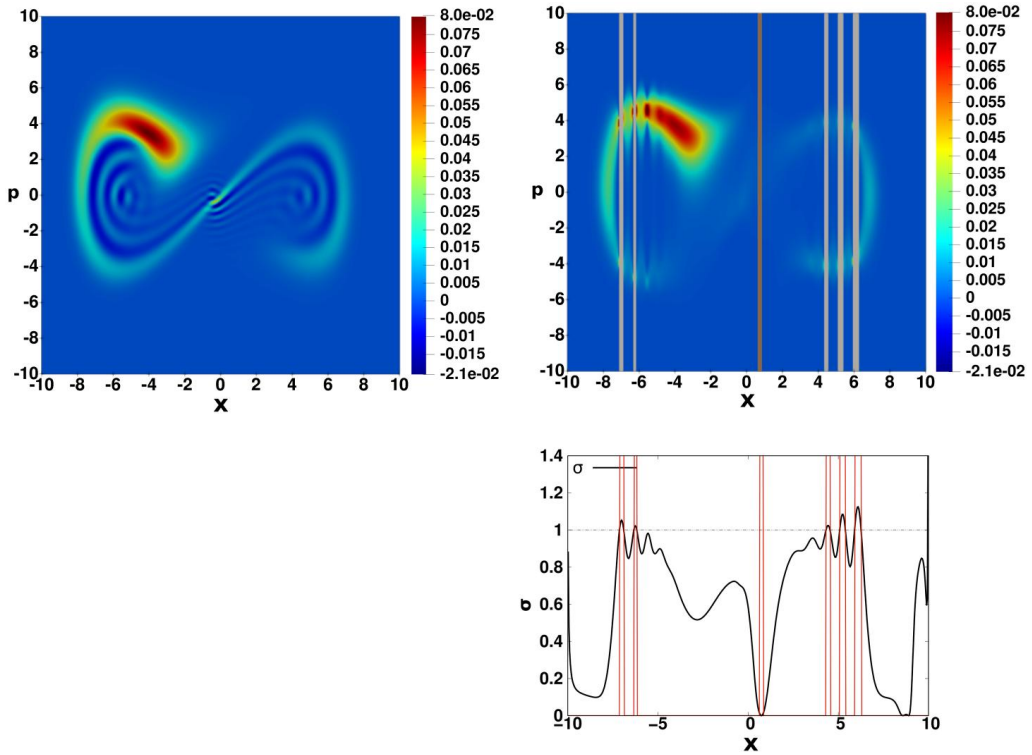

Figure 10. Wigner distribution in phase space (on the right), five-moments distribution in phase space (on the left) with associated x-σ plot at a non-dimensional time $t = 4.0$.

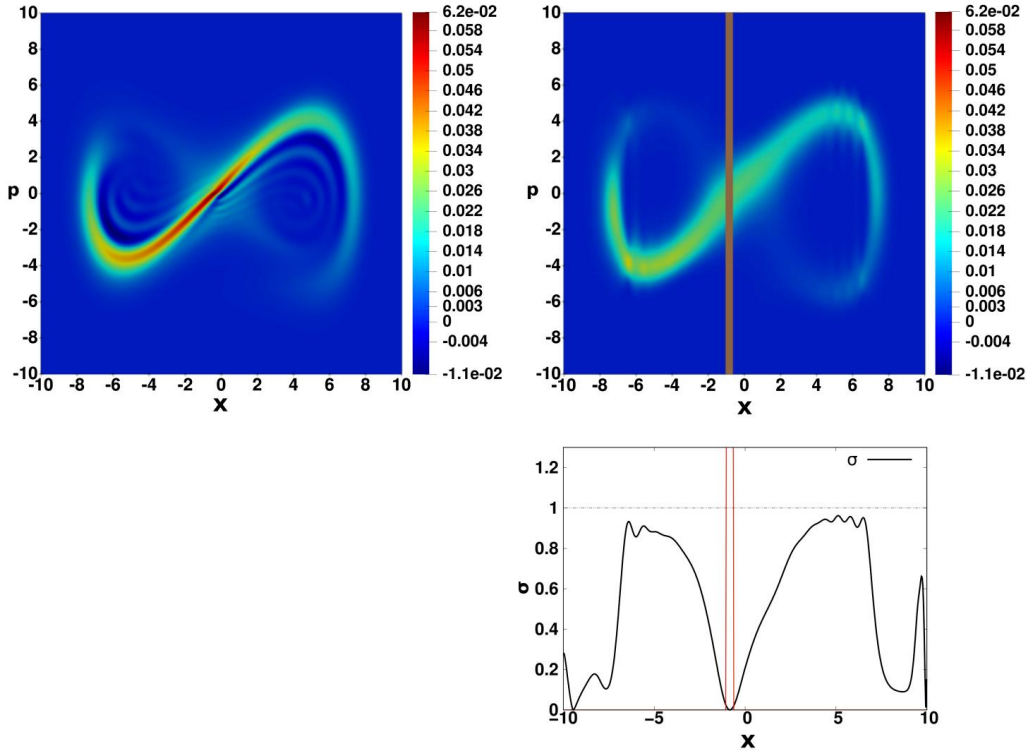

Figure 11. Wigner distribution in phase space (on the right), five-moments distribution in phase space (on the left) with associated x-σ plot at a non-dimensional time $t = 7.0$.

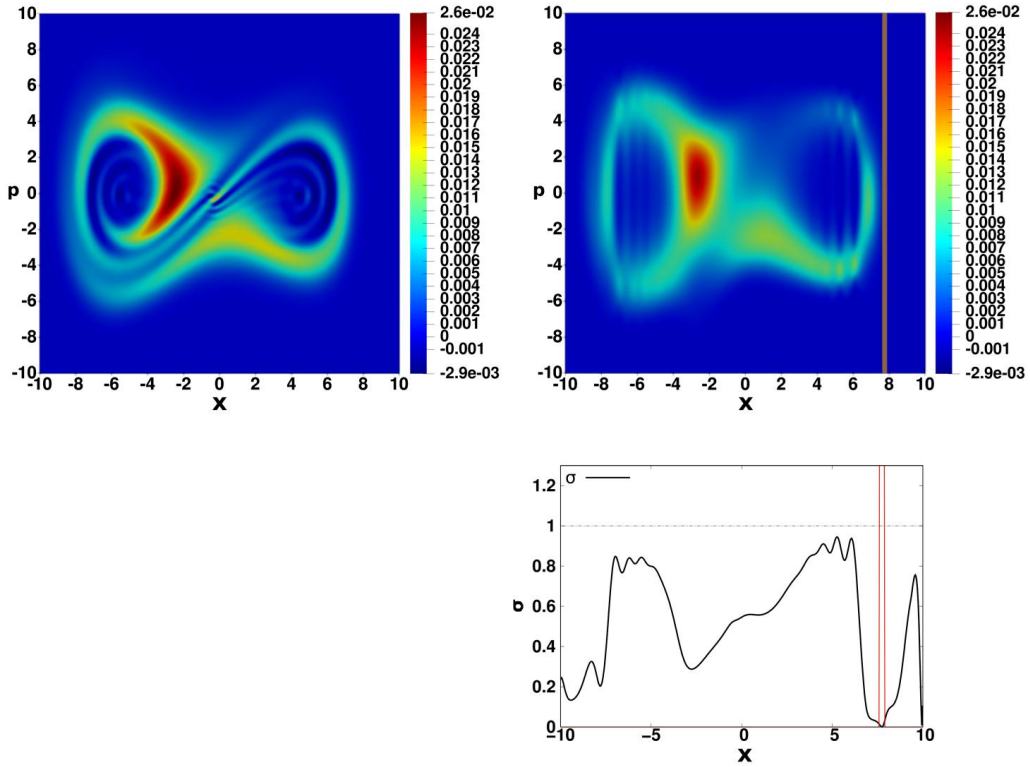

Figure 12. Wigner distribution in phase space (on the right), five-moments distribution in phase space (on the left) with associated x-σ plot at a non-dimensional time $t = 10.0$.

the Wigner function is observed, the prediction obtained from the five-moment model starts to diverge from the expected solution. The grey boxes in the five-moment distribution represent regions where σ is above one, thus the state leaves the region of classical realizability. One can see that the regions coincide with negativity begin present in the Wigner distribution. The brown boxes, on the other hand, are associated with regions where σ goes to zero, thus approaching the Junk half line. In all these regions, the distribution function cannot be computed due to ill-conditioning caused by the singularity. Figures 11 and 12 show both distributions for $t = 7$ and $t = 10$, respectively. Although the distributions obtained using the five-moment model recover the general shape given by the Wigner function, one can clearly see that the sharpness of the solutions deteriorates, especially around regions where negative density is predicted by the Wigner distribution. The rigidity of the five-moment model comes from the choice of closure that aims to maximize the entropy of a classical gas which is seemingly not optimally suited to quantum systems.

As a final demonstration, Figure 13 shows the expectation values for the position, $\langle x \rangle$, and momentum, $\langle p \rangle$, predicted by the five-moment model for four different cases, as compared to the prediction from the direct solution of the Wigner equation. The above cases with V_2, V_3, V_4, and V_5 potentials are illustrated. All calculations have been run to a final non-dimensional time of $t = 30$. One can observe that the five-moment solution has more oscillations and converges faster to a steady state than the direct solution. However, in all cases, both calculations approach the same steady-state value.

5. Conclusion

This work demonstrates that a closed-form moment closure offers promising alternatives to typical Wigner solvers. In this work, an approximation to the second one-dimensional member of the maximum-entropy moment closure hierarchy has been used to compute the time evolution of a one-dimensional low-energy quantum wave-packet in various unbounded double-well potentials. By comparing the probability density, the expected values for both the position and momentum, and the quasi-probability distributions, the general accuracy of this moment method as well as the major challenges that it poses as a quantum hydrodynamic model are assessed.

The inability of distribution functions from classical maximum-entropy closures to admit negative regions seems to limit their immediate applicability to a Wigner-equation treatment of quantum mechanics. It was shown that deviations between moment- and Wigner-based predictions become larger when

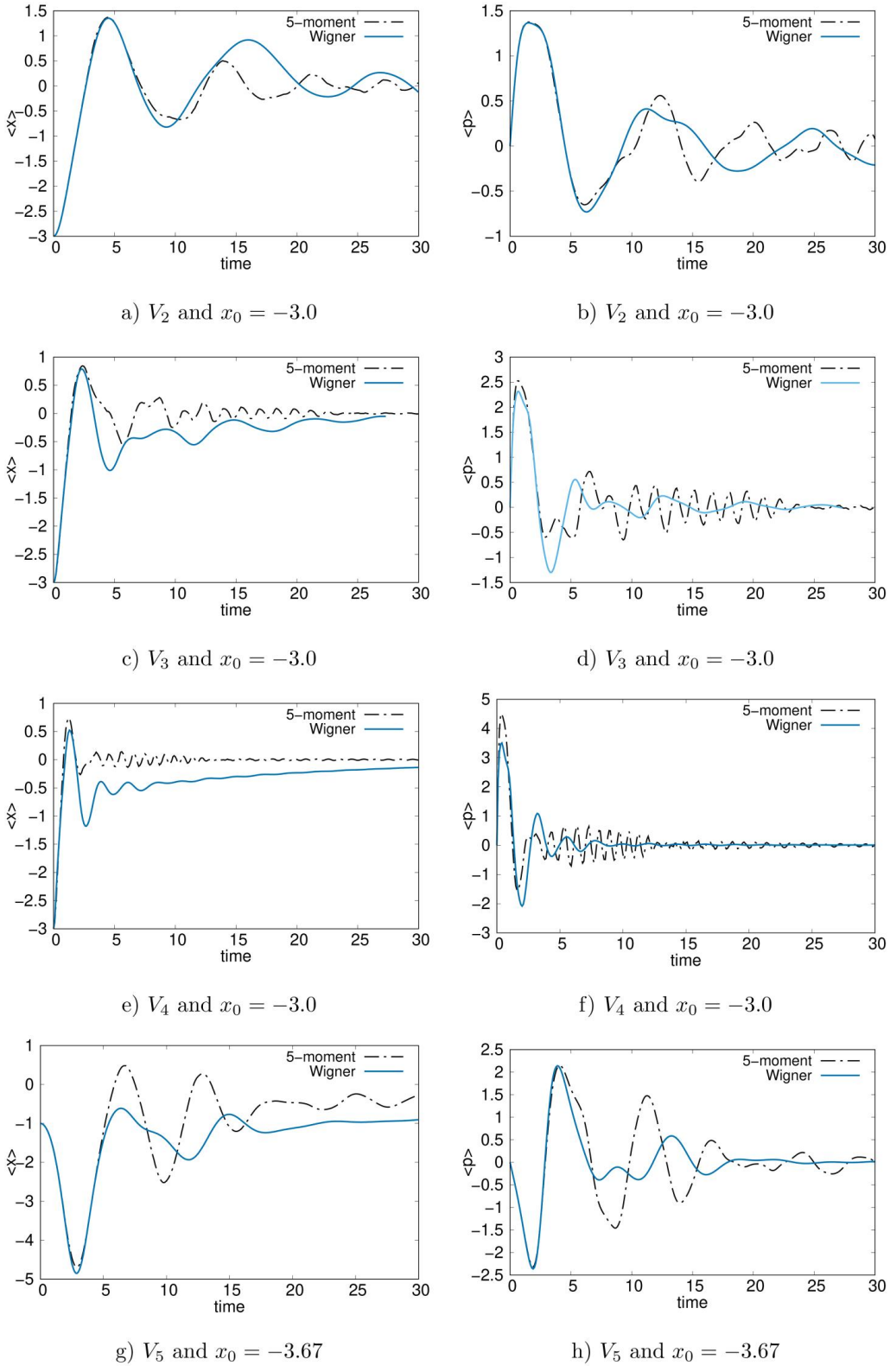

a) V_2 and $x_0 = -3.0$

b) V_2 and $x_0 = -3.0$

c) V_3 and $x_0 = -3.0$

d) V_3 and $x_0 = -3.0$

e) V_4 and $x_0 = -3.0$

f) V_4 and $x_0 = -3.0$

g) V_5 and $x_0 = -3.67$

h) V_5 and $x_0 = -3.67$

Figure 13. Expected values of position, $\langle x \rangle$ (on the left) and momentum, $\langle p \rangle$ (on the right) for V_2, V_3, V_4, and V_5 potentials.

these negative regions became significant. Notwithstanding this limitation, it was demonstrated that moment methods with relatively low numbers of moments do hold the promise of eventually providing affordable and accurate models for quantum-mechanical systems.

Disclosure statement

No potential conflict of interest was reported by the author(s).

Funding

This work was supported by the Natural Sciences and Engineering Research Council of Canada (Grant No. RGPIN-2020-06295). The authors are very grateful for the support.

References

Abdelmalik, M. R. A., and E. H. van Brummelen. 2016. Moment closure approximations of the Boltzmann Equation based on φ-divergences. J. Stat. Phys. 164 (1):77-104.

Allegretto, W., C. Ringhofer, G. Mascali, V. Romano, A. M. Anile, G. Mascali, and V. Romano. 2003. Recent developments in hydrodynamical modeling of semiconductors. In *Mathematical problems in semiconductor physics: Lectures given at the CIME Summer School held in Cetraro, Italy, July 15–22, 1998. With the collaboration of G. Mascali and V. Romano*, 1–56.

Anile, A. M., and M. Trovato. 1997. Nonlinear closures for hydrodynamical semiconductor transport models. *Phys. Lett. A* 230 (5–6):387–95. doi:10.1016/S0375-9601(97)00278-8

Anile, A. M., and O. Muscato. 1995. Improved hydrodynamical model for carrier transport in semiconductors. *Phys. Rev. B Condens. Matter* 51 (23):16728–40. doi:10.1103/physrevb.51.16728

Anile, A. M., and V. Romano. 1999. Non parabolic band transport in semiconductors: Closure of the moment equations. *Continuum Mech. Thermodyn.* 11 (5):307–25. doi:10.1007/s001610050126

Cai, Z., Y. Fan, and R. Li. 2013. Globally hyperbolic regularization of grad's moment system in one dimensional space. *Commun. Math. Sci.* 11 (2):547–71. doi:10.4310/CMS.2013.v11.n2.a12

Cai, Z., Y. Fan, and R. Li. 2014. On hyperbolicity of 13-moment system. *Kinet. Relat. Models* 7 (3):415–32. doi:10.3934/krm.2014.7.415

Cai, Z., Y. Fan, R. Li, T. Lu, and Y. Wang. 2012. Quantum hydrodynamic model by moment closure of Wigner equation. *J. Math. Phys.* 53 (10):1–18. doi:10.1063/1.4748971

Case, W. B. 2008. Wigner functions and Weyl transforms for pedestrians. *Am. J. Phys.* 76 (10):937–46. doi:10.1119/1.2957889

Chen, Z., Y. Xiong, and S. Shao. 2019. Numerical methods for the Wigner equation with unbounded potential. *J. Sci. Comput.* 79 (1):345–68. doi:10.1007/s10915-018-0853-0

Cordes, J. G., and A. K. Das. 2001. Tunnelling in asymmetric double-well potentials: Varying initial states. *Superlattices Microstruct.* 29 (2):121–32. doi:10.1006/spmi.2000.0964

Degond, P., and C. Ringhofer. 2003. Quantum moment hydrodynamics and the entropy principle. *J. Stat. Phys.* 112 (3/4):587–628. doi:10.1023/A:1023824008525

Dreyer, W. 1987. Maximization of the entropy in non-equilibrium. *J. Phys. A Math. Gen.* 20 (18):6505–17. doi:10.1088/0305-4470/20/18/047

Ferry, D. K., and H. L. Grubin. 1996. Modeling of quantum transport in semiconductor devices. *Solid State Phys.* 49:283–448.

Fox, R. O., and F. Laurent. 2022. Hyperbolic quadrature method of moments for the one-dimensional kinetic equation. *SIAM J. Appl. Math.* 82 (2):750–71. doi:10.1137/21M1406143

Frommlet, F., P. A. Markowich, and C. Ringhofer. 1999. A Wigner function approach to phonon scattering. *VLSI Des.* 9 (4):339–50. doi:10.1155/1999/30381

Gardner, C. L. 1994. The quantum hydrodynamic model for semiconductor devices. *SIAM J. Appl. Math.* 54 (2):409–27. doi:10.1137/S0036139992240425

Grad, H. 1949. On the kinetic theory of rarefied gases. *Comm. Pure Appl. Math.* 2 (4): 331–407. doi:10.1002/cpa.3160020403

Hamburger, H. L. 1944. Hermitian transformations of deficiency-index (1, 1), Jacobian matrices, and undetermined moment problems. *Am. J. Math.* 66 (4):489–552. doi:10.2307/2371763

Junk, M. 1998. Domain of definition of Levermore's five-moment system. *J. Stat. Phys.* 93 (5/6):1143–67. doi:10.1023/B:JOSS.0000033155.07331.d9

Levermore, C. D. 1996. Moment closure hierarchies for kinetic theories. *J. Stat. Phys.* 83 (5–6):1021–65. doi:10.1007/BF02179552

McDonald, J. G., and M. Torrilhon. 2013. Affordable robust moment closures for CFD based on the maximum-entropy hierarchy. *J. Comput. Phys.* 251:500–23. doi:10.1016/j.jcp.2013.05.046

Müller, I., and T. Ruggeri. 1993. *Extended thermodynamics*. New York, NY: Springer-Verlag.

Somorjai, R. L., and D. F. Hornig. 2004. Double-minimum potentials in hydrogen-bonded solids. *J. Chem. Phys.* 36 (8):1980–1987.

Torrilhon, M. 2016. Modeling nonequilibrium gas flow based on moment equations. *Annu. Rev. Fluid Mech.* 48 (1):429–58. doi:10.1146/annurev-fluid-122414-034259

Weinbub, J., and D. K. Ferry. 2018. Recent advances in Wigner function approaches. *Appl. Phys. Rev.* 5 (4):041104. doi:10.1063/1.5046663

Weiner, J. H., and S. T. Tse. 1981. Tunneling in asymmetric double-well potentials. *J. Chem. Phys.* 74 (4):2419–26. doi:10.1063/1.441364

Wigner, E. 1932. On the quantum correction for thermodynamic equilibrium. *Phys. Rev.* 40 (5):749–59. doi:10.1103/PhysRev.40.749

Chapter 4

Second Journal Publication: Development of Globally Hyperbolic One-Dimensional Moment Closures Based on Orthogonal Polynomials

Following the conclusions of the first paper, one of the problems observed is the impact of relatively low-order moment methods on the accuracy of highly oscillatory solutions. The need for higher-order moment methods is the driving factor motivating the study presented in the second journal paper. Higher-order moment closures based on maximum-entropy approximations have proven difficult to obtain. This paper presents a new method for the constructions of hyperbolic, high-order moment methods along with a new hierarchy of Galilean invariant moment closures maintaining balance-law form.

Journal of Computational Physics 523 (2025) 113659

Contents lists available at ScienceDirect

Journal of Computational Physics

journal homepage: www.elsevier.com/locate/jcp

Development of globally hyperbolic one-dimensional moment closures based on orthogonal polynomials

William Morin *, James G. M^{c}Donald

Department of Mechanical Engineering, University of Ottawa, 161 Louis-Pasteur, Ottawa, K1N 6N5, ON, Canada

ARTICLE INFO

Keywords:
Hyperbolic moment closures
Kinetic theory of gases
Quadrature method of moment

ABSTRACT

The use of moment closure techniques for the prediction of non-equilibrium flows has gained in popularity in the past decades. However, many moment models lack robustness which make them impractical for many engineering applications. Ideally, moment models should always predict realizable moments while maintaining global hyperbolicity and yielding a system in balance-law form. Quadrature-based methods have been shown to offer promising alternatives to more traditional moment methods. Building on the works by Fox and Laurent, a novel approach to moment closure construction is presented. This technique is used to build a new robustly hyperbolic hierarchy for closures with even numbers of moments. Numerical solutions for a typical Riemann problem along with shock waves at a variety of incoming flow Mach numbers are used to compare the robustness and accuracy of the various models.

1. Introduction

The development of models that accurately predict non-equilibrium gas flows for a wide range of Knudsen number has proven difficult. Traditional models, such as the Navier-Stokes equations, fail to produce accurate solutions, while particle-based methods, such as direct-simulation Monte Carlo (DSMC) [1], can be computationally taxing. The cost linked to stochastic particle methodologies becomes particularly prohibitive in cases of low-speed flows or when aiming for time-accurate computations [2]. Methods that attempt to enhance the Navier–Stokes equations by introducing higher-order terms through expansion techniques have not succeeded in producing consistent sets of partial differential equations (PDEs) [3]. The use of moment methods for the prediction of non-equilibrium flows have been shown to offer some modelling and numerical advantages over other methods [4,5].

Kinetic theory of gases commonly describes the motion of classical gas particles through a velocity distribution function in phase space. The time evolution of this distribution function is governed by the Boltzmann equation. However, the accurate discretization of the Boltzmann equation presents several numerical difficulties that are mostly associated with the large number of dimensions involved. Moment closure was found to be a promising method for simplifying kinetic equations into fluid models [6–9]. The problem of constructing a suitable moment model has been widely studied over the past decades. Ideally, a well-posed moment model should always predict realizable moments while maintaining global hyperbolicity and yielding a system of equations in balance-law form. As is demonstrated in this work, strict conditions need to be followed in order to produce such moment systems. Many successful

* Corresponding author.
E-mail address: wmori104@uottawa.ca (W. Morin).

https://doi.org/10.1016/j.jcp.2024.113659
Received 1 February 2024; Received in revised form 21 November 2024; Accepted 3 December 2024

Available online 6 December 2024

moment models were developed in the past decades, however, they almost all fail to observe at least one of the above critera or suffer from numerical difficulties. A non-exhaustive review of some of these methods is presented herein.

One of the first moment-closure hierarchies was proposed by Grad [4]. It is built using an expansion of the equilibrium distribution in Hermite polynomials. This closure was found to suffer from a restrictive region of hyperbolicity, only allowing accurate solution near equilibrium. Furthermore, due to the polynomial expansion, this method is not guaranteed to predict strictly positive distribution functions. Other authors have proposed a regularized moment system to extend the mathematical robustness of the closures, consequently adding non-conservative terms into the moment system [10,11]. An alternate idea based on the maximization of the Boltzmann entropy was proposed by Dreyer [12], Muller & Ruggeri [13] and Levermore [14]. The maximum-entropy hierarchy was shown to produce accurate predictions of non-equilibrium flows, while guaranteeing global hyperbolicity and producing system of equations in conservative form [15]. However, as shown by Junk [16], there exist states for which a maximum-entropy distribution function cannot be constructed. Moreover, due to the specific form of distribution function, the closing flux cannot be integrated in closed form, thus requiring approximations, which are currently only available for a limited number of moments [15,17]. Quadrature based methods, on the other hand, were shown to offer more flexibility in producing stable hyperbolic moment equations while yielding a system of hyperbolic balance-laws. First introduced by McGraw [18] in the context of aerosol dynamics description, Fox developed the QMOM hierarchy [19] and later, with the contribution of Laurent, the HyQMOM hierarchy, providing hyperbolic stable moment closure models [20]. As shown in this work, the question of hyperbolicity is only relevant when moments of the particle velocities present in a flux vector are of interest. In many population-balance applications, where moments of the differentiating properties of distinguishable particles are the focus, the question of hyperbolicity is not relevant. This is the case, for example, in the GQMOM approach of Fox et al. [21]. However, when applied to the current setting, the GQMOM reduces to HyQMOM, with the possibility of defining higher-order moments. For the present application (a gas of indistinguishable particles), the robust hyperbolicity of the resulting moment equations is the focus. This leads to the development of new constraints that are not relevant in the classical population-balance setting.

1.1. Scope of study

This paper begins with a quick review of one-dimensional moment closure theory with emphasis on the quadrature-based moment closure. A technique for the construction of hyperbolic closure in balance-law form is presented. This technique builds directly on the works of Fox and Laurent [22,20]. The QMOM and HyQMOM hierarchies are also discussed along with their place in the proposed framework. A new even-order moment hierarchy is presented. This hierarchy of new strongly hyperbolic even-order moment closures expands the hierarchy started by Fox and Laurent with their HyQMOM. The long-term outcome of the work is to use this new technique as a stepping stone for the eventual construction of 3D globally hyperbolic closures. The construction of these multi-dimensional practical closures will be presented in a following paper and requires robustly hyperbolic one-dimensional closures of both even and odd order. The even-order closures developed in this work complement the existing odd-order closures of Fox and Laurent [20] in this endeavor. Finally, numerical solutions of a typical Riemann problem along with shock-waves of various strength are used to compare the different closures against the BGK kinetic equation solutions.

2. Moment closures

The method of moment-closure descends from the traditional kinetic theory of gases, in which a probability distribution function is used to statistically describe a gas. Since directly tracking every single particle is prohibitive for most applications, a distribution function, $\mathcal{F}(x_i, v_i, t)$, describing the phase-space density of particles at a location, x_i, with velocity, v_i, at time, t, is used. In most cases, only a small number of macroscopic properties are of interest and not all the information contained in the distribution function is necessary. These macroscopic properties can be obtained by multiplying the distribution function by a monomial velocity weight and integrating over all velocity space. This process is commonly known as taking moments of the distribution function.

It is important to note that, in the present study, only a one-dimensional velocity distribution function is considered. That is, $\mathcal{F}(x, v, t)$, is defined for $(x, v, t) \in \mathbb{R} \times \mathbb{R} \times \mathbb{R}^+$. For a one-dimensional treatment, the following are examples of moments of the distribution function yielding macroscopic properties of interest:

$$\rho = \int m\mathcal{F}\, \mathrm{d}v = \langle m\mathcal{F} \rangle ,$$
$$\rho u = \langle mv\mathcal{F} \rangle ,$$
$$\rho\theta = \left\langle mc^2\mathcal{F} \right\rangle ,$$
$$q = \left\langle mc^3\mathcal{F} \right\rangle ,$$
$$r = \left\langle mc^4\mathcal{F} \right\rangle ,$$
$$s = \left\langle mc^5\mathcal{F} \right\rangle .$$

The notation, $\langle \cdot \rangle$, is used to denote the integral over all velocity space. The bulk velocity is given by u, while c represents the random velocity, which is expressed as $c = v - u$. The variables ρ, θ and q are the mass density, the temperature, and the heat flux respectively, while r and s are associated with the fourth- and fifth-order moment. Moments of the full particle velocity, often called convective moments, are denoted by U_n,

$$U_n = \langle m v^n \mathcal{F} \rangle \,, \tag{1}$$

with $n \in \mathbb{N}$. A vector of such moments can be defined as, $\boldsymbol{U} = [U_0, U_1, \cdots, U_n]^{\mathrm{T}}$.

2.1. Normalized moments

Throughout this paper normalized moments, W_n, are used. These moments are constructed by shifting the probability distribution function in velocity space resulting in a zero bulk velocity, followed by a non-dimensionalization such that $\rho = 1$ and $\theta = 1$,

$$W_n = \frac{1}{\rho}\left(\frac{1}{\theta}\right)^{n/2} \langle m c^n \mathcal{F} \rangle \,. \tag{2}$$

The resulting normalized moment vectors is defined as $\boldsymbol{W}_n = [1, 0, 1, W_3 \cdots, W_n]^{\mathrm{T}}$.

2.2. Physical realizability of one-dimensional moment closures

Physical realizability of a classical gas is defined as the moment space where states, $\boldsymbol{U}$, can be reached by at least one non-negative distribution function, thus only allowing certain moment arrangements. The set of realizable moment states can be calculated through the solution of the Hamburger problem [23]. This is typically done using a vector of velocity weights, $\boldsymbol{\mathcal{W}} = [1, v, v^2, \cdots, v^n]^{\mathrm{T}}$, to define a matrix,

$$\boldsymbol{M} = \left\langle m \boldsymbol{\mathcal{W}} \boldsymbol{\mathcal{W}}^{\mathrm{T}} \mathcal{F} \right\rangle \,. \tag{3}$$

For any non-negative distribution, $\mathcal{F}$, it can be shown that the resulting matrix,

$$\boldsymbol{M}_{2l} = \begin{bmatrix} U_0 & U_1 & U_2 & U_3 & \cdots & U_l \\ U_1 & U_2 & U_3 & U_4 & \cdots & U_{l+1} \\ U_2 & U_3 & U_4 & U_5 & \cdots & U_{l+2} \\ U_3 & U_4 & U_5 & U_6 & \cdots & U_{l+3} \\ \vdots & & & \ddots & & \\ U_l & U_{l+1} & U_{l+2} & U_{l+3} & \cdots & U_{2l} \end{bmatrix}, \qquad l \in \{0, 1, 2, \cdots, n\} \,, \tag{4}$$

must be positive semi-definite. The principal minors of $\boldsymbol{M}_{2l}$ define the lower-boundaries of physical realizability for a given moment set,

$$\begin{aligned} M_0 &= U_0 \geq 0 \\ M_2 &= U_0 U_2 - U_1^2 \geq 0 \\ M_4 &= U_0 U_2 U_4 - U_0 U_3^2 - U_1^2 U_4 + 2 U_1 U_2 U_3 - U_2^3 \geq 0 \\ &\vdots \\ M_{2l} &= \det(\boldsymbol{M}_{2l}) \geq 0 \end{aligned}$$

For simplicity, the minors are often written in terms of the normalized moments, i.e. ($M_2 = W_4 - W_3^2 - 1$).

2.3. The Boltzmann equation

For a classical gas, the time evolution of the distribution function is described by the Boltzmann equation,

$$\frac{\partial \mathcal{F}}{\partial t} + v \frac{\partial \mathcal{F}}{\partial x} + \frac{\partial (a\mathcal{F})}{\partial v} = \frac{\delta \mathcal{F}}{\delta t} \,. \tag{5}$$

The second term of Eq. (5) represents the convective contribution to the time evolution while the third term describes the acceleration effects on the particles due to external fields. In this work the acceleration is assumed to be zero. The right-hand side of the equation represents the effects of inter-particle collisions on the distribution function. This collision operator contains a high-dimensional integral that, in general, cannot be evaluated in closed form. Nevertheless, information about this operator is available. The collision operator can be shown to conserves mass, momentum, and energy. It was also shown by Boltzmann that it always increases the entropy until the distribution function has the form of a Maxwellian,

$$\mathcal{M} = \frac{\rho}{m}\left(\frac{1}{2\pi\theta}\right)^{\frac{3}{2}} \exp\left(\frac{1}{2\theta} c^2\right) \,. \tag{6}$$

When equilibrium is reached, the collision operator has no further effects. As the goal of this work is the investigation of suitable conditions for the development of hyperbolic moment closures, the simple BGK relaxation-time collision operator [24] is used to close the right hand-side of Eq. (5),

$$\frac{\delta \mathcal{F}}{\delta t} = -\frac{\mathcal{F} - \mathcal{M}}{\tau} \,. \tag{7}$$

55

In order to obtain a set of PDEs describing the evolution of the properties of interest, velocity moments of the Boltzmann equation are taken,

$$\frac{\partial}{\partial t}\langle \boldsymbol{\mathcal{W}}\mathcal{F}\rangle + \frac{\partial}{\partial x}\langle v\boldsymbol{\mathcal{W}}\mathcal{F}\rangle = \left\langle m\boldsymbol{\mathcal{W}}\frac{\delta\mathcal{F}}{\delta t}\right\rangle . \tag{8}$$

This equation can be written in the form,

$$\frac{\partial \boldsymbol{U}}{\partial t} + \frac{\partial \boldsymbol{F}}{\partial x} = \boldsymbol{C}\,, \tag{9}$$

where $\boldsymbol{U}$ is the solution vector containing the convective moment of interest, $\boldsymbol{F}$ is the flux vector, and $\boldsymbol{C}$ is the source vector representing the effect of the collision operator. Unfortunately, this method does not lead to a closed set of equations, since the time evolution of a given moment always depend on the spacial divergence of a moment that is one order higher.

One method to close the system of equations is to assume a form for $\mathcal{F}$. This technique has been particularity successful and is at the centre of many moment closure hierarchies. The assumed distribution function should contain the same number of free parameters as there are moments of interest. The free parameters are chosen to be in agreement with the macroscopic properties of interest. It is then possible to express the closing flux as a function of the known moments by integrating the now known distribution function. Though this has been the traditional method, one does not necessarily need to assume a form for the distribution function. As is demonstrated in the following section, restrictions on the system homogeneity and hyperbolicity provide sufficient constraints to construct closures, leading to robust moment equations more directly.

2.4. Flux Jacobian

The flux jacobian, $\frac{\mathrm{d}\boldsymbol{F}}{\mathrm{d}\boldsymbol{U}}$, of the moment system can be found from Eq. (9),

$$\frac{\partial \boldsymbol{U}}{\partial t} + \frac{\mathrm{d}\boldsymbol{F}}{\mathrm{d}\boldsymbol{U}}\frac{\partial \boldsymbol{U}}{\partial x} = \boldsymbol{C}\,. \tag{10}$$

For a one-dimensional treatment of an n-moment system, the flux Jacobian takes the form of a companion matrix,

$$\frac{d\boldsymbol{F}}{d\boldsymbol{U}} = \begin{bmatrix} 0 & 1 & 0 & \cdots & 0 \\ 0 & 0 & 1 & \cdots & 0 \\ \vdots & & & \ddots & \vdots \\ 0 & 0 & 0 & \cdots & 1 \\ \frac{\partial U_{n+1}}{\partial U_0} & \frac{\partial U_{n+1}}{\partial U_1} & \frac{\partial U_{n+1}}{\partial U_2} & \cdots & \frac{\partial U_{n+1}}{\partial U_n} \end{bmatrix}, \tag{11}$$

where, U_{n+1} is the closing flux ($F_n = U_{n+1}$). The eigenvalues of this matrix, $\lambda_n = [\lambda_0, \lambda_1, \cdots, \lambda_n]^{\mathrm{T}}$, are the wave speeds of the system. Due to this specific structure, the characteristic polynomial of $\frac{d\boldsymbol{F}}{d\boldsymbol{U}}$ can be expressed as

$$P_{n+1}(v) = -v^{n+1} + A_n v^n + A_{n-1}v^{n-1} + \cdots + A_2 v^2 + A_1 v + A_0\,, \tag{12}$$

where,

$$A_n = \frac{\partial U_{n+1}}{\partial U_n} \qquad A_{n-1} = \frac{\partial U_{n+1}}{\partial U_{n-1}} \qquad \cdots \qquad A_1 = \frac{\partial U_{n+1}}{\partial U_1} \qquad A_0 = \frac{\partial U_{n+1}}{\partial U_0} \tag{13}$$

In order for the moment equations to be strongly hyperbolic, the system must produce distinct real wave speeds, while keeping the relation between the closing flux and the coefficients of the characteristic polynomial. This important condition is addressed in detail in the next section.

2.5. Homogeneous property of moment closures

The Euler equations are known, among other things, for their homogeneous properties. These special properties are often used for the accurate construction of numerical methods. However, this homogeneity is not only specific to the Euler equations. It is, in fact, an important characteristic observed in well defined moment closures. These properties provide further constraints on the moment system.

Using Euler's theorem for homogeneous function,

$$\boldsymbol{F}(\alpha \boldsymbol{U}) = \alpha^m \boldsymbol{F}(\boldsymbol{U})\,, \tag{14}$$

for a fixed m, then $\boldsymbol{F}$ is said to be homogeneous of degree m. Differentiating on both sides with respect to α and setting $m = 1$ leads to,

$$\frac{\mathrm{d}\boldsymbol{F}}{\mathrm{d}\boldsymbol{U}}\boldsymbol{U} = \boldsymbol{F}(\boldsymbol{U})\,, \tag{15}$$

where $\boldsymbol{F}$ and $\boldsymbol{U}$ are homogeneous of degree 1. This puts constraints on the allowed form of the closing flux, U_{n+1}. In order to respect the homogeneity described in Eq. (15), the flux Jacobian coefficients must only be function of the scaled moments,

$$\tilde{U}_k = \frac{U_k}{U_0} \quad \text{for} \quad k \in \{1, ..., n\}\,, \tag{16}$$

thus forcing the closing flux to have the form

$$U_{n+1} = U_0\, A_0\left(\tilde{U}_1, \cdots, \tilde{U}_n\right) + \cdots + U_n\, A_n\left(\tilde{U}_1, \cdots, \tilde{U}_n\right)\,, \tag{17}$$

with the coefficients, A_i defined in Eq. (13).

3. Strongly hyperbolic moment closures

In this section two different techniques for the construction of hyperbolic quadrature-based moment closures are presented. The first idea, summarized in Section 3.1, investigates hyperbolic closure construction by directly choosing a form for the wave speeds as function of the known moments, $\boldsymbol{U}$. This technique was found to be challenging and is therefore not considered further. However, important insights on the necessary conditions for the construction of such hyperbolic quadrature-based models were obtained through the analysis, thus the inclusion in this paper. In Section 3.2, a new technique for the construction of globally hyperbolic quadrature-based moment closures based in the orthogonality of polynomials is presented. Using this approach a new hierarchy of hyperbolic moment equations is introduced along with several individual new closures. This new hierarchy is shown to be a good supplement to the well known QMOM system as it covers the even-order moments.

3.1. Quadrature-based closure from eigenvalue construction

Every hyperbolic one-dimensional closure is equivalent to a quadrature-based method. A well known example, is the maximum-entropy hierarchy, where the wave speeds can be shown to always be located at the optimum Gaussian quadrature points of the underlying distribution function [25]. However, general conditions for the construction of strongly hyperbolic moment closure are still elusive. One obvious method is to attempt to propose the wave speeds directly as function of the known moments. Unfortunately, this proves to be more difficult than anticipated since, as is shown in this section, building the closing flux from a proposed quadrature rule does not automatically make the associated quadrature points the wave speeds of the system.

In general, when dealing with quadrature-based closures, finding a closed form for the velocity distribution function is not necessary since the closing flux is not computed by taking a moment of $\mathcal{F}$. However, in this case, it is convenient to represent the velocity distribution function as a weighted sum of Dirac deltas,

$$\mathcal{F} = \sum_{i=0}^{i=n} \mathfrak{W}_i \delta(v - \zeta_i) \tag{18}$$

where, ζ_i, is the position of each quadrature point and $\mathfrak{W}_i$ is the associated weight. The weights are linked to the known moments through,

$$\boldsymbol{V}\boldsymbol{\mathfrak{W}} = \boldsymbol{U}\,, \tag{19}$$

while the flux is computed as,

$$\boldsymbol{F} = \boldsymbol{V}\boldsymbol{\Omega}\boldsymbol{\mathfrak{W}} = \boldsymbol{V}\boldsymbol{\Omega}\boldsymbol{V}^{-1}\boldsymbol{U} \tag{20}$$

with

$$\boldsymbol{V} = \begin{bmatrix} 1 & 1 & 1 & \cdots & 1 \\ \zeta_0 & \zeta_1 & \zeta_2 & \cdots & \zeta_n \\ \zeta_0^2 & \zeta_1^2 & \zeta_2^2 & \cdots & \zeta_n^2 \\ \vdots & & \cdots & & \vdots \\ \zeta_0^n & \zeta_1^n & \zeta_2^n & \cdots & \zeta_n^n \end{bmatrix}, \qquad \boldsymbol{\Omega} = \begin{bmatrix} \zeta_0 & 0 & 0 & \cdots & 0 \\ 0 & \zeta_1 & 0 & \cdots & 0 \\ \vdots & 0 & \ddots & 0 & \vdots \\ 0 & \cdots & 0 & \zeta_{n-1} & 0 \\ 0 & \cdots & 0 & 0 & \zeta_n \end{bmatrix}. \tag{21}$$

However, as mentioned earlier, simply choosing the quadrature points in terms of $\boldsymbol{U}$ does not necessarily produce a hyperbolic set of moment equations, since for most cases the quadrature points will not agree with the system wave speeds found through the eigenvalues of the flux Jacobian. The system wave speeds are required to be the quadrature points, that is $\boldsymbol{\zeta} = \boldsymbol{\lambda}$, allowing the flux Jacobian to be written as,

$$\frac{d\boldsymbol{F}}{d\boldsymbol{U}} = \boldsymbol{V}\,\boldsymbol{\Omega}\,\boldsymbol{V}^{-1}\,, \tag{22}$$

$$\boldsymbol{V}\,\boldsymbol{\Omega}\,\boldsymbol{V}^{-1} = \begin{bmatrix} 0 & 1 & 0 & \cdots & 0 \\ 0 & 0 & 1 & \cdots & 0 \\ \vdots & & \ddots & & \vdots \\ 0 & 0 & 0 & \cdots & 1 \\ A_0(\lambda) & A_1(\lambda) & A_2(\lambda) & \cdots & A_n(\lambda) \end{bmatrix}, \tag{23}$$

57

where, the first coefficient is the product of the wave speeds, $A_0 = \prod_{k=0}^{n} \lambda_k$, the second coefficient, A_1, is the negative of the sum of all possible combination of n wave speeds. Similarly, the third coefficient, A_2, is the sum of all possible combination of $n-1$ wave speeds. This pattern continues until the last coefficient $A_n = (-1)^{n+1} \sum_{k=0}^{n} \lambda_k$. Then coefficient, A_k shown in Eq. (13), are only function of the wave speeds which in turn depends on $\boldsymbol{U}$. This situation will only happen if the wave speeds are chosen in such a way that, for any small variation in the solution vector, $\delta\boldsymbol{U}$, the corresponding change in the flux, $\delta\boldsymbol{F}$, is only affected by the variation in $\boldsymbol{U}$ and not by the subsequent change in the wave speeds position, $\delta\lambda$. That is,

$$\delta \boldsymbol{F} = \frac{\partial \boldsymbol{F}}{\partial \boldsymbol{U}} \delta \boldsymbol{U} + \cancelto{0}{\frac{\partial \boldsymbol{F}}{\partial \lambda} \delta \lambda} \,. \tag{24}$$

To enforce this condition, one can rewrite the closing flux as $U_{n+1}(\boldsymbol{U}, \lambda(\boldsymbol{U}))$ where $\lambda(\boldsymbol{U})$ is a vector containing the systems wave speeds, $\lambda(\boldsymbol{U}) = [\lambda_0(\boldsymbol{U}), \lambda_1(\boldsymbol{U}), \cdots, \lambda_n(\boldsymbol{U})]^{\mathrm{T}}$. The flux-dyad can be written as,

$$\boldsymbol{F} = [U_1, U_2, \cdots, U_{n+1}(\boldsymbol{U}, \lambda(\boldsymbol{U}))]^{\mathrm{T}} \,. \tag{25}$$

Using the chain rule, the flux-Jacobain can be decomposed as,

$$\frac{d\boldsymbol{F}}{d\boldsymbol{U}} = \left(\frac{\partial \boldsymbol{F}}{\partial \boldsymbol{U}}\right)_{\lambda} + \left(\frac{\partial \boldsymbol{F}}{\partial \lambda}\right)_{U} \left(\frac{\partial \lambda}{\partial \boldsymbol{U}}\right) , \tag{26}$$

where the first term represent the variation of the flux vector due to changes of the state vector holding the wave speeds, λ, constant, while the second term gives the variation of the flux vector due to changes of the wave speeds holding the solution vector constant. Forcing the second term to be zero ensures that the prescribed real-valued quadrature points correspond to the system wave speeds.

Since only the last row of the flux vector depends on the λs, this condition can be further simplified as,

$$\left(\frac{\partial U_{n+1}}{\partial \lambda}\right)_{U} \left(\frac{\partial \lambda}{\partial \boldsymbol{U}}\right) = 0 \qquad \text{with} \qquad \left(\frac{\partial U_{n+1}}{\partial \lambda}\right)_{U} = \left[\frac{\partial U_{n+1}}{\partial \lambda_0}, \frac{\partial U_{n+1}}{\partial \lambda_1}, \cdots, \frac{\partial U_{n+1}}{\partial \lambda_n}\right] , \tag{27}$$

requiring the vector $\left(\frac{\partial U_{n+1}}{\partial \lambda}\right)_{U}$ to be in the left null space of the matrix $\left(\frac{\partial \lambda}{\partial \boldsymbol{U}}\right)$. The first-order homogeneity of the system ensures that $\boldsymbol{U}$ is the right nullspace of $\left(\frac{\partial \lambda}{\partial \boldsymbol{U}}\right)$. It is important to note that this restricts the form of the wave speeds, as shown in Eq. (17), to only be function of the scaled moments, $\tilde{\boldsymbol{U}}$,

$$\lambda_0\left(\tilde{U}_1, \cdots, \tilde{U}_n\right) \qquad \lambda_1\left(\tilde{U}_1, \cdots, \tilde{U}_n\right) \qquad \cdots \qquad \lambda_n\left(\tilde{U}_1, \cdots, \tilde{U}_n\right) . \tag{28}$$

Picking the wave speeds to be a real function of the scaled moments while also satisfying Eq. (27) provide necessary and sufficient conditions for the construction of strongly hyperbolic closures. Unfortunately, this approach requires one to solve a system of differential equations which is often difficult. An example for the 3-moment case is presented in Appendix A.

3.2. Quadrature-based closure from orthogonal polynomials

Instead of proposing a form for the wave speeds from the known moments. Monic orthogonal polynomials can be used to build the flux Jacobian characteristic polynomial directly. Expanding on the works done by Fox and Laurent [19,22], this section presents a general technique for the construction of hyperbolic closures along with a new hierarchy covering the even-order moments.

3.2.1. Orthogonal polynomials

Orthogonal polynomials of a single variable defined by moment of a non-negative velocity distribution function have interesting properties. The orthogonal polynomials, P_n, can always be expressed in terms of the moments by applying the Gram-Schmidt process to the monomials,

$$P_n = \det \begin{bmatrix} U_0 & U_1 & U_2 & \cdots & U_n \\ U_1 & U_2 & U_3 & \cdots & U_{n+1} \\ \vdots & \vdots & \vdots & \ddots & \vdots \\ U_{n-1} & U_n & U_{n+1} & \cdots & U_{2n-1} \\ 1 & v & v^2 & \cdots & v^n \end{bmatrix} , \tag{29}$$

imposing each polynomial to be orthogonal with respect to each other, i.e., $\langle P_n P_m \rangle = \left\langle P_n^2 \right\rangle \, \delta_{nm}$. They also satisfy the three-term recurrence relation, allowing one to build the following sequence,

$$P_{n+1} = (v - a_n) P_n - b_n P_{n-1} \,, \tag{30}$$

with, $P_0 = 1$ and

$$a_n = \frac{\left\langle v P_n^2 \right\rangle}{\left\langle P_n^2 \right\rangle} , \qquad b_n = \frac{\left\langle P_n^2 \right\rangle}{\left\langle P_{n-1}^2 \right\rangle} = \frac{\boldsymbol{M}_{2n} \boldsymbol{M}_{2n-4}}{\boldsymbol{M}_{2n-2}^2} . \tag{31}$$

58

More importantly, following Favard's theorem, the roots of P_{n+1} are guaranteed to be real if the recurrence coefficient a_n are real valued and the b_n are positive.

3.2.2. Closure construction using orthogonal polynomials

In order to build hyperbolic moment systems using orthogonal polynomials, one first need to construct the flux Jacobian from the monic polynomials following the recurrence relation, Eq. (30), up to the $n+1$ order. The first recurrence coefficients of the series in terms of normalized moments, $\boldsymbol{W} = [1, 0, 1, W_3, W_4, \cdots, W_n]^{\mathrm{T}}$, are

$$
\begin{aligned}
a_0 &= \left\langle v P_0^2 / P_0^2 \right\rangle = 0 \\
a_1 &= W_3 & b_1 &= 1 \\
a_2 &= \frac{W_3^3 - 2W_3 W_4 + W_5}{W_4 - W_3^2 - 1} & b_2 &= W_4 - W_3^2 - 1 \\
&\vdots & &\vdots \\
a_n &= \left\langle v P_n^2 \right\rangle / \left\langle P_n^2 \right\rangle & b_n &= \left\langle P_n^2 \right\rangle / \left\langle P_{n-1}^2 \right\rangle .
\end{aligned}
$$

However, the closing flux cannot be calculated directly by taking moments of the resulting polynomial, since it contains higher-order moments that are not part of the solution vector. In order to close the system one needs to choose the form of the closing flux such that all the recurrence coefficients fulfill the requirements of Favard's theorem. The closing flux, U_{n+1}, is always completely determined by choosing the form of the closing coefficient. The term "closing coefficient" does not refer to the highest-order recurrence coefficient of the characteristic polynomial, but rather to the first coefficient containing the closing flux. For even moment systems, the associated closure coefficient is always given by $b_{(n+1)/2}$. Similarly, for odd moment systems, the closure coefficient is given by $a_{n/2}$. All higher recurrence coefficients become fixed after this choice as there is a one to one relation between the closure coefficient and the closing flux. However, choosing the closing coefficient such that Favards theorem is fulfilled is not trivial.

3.2.3. Galilean invariance and correct temperature scaling

In order for any system to be Galilean invariant and scale correctly with the temperature, restrictions on the form of the closing flux needs to be observed. These restrictions can be expressed in many different forms. However, in this section, it is convenient to write them using the characteristic polynomial, P_{n+1}, as discussed by Fox and Laurent [20],

$$
\left\langle P'_{n+1} \right\rangle = 0 \qquad \left\langle v P'_{n+1} \right\rangle = 0 . \tag{32}
$$

Interestingly, it is believed that these two restrictions are exactly equivalent to Eq. (A.10), as shown for the 3-moment case in Appendix B. This equivalence was tested for moment system up to order nine. However, no formal proof is presented in this work.

3.2.4. The QMOM and HyQMOM hierarchies

As mentioned above, the QMOM and HyQMOM closures are central to this present work [22,20]. They were proven to be a very successful method for the construction of Galilean invariant hyperbolic quadrature-based closures. Without going into extensive details, the QMOM closure provides a technique to build the even-order moment closures. The closing flux, U_{n+1}, is constructed by setting the closure coefficient, $b_{(n+1)/2} = 0$. This allows, U_{n+1}, to be solved from the definition of the recurrence coefficient since it only appears once on the left hand side,

$$
b_{\frac{(n+1)}{2}} = \frac{\left\langle P^2_{\frac{n+1}{2}} \right\rangle}{\left\langle P^2_{\frac{n-1}{2}} \right\rangle} = 0 . \tag{33}
$$

The resulting closures reside on the realizability boundary thus never recovering equilibrium and always predicting repeated wave speeds. The HyQMOM closure, on the other hand, provides a methods for the construction the odd-order closures. The resulting closures are strongly hyperbolic meaning that they are not restricted to the physical realizable boundary. Similarly, they are constructed by setting the closure coefficient, $a_{n/2} = \frac{1}{k} \sum_{k=0}^{k=\frac{n}{2}-1} a_k$. Again the closing flux can be found directly from the definition of the recurrence coefficient.

$$
a_{\frac{n}{2}} = \frac{\left\langle v P^2_{\frac{n}{2}} \right\rangle}{\left\langle P^2_{\frac{n}{2}} \right\rangle} = \frac{1}{n/2} \sum_{k=0}^{k=\frac{n}{2}-1} a_k . \tag{34}
$$

As an example, one can look at the 5-moment closure obtained by the HyQMOM hierarchy. The normalized closing flux, W_5, can be found by proposing a form for the corresponding closure coefficient a_2,

$$a_2 = \frac{1}{k}\sum_{0}^{n/2} a_k = \left\langle v P_2^2 / P_2^2 \right\rangle \tag{35}$$

$$\frac{1}{2}W_3 = \frac{W_3^3 - 2W_3W_4 + W_5}{W_4 - W_3^2 - 1} \tag{36}$$

$$W_5 = \frac{1}{2}W_3(5W_4 - 3W_3^2 - 1)\,. \tag{37}$$

3.2.5. A new approach to quadrature-based closure construction

Building a characteristic polynomial such that the recurrence coefficients, a_n and b_n, remain real and non-negative, respectively, is not enough to guarantee hyperbolicity. One also needs to ensure that the resulting polynomial is in fact the characteristic polynomial of the flux Jacobian, thus providing necessary and sufficient conditions for the construction of strongly hyperbolic closures. One way to enforce this condition is to consider the closing flux as $U_{n+1} = \boldsymbol{A}(\boldsymbol{U}) \cdot \boldsymbol{U}$ as was required by Eq. (17). The flux Jacobian $\frac{\partial \boldsymbol{F}}{\partial \boldsymbol{U}}$ can then be decomposed into two terms.

$$\frac{d\boldsymbol{F}}{d\boldsymbol{U}} = \left(\frac{\partial \boldsymbol{F}}{\partial \boldsymbol{U}}\right)_A + \left(\frac{\partial \boldsymbol{F}}{\partial \boldsymbol{A}}\right)_U \left(\frac{\partial \boldsymbol{A}}{\partial \boldsymbol{U}}\right). \tag{38}$$

Building the closing flux such that the second term is zero is necessary for Eq. (13) to be true. Simplifications can be made since only the closing flux, U_{n+1} is unknown,

$$\frac{dU_{n+1}}{d\boldsymbol{U}} = \left(\frac{\partial U_{n+1}}{\partial \boldsymbol{U}}\right)_A + \left(\frac{\partial U_{n+1}}{\partial \boldsymbol{A}}\right)_U \left(\frac{\partial \boldsymbol{A}}{\partial \boldsymbol{U}}\right), \tag{39}$$

$$\frac{dU_{n+1}}{d\boldsymbol{U}} = \boldsymbol{A} + \boldsymbol{U}^{\mathrm{T}} \left(\frac{\partial \boldsymbol{A}}{\partial \boldsymbol{U}}\right). \tag{40}$$

Finally, Eq. (13) leads to,

$$\frac{dU_{n+1}}{d\boldsymbol{U}} = \boldsymbol{A} + \boldsymbol{U}^{\mathrm{T}} \left(\frac{\partial^2 \boldsymbol{U_{n+1}}}{\partial^2 \boldsymbol{U}}\right). \tag{41}$$

For the closing flux to produce a system of first-order hyperbolic equations, the solution vector needs to be in the left null space of $\left(\frac{\partial \boldsymbol{A}}{\partial \boldsymbol{U}}\right)$,

$$\boldsymbol{U}^{\mathrm{T}} \left(\frac{\partial \boldsymbol{A}}{\partial \boldsymbol{U}}\right) = 0 \qquad \text{or} \qquad \boldsymbol{U}^{\mathrm{T}} \left(\frac{\partial^2 \boldsymbol{U_{n+1}}}{\partial^2 \boldsymbol{U}}\right) = 0\,. \tag{42}$$

This constraint provides a system of differential equations only containing derivatives of the closing coefficient ($b_{(n+1)/2}$ or $a_{n/2}$). Once the forms of the closing coefficient is chosen, the other recurrence coefficient can be solved algebraically. The effect of different form of closing coefficients on the system hyperbolicity can then be studied allowing for the constructions of a variety of new closures.

In order to illustrate this approach, one can consider a simple 3-moment system. The sequence of orthogonal polynomials are first built until P_3 using the recurrence relations,

$$\begin{aligned}
P_0 &= 0 \\
P_1 &= (v - a_0) \\
P_2 &= v^2 - (a_1 + a_0)v + a_1a_0 - b_1 \\
P_3 &= v^3 - (a_2 + a_1 + a_0)v^2 + (-a_2(-a_1 - a_0) + a_1a_0 - b_1 - b_2)v - a_2(a_1a_0 - b_1) + b_2a_0\,,
\end{aligned}$$

where the coefficient of the resulting characteristic polynomial are,

$$\begin{aligned}
A_0 &= a_2(a_1a_0 - b_1) - b_2a_0 \\
A_1 &= a_2(-a_1 - a_0) - a_1a_0 + b_1 + b_2 \\
A_2 &= a_2 + a_1 + a_0\,.
\end{aligned}$$

The first two recurrence coefficients $a_0 = U_1/U_0$ and $b_1 = U_2/U_0 - U_1^2/U_0^2$ can be computed directly using Eq. (31), while the others contain higher moments of the distribution that are not part of the solution vector. Eq. (42) is then used to provide a system of equations,

$$\begin{aligned}
U_0\frac{\partial A_0}{\partial U_0} + U_1\frac{\partial A_1}{\partial U_0} + U_2\frac{\partial A_2}{\partial U_0} &= 0\,, \\
U_0\frac{\partial A_0}{\partial U_1} + U_1\frac{\partial A_1}{\partial U_1} + U_2\frac{\partial A_2}{\partial U_1} &= 0\,,
\end{aligned}$$

$$U_0\frac{\partial A_0}{\partial U_2}+U_1\frac{\partial A_1}{\partial U_2}+U_2\frac{\partial A_2}{\partial U_2}=0\,,$$

where the first equation is always automatically satisfied by choosing the closing coefficients, a_1 to be function of the scaled moments, $\tilde{\boldsymbol{U}}$, forcing the system to be first-order homogeneous. After substituting a_0 and b_1, the equations can be simplified as,

$$\frac{\partial a_1}{\partial \tilde{U}_1}\left(\tilde{U}_2-\tilde{U}_1^2\right)+a_2a_1+a_2\tilde{U}_1-b_2-a_1\tilde{U}_1+\tilde{U}_2-2\tilde{U}_1^2=0\,,$$

$$\frac{\partial a_1}{\partial \tilde{U}_2}\left(\tilde{U}_2-\tilde{U}_1^2\right)-a_2+\tilde{U}_1=0\,.$$

One can see that the system only depends on the choice of the closing coefficient, a_1, and its derivatives, meaning that the higher-order coefficients can be found algebraically,

$$a_2=\frac{\partial a_1}{\partial \tilde{U}_2}\left(\tilde{U}_2-\tilde{U}_1^2\right)+\tilde{U}_1\,,$$

$$b_2=\left(\frac{\partial a_1}{\partial \tilde{U}_2}\left(a_1+\tilde{U}_1\right)+\frac{\partial a_1}{\partial \tilde{U}_1}+1\right)\left(\tilde{U}_2-\tilde{U}_1^2\right)\,.$$

Multiple forms of a_1 can produce a real valued a_2 and non-negative b_2, the only requirements are that the chosen closing coefficient is dimensionally consistent and a function of the scaled moments. However, only one was found to produce Galilean invariant equations, $a_1=a_0$, leading to the Euler equations. It is easy to see that setting $a_1=0$ also produces a 3-moment hyperbolic system since simplifying the equations lead to $a_2=a_0$ and $b_2=M_2$. Moreover the resulting closure scales correctly with the pressure, $\left\langle vP'_{n+1}\right\rangle=0$. However, it is not Galilean invariant anywhere except on the realizability boundary corresponding to a zero temperature since $\left\langle vP'_{n+1}\right\rangle=\frac{U_2}{U_0}-\frac{U_1^2}{U_0^2}$.

Using this technique, one can easily show that setting the closing coefficient $a_{n/2}=0$ always leads to hyperbolic systems, even for higher closures. However, all resulting closures were found to only be Galilean invariant for states on the realizability boundary. These solutions are therefore not considered further in this work. An infinite number of closures can be found using this technique, however the complexity increases rapidly with the number of moments. Ideally, a pattern needs to emerge from the easier lower-order closures leading to a hierarchy spanning all moment.

3.2.6. Some ad-hoc odd-order closures

Using this technique, multiple hyperbolic, Galilean invariant 5-moment closures have been found. For any 5-moment system, the coefficients a_0, a_1, b_1 and b_2 can be calculated analytically from Eq. (31). The closing coefficient, a_2, needs to be chosen in such a way that a_3, a_4, b_3 and b_4 are real valued and non-negative respectively.

The first closure considered in this study, denoted $\mathrm{C0}_5$, is found by setting $a_2=a_0$. The associated closing flux, $W_5=-W_3(W_3^2-2W_4)$, resulting in $a_3=W_3$, $a_4=0$, $b_3=W_4-W_3^2$ and $b_4=0$, is globally hyperbolic, scales correctly with temperature, and is Galilean invariant. Unfortunately, it was found that choosing a value of a_0 for the closing coefficient only produce 3-moment and 5-moment hyperbolic systems. The pattern does not extend to higher-order moment closures.

The next logical form to be considered is $a_2=a_0+a_1$ which leads to a hyperbolic but not Galilean invariant system. In order to ensure that $\left\langle P'_5\right\rangle=0$ and $\left\langle vP'_5\right\rangle=0$ the closing coefficient needs to be multiplied by a factor of $\frac{1}{2}$. This choice exactly recovers the HyQMOM_5 model of Fox and Laurent. This closure leads to $a_3=W_3$, $a_4=0$, $b_3=W_4-W_3^2$ and $b_4=0$.

Other expression were also found to produce hyperbolic and Galilean invariant systems, i.e. $a_2=\frac{1}{4}\left(\frac{U1}{U0}+\frac{U3}{U2}\right)$. However the resulting closure was found to be very similar to HyQMOM_5 and therefore not considered further.

Finally the last 5-moment closure studied in this work, denoted $\mathrm{C1}_5$, was found by setting $a_2=a_0+\frac{b_2}{b_1}(a_1-a_0)$. The resulting moment equations are Galilean invariant and scale correctly with temperature, but are not globally hyperbolic. This can be seen in Fig. 1 as large negative regions can be observed in the normalized b_3 and b_4 coefficients plotted over realizable space. This limits the use of this closure only to low speed flow or below $\mathrm{Ma}=2$ shock waves. However, using this closure a 7-moment approximation can also be built by setting $a_3=a_0+a_1+\frac{b_3}{b_2}(a_2-a_1)$. After numerical investigations, this closure, denoted $\mathrm{C1}_7$, seems to a similar region of hyperbolicity making it adequate for low-speed flows.

3.2.7. A new even-order hierarchy

Apart from the QMOM hierarchy, no other method reliably produces robust high even-order quadrature-based closures. As mentioned previously, the QMOM hierarchy always predicts moments on the realizability boundary thus being unable to recover equilibrium. Using the new technique presented above, a new hyperbolic and Galilean invariant even-moment hierarchy is constructed.

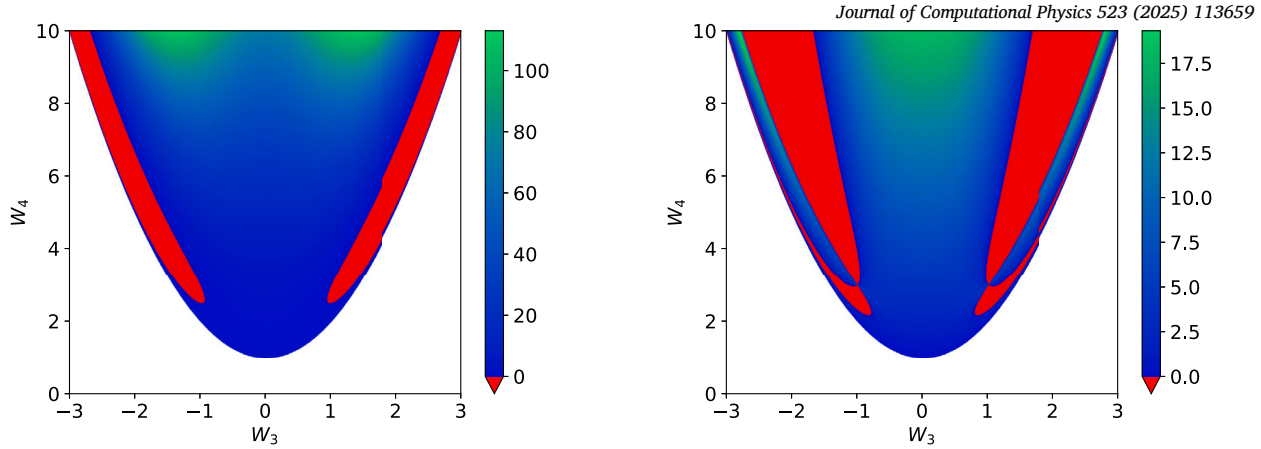

(a) Normalized b_3 (b) Normalized b_4

Fig. 1. Normalized b_3 and b_4 recurrence coefficients of the $C1_5$ closure. (For interpretation of the colours in the figure(s), the reader is referred to the web version of this article.)

Starting with the 4-moment closure, denoted B_4, the closing coefficient is chosen to be

$$b_2 = \beta_1 b_1 + \beta_2 (a_1 - a_0)^2 \,. \tag{43}$$

The constant $\beta_1 = 2$ was chosen in order to recover the equilibrium state while $\beta_2 = 1$ is necessary fulfill the requirement of Favard's theorem. The corresponding closing flux is,

$$W_4 = 2W_3^2 + 3 \,, \tag{44}$$

while the remaining recurrence coefficients are found as,

$$a_2 = \frac{W_3(3W_3^2+4)}{W_3^2+2} \qquad a_3 = \frac{2W_3}{W_3^2+2} \qquad b_3 = \frac{9W_3^4 + 20W_3^2 + 12}{(W_3^2+2)^2} \,. \tag{45}$$

The detailed derivation is presented in Appendix C. The same procedure, as shown for the 3-moment system, is followed. The derivations of the other higher-order closures are not included in this work since the resulting expressions are too large. However, they can be done easily using symbolic computing software. The 6-moment closure is found by assigning the closing coefficient to be,

$$b_3 = \beta_3 (b_1 + b_2) + \beta_4 \left[(a_2 - a_0)^2 + (a_2 - a_1)^2 \right] \,, \tag{46}$$

where, the constants are set to $\beta_3 = 1$ and $\beta_4 = \frac{1}{2}$ in order to recover equilibrium and maintain hyperbolicity. The closing flux can then be found to be,

$$\begin{aligned} W_6 = &-\frac{1}{2}\frac{3W_3^6 - 10W_3^4W_4 - 2W_3^4 + 6W_3^3W_5 + 7W_3^2W_4^2 + 8W_3^2W_4}{W_3^2 - W_4 + 1} \\ &+\frac{1}{2}\frac{14W_3W_4W_5 + 4W_4^3 - W_3^2 - 2W_3W_5 - 6W_4^2 + 4W_5^2 + 2W_4}{W_3^2 - W_4 + 1} \,. \end{aligned}$$

The recurrence coefficients a_4, a_5, b_4 and b_5 contain too many terms to be shown here. However, plots of the normalized b_4 and b_5 are shown for different values of W_5 in Figs. 2, 3 and 4. Observation of more than 100 slices, ranging from $W_5 = 0$ to $W_5 = 300$, along with extensive numerical experimentation show that the resulting closure seems to be strongly hyperbolic. As can be observed the b_4 and b_5 remain positive throughout the realizability domain. Furthermore, the resulting a_4, a_5 are real valued functions. Finally, following this pattern, the next member of this hierarchy, the 8-moment system, denoted B_8, is found by setting,

$$b_4 = \frac{2}{3}(b_1 + b_2 + b_3) + \frac{1}{3}\left[(a_3 - a_0)^2 + (a_3 - a_1)^2 + (a_3 - a_2)^2 \right] \,. \tag{47}$$

Again, the hyperbolicity of the 8-moment system has been investigated numerically. A general form for the closing coefficient, $b_{(n+1)/2}$, can be expressed as,

$$b_{(n+1)/2} = \frac{4}{(n-1)} \sum_{k=1}^{(n-1)/2} b_k + \frac{2}{(n-1)} \sum_{l=0}^{(n-1)/2} (a_{(n-1)/2} - a_l)^2 \tag{48}$$

allowing the computation of a closing flux, U_{n+1} of any even-order moment. Although no formal proof is available for hyperbolicity, extensive numerical investigation suggest that the hierarchy is robustly hyperbolic.

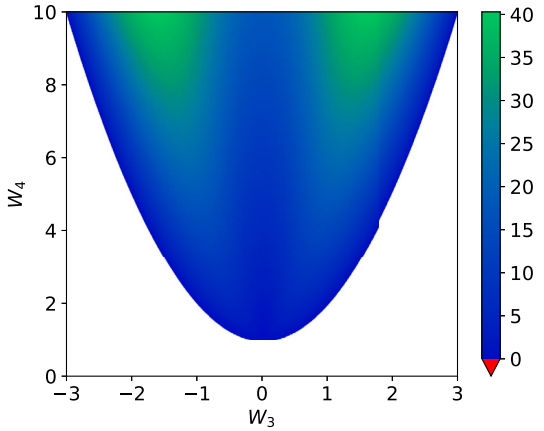

(a) Normalized b_4, $W_5 = 0$

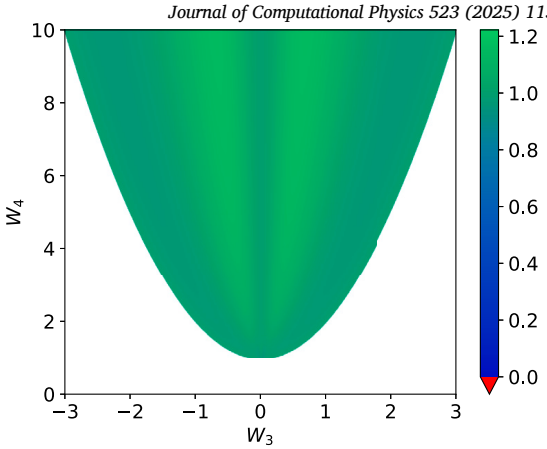

(b) Normalized b_5, $W_5 = 0$

Fig. 2. Normalized b_4 and b_5 recurrence coefficients of the B_6 closure for $W_5 = 0$.

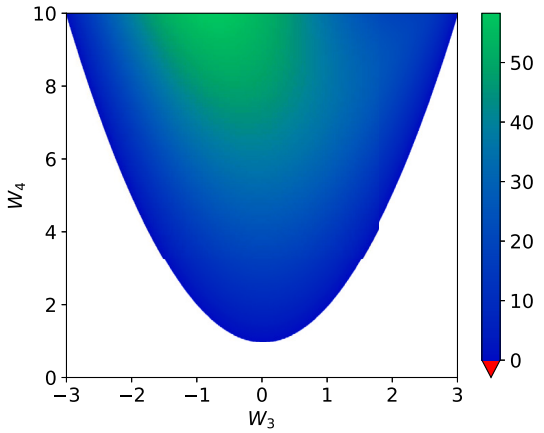

(a) Normalized b_4, $W_5 = 50$

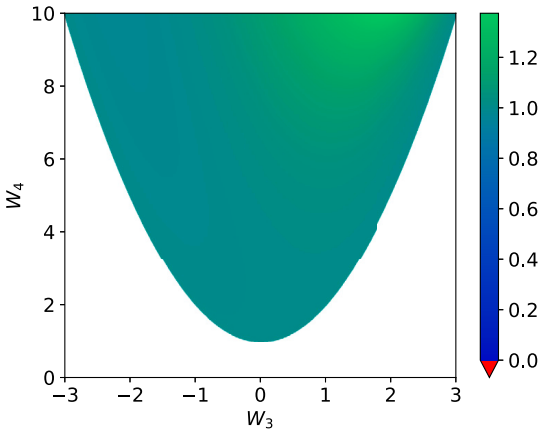

(b) Normalized b_5, $W_5 = 50$

Fig. 3. Normalized b_4 and b_5 recurrence coefficients of the B_6 closure for $W_5 = 50$.

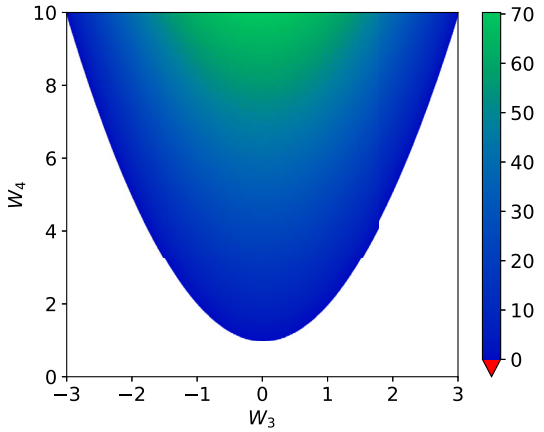

(a) Normalized b_4, $W_5 = 200$

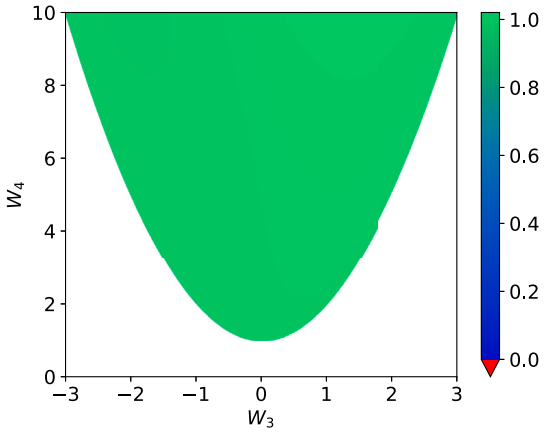

(b) Normalized b_5, $W_5 = 200$

Fig. 4. Normalized b_4 and b_5 recurrence coefficients of the B_6 closure for $W_5 = 200$.

4. Numerical results

In order to investigate the behaviour of the various moment closures discussed in the previous sections, solutions of a typical 1-D Riemann problem in the free-molecular, transition and continuum regimes are presented. Furthermore, a numerical investigation of the internal structure of stationary shock waves is shown. Comparisons are made between the moment models and the direct

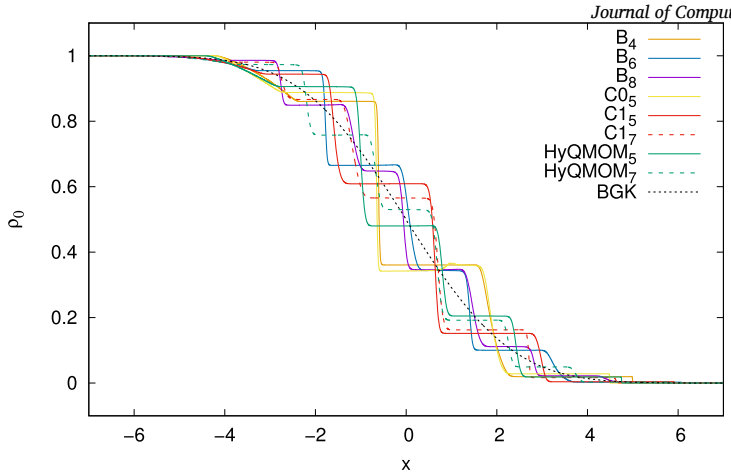

(a) Normalized density, Free-molecular

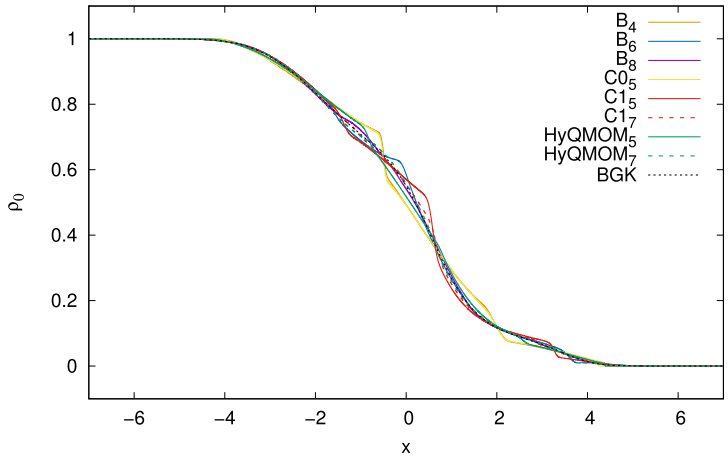

(b) Normalized density, $\tau = 10^{-3}$ s

Fig. 5. Numerical solution for the normalized density of 1-D Riemann problems as determined by moment models and direct numerical solutions of the BGK kinetic equation: (a) free-molecular regime, (b) transition regime.

numerical solution of the BGK equation, using the discrete-velocity method of Mieussens [26]. An upwind Godunov-type finite-volume scheme with HLL flux function [27] is used for the numerical solution of the moment equations. Wave speeds are determined by numerically computing the eigenvalues of the flux Jacobian. A first-order-accurate time-marching scheme is used that treats the hyperbolic left-hand side of the moment equations explicitly while employing a point-implicit treatment for the stiff right-hand side [25].

4.1. Numerical solutions of 1-D Riemann problems

Numerical solutions of a Riemann problem in the free-molecular, transition, and continuum regimes are used to illustrate the predictions of the different closures. For the free-molecular regime, the BGK source term was set to zero for all models, thus only displaying the collision less solution. The transition and continuum regime calculations were computed using $\tau = 10^{-3}$ s and $\tau = 10^{-6}$ s respectively. For all solutions of the BGK equation, velocity space is discretized using 1500 velocities spanning -5000 m/s to 5000 m/s. The initial conditions are given as,

$$x \leq 0 \begin{cases} \rho = 4.696 \quad \text{kg/m}^3 \\ u = 0 \quad \text{m/s} \\ p = 404400 \quad \text{Pa} \end{cases} \qquad x > 0 \begin{cases} \rho = 1.408 \quad \text{kg/m}^3 \\ u = 0 \quad \text{m/s} \\ p = 101100 \quad \text{Pa} \end{cases} . \tag{49}$$

For all calculations, a spacial discretization of 10,000 equal-sized cells is used on a computational domain -7 m $\leq x < 7$ m. All cases were run to a final $t = 0.006$ s. Figs. 5, 6, and 7 show the normalized density, the velocity, and the normalized heat transfer for both free-molecular and transition regimes. As expected, for the free-molecular case, a collection of discontinuities representing individual wave

64

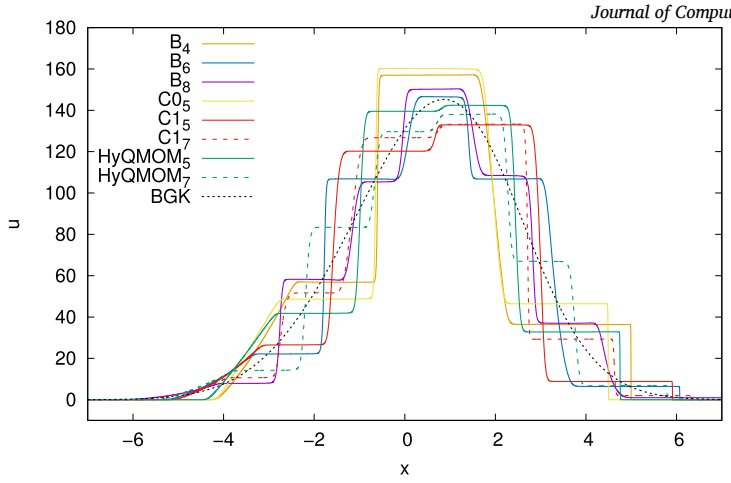

(a) Velocity, Free-molecular

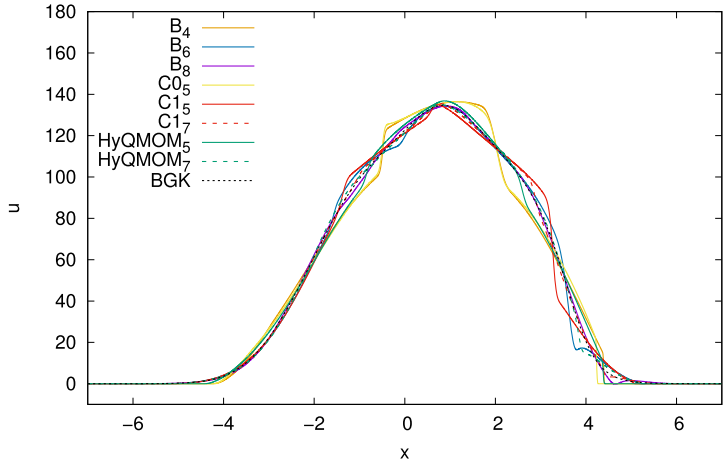

(b) Velocity, $\tau = 10^{-3}$ s

Fig. 6. Numerical solution for the velocity of 1-D Riemann problems as determined by moment models and direct numerical solutions of the BGK kinetic equation: (a) free-molecular regime, (b) transition regime.

speeds can be seen for each closure. Furthermore, higher-order moment models seems to provide better approximations, suggesting that in the limit of a large number of moments the BGK solution would be recovered. In the transition regime, a closer agreement from all the models is observed. However, minor deviations coming from the lower-order models are still present. Fig. 8 shows the density and velocity distributions in the continuum regime. As expected all models recover the Euler solution. The heat flux is not shown for the continuum regime as all models correctly predict essentially zero heat flux.

4.2. Numerical solutions of 1-D stationary shock waves

Numerical solutions of stationary shock waves of various strength are presented. This investigation allows for a better understanding of the different behaviour of the presented quadrature based closures. Numerical solutions are compared to the discretized BGK kinetic equation as well as a 5-moment maximum-entropy based approximations that has proven particularly successful in predicting strong shock wave internal structure. The maximum-entropy approximation, denoted MEF in this paper, was adopted from McDonald and Torrilhon [15].

For all calculations a spacial discretization of four thousand equal-sized cell is used. The relaxation time for the BGK collision operator is held fixed at a value of $\tau = 10^{-7}$ s. The computed results are therefore not physically accurate, since the relaxation time is expected to vary as function of the gas macroscopic properties. However, it does allow an evaluation of the behaviour of the closures for non-equilibrium flows. The upstream values of pressure and density are taken to be standard atmospheric values, 101 325 Pa and 1.225 kg/m^3, respectively. The upstream mean free path, λ, is taken to be $\lambda = 3.67 \times 10^{-7}$ m. This follows from the expression for hard-sphere collisional processes given by Bird [1]. Combined with the relation provided by the BGK collision operator linking the relaxation time and fluid viscosity, the mean free path can be expressed as

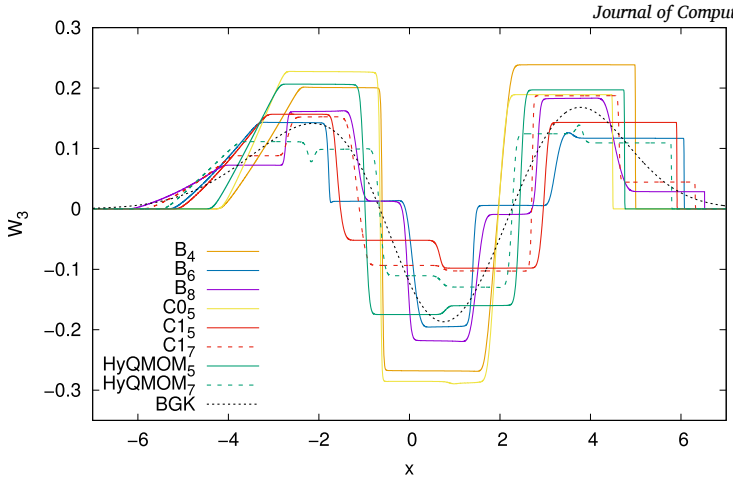

(a) Normalized heat flux, Free-molecular

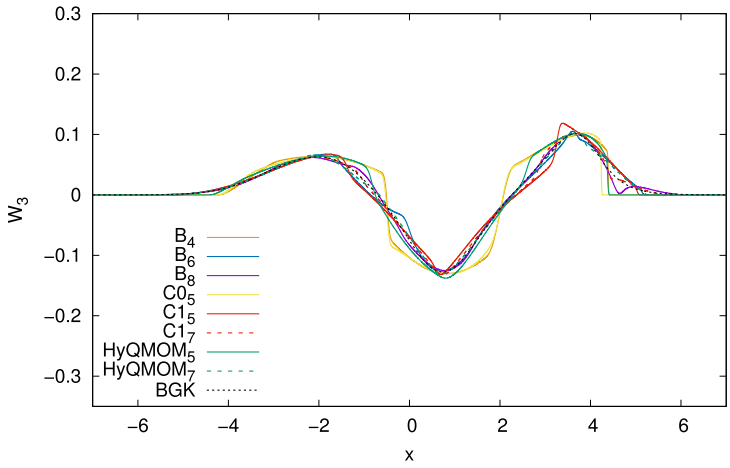

(b) Normalized heat flux, $\tau = 10^{-3}$ s

Fig. 7. Numerical solution for the normalized heat flux of 1-D Riemann problems as determined by moment models and direct numerical solutions of the BGK kinetic equation: (a) free-molecular regime, (b) transition regime.

$$\lambda = \frac{16\tau}{5}\sqrt{\frac{p}{2\pi\rho}}. \tag{50}$$

For the solution of the BGK equation, velocity space is discretized using 1500 velocities spanning -5000 m/s to 5000 m/s for the cases with an upstream Mach number of 2 and 4. For the case with an upstream Mach number of 6, 3000 velocities spanning -10,000 m/s to 10,000 m/s were used. Comparison is made to the BGK equation rather than the Boltzmann equation with the true collision operator so as to more accurately make a comparison to the moment closure. Since both solutions have the same collision operator, the only source of deviation is the moment approximation, which is the interest of this study.

Figs. 9, 11, and 13 show the numerical solutions of the density profile for the three different stationary shock waves, while Figs. 10, 12, and 14 display the normalized heat flux. The density was normalized to go from zero to one. As expected the maximum-entropy approximation performs well in capturing the shocks internal structures, as minimal deviation can be observed from the BGK solutions. It can be seen that the higher-order quadrature-based closures (B_6, $HyQMOM_7$, $C1_7$ and B_8) were also successfully predicting the BGK solutions especially for Ma $= 2$ shock wave. As the shock strength increases, discontinuities in the solutions, called sub-shocks becomes more apparent. This can be more easily seen in the normalized heat flux calculations. As expected, the lower-order closures (B_4, $C1_5$, and $HyQMOM_5$) do not perform nearly as well, even if the density profile is captured relatively well, strong sub-shocks can be observed even in the weakest shock wave calculations. Interestingly, the B_4 model perform surprisingly well, often displaying smaller sub-shocks than its 5-moments counterparts.

For hyperbolic balance laws, information travels at finite velocities that are described by the eigenvalues of the flux Jacobian. When considering 1D physics, the equilibrium speed of sound is given by $\sqrt{3\theta}$. For shock-structure predictions, if the incoming flow velocity is larger than the fastest equilibrium wave speed of the system, then all characteristics will point in the downstream direction and there is no possibility of upstream information propagation for smooth solutions. The only way the flow can transition

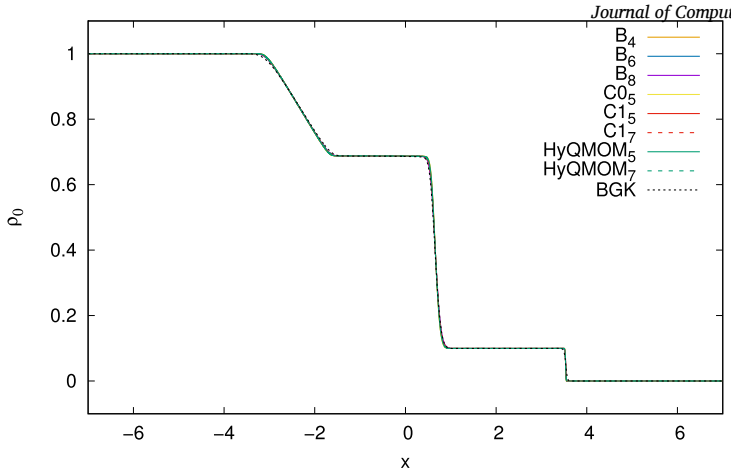

(a) Normalized density, $\tau = 10^{-6}$ s

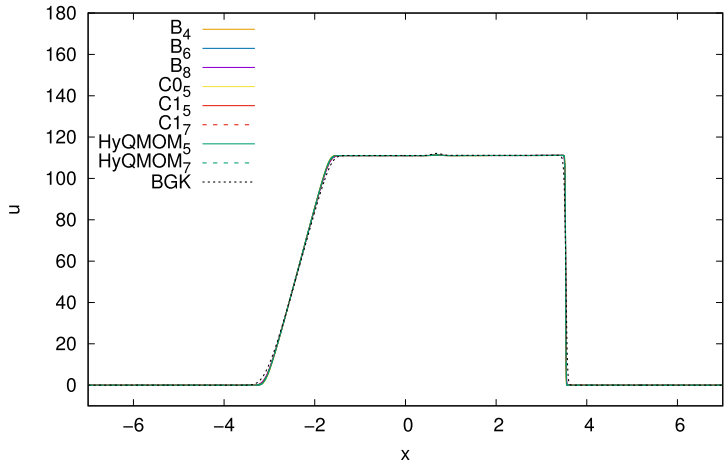

(b) Velocity, $\tau = 10^{-6}$ s

Fig. 8. Numerical solution of 1-D Riemann problems, in the continuum regime, as determined by moment models and direct numerical solutions of the BGK kinetic equation: (a) Normalized density, (b) Velocity.

to the downstream state is through an initial discontinuity, or sub-shock. Every quadrature based model presented in this study with the exception of the B_8 model posses equilibrium wave speeds that are insufficiently large for the smooth prediction of a Ma $= 2$ shock wave, corresponding to a normalized velocity of $2\sqrt{3} = 3.4641$. The B_4, HyQMOM$_5$, C0$_5$ and C1$_5$ models have an normalized equilibrium maximum wave speeds of $\lambda_{\max} = 2.33$, $\lambda_{\max} = 2.45$, $\lambda_{\max} = 2.33$ and $\lambda_{\max} = 2.87$ respectively. Furthermore, the B_6, HyQMOM$_7$, C1$_7$ and B_8 models have maximum wave speed of $\lambda_{\max} = 2.93$, $\lambda_{\max} = 3.04$, $\lambda_{\max} = 3.38$ and $\lambda_{\max} = 3.45$ respectively. For one-dimensional physics, this translates into a maximum Mach number under Ma $= 2$ for all closures expect for the B_8 model. The slow increase in equilibrium wave speed value with respect to the number of moments suggest that the presented quadrature-based moment closure hierarchies may not be ideal for high speed non-equilibrium flows if the internal structure of shock wave is of interest.

The 5-moment maximum-entropy based system seems to always produce smooth solutions. This can be explained by the presence of the Junk subspace, located above equilibrium [16]. This well documented artifact is also the reason why maximum-entropy based closure are generally able to produce smooth solutions. As the Junk subspace is approached and the closing flux becomes singular, the maximum wave speeds also become arbitrarily large. If the solution leaves equilibrium with a trajectory that takes it into a region of very high wave speeds, no sub-shock structure is expected as can be seen in the numerical results. This behaviour is explored and explained by M^{c}Donald and Torrilhon [25].

5. Conclusions

It as been demonstrated that globally hyperbolic closures can be reliably constructed using the technique presented in this work. This new technique is based on the HyQMOM theory, previously proposed by Fox and Laurent [20]. A novel even-order moment clo-

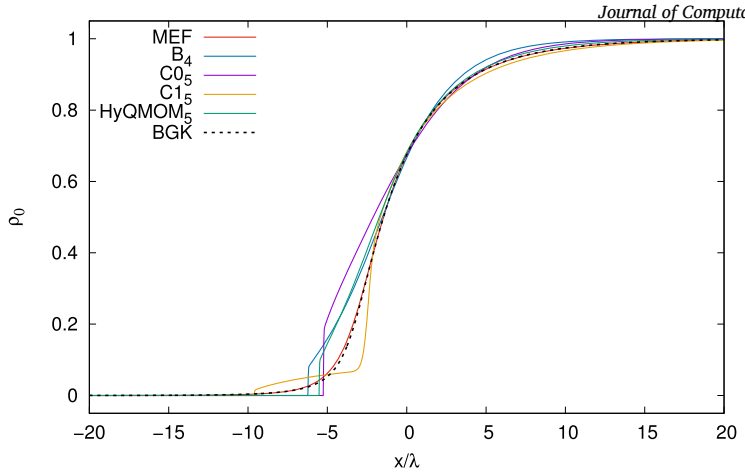

(a) Normalized density, lower-order closures

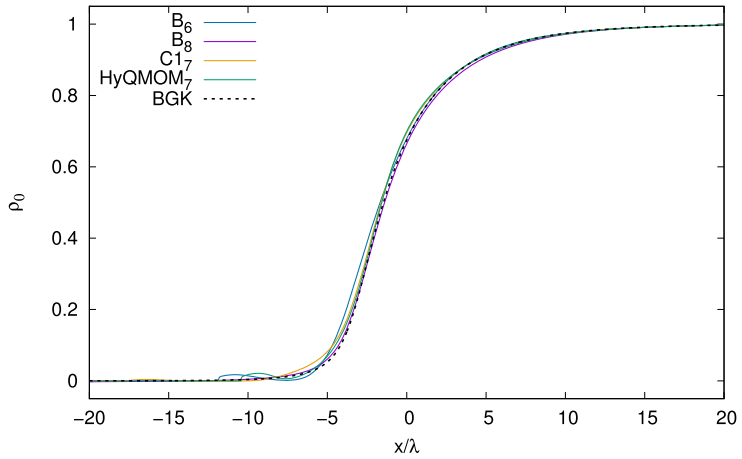

(b) Normalized density, higher-order closures

Fig. 9. Predicted normalized density across a Ma = 2, 1-D stationary shock wave as determined by quadrature-based moment models and direct numerical solutions of the BGK kinetic equation: (a) lower-order closures, (b) higher-order closures.

sure hierarchy has been developed using this method, along with several other ad-hock lower order closures. Numerical investigation into the accuracy and robustness of these new closure was conducted by solving a 1-D Riemann problem and shack waves structures. It was demonstrated that, the moment closures performs well for moderate shock strength. However, for high Mach number shocks, the presence of sub-shocks was observed in all moment methods.

CRediT authorship contribution statement

William Morin: Writing – original draft, Visualization, Software, Investigation, Formal analysis, Conceptualization. **James G. M^{c}Donald:** Writing – review & editing, Supervision, Resources, Conceptualization.

Funding

This work was supported by the Natural Sciences and Engineering Research Council of Canada (Grant No. RGPIN-2020-06295). The authors are very grateful for the support.

Declaration of competing interest

The authors declare that they have no known competing financial interests or personal relationships that could have appeared to influence the work reported in this paper.

68

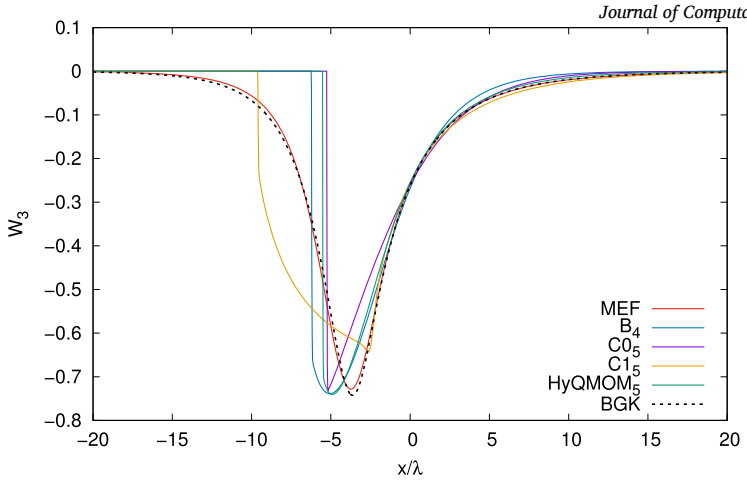

(a) Normalized heat flux, lower-order closures

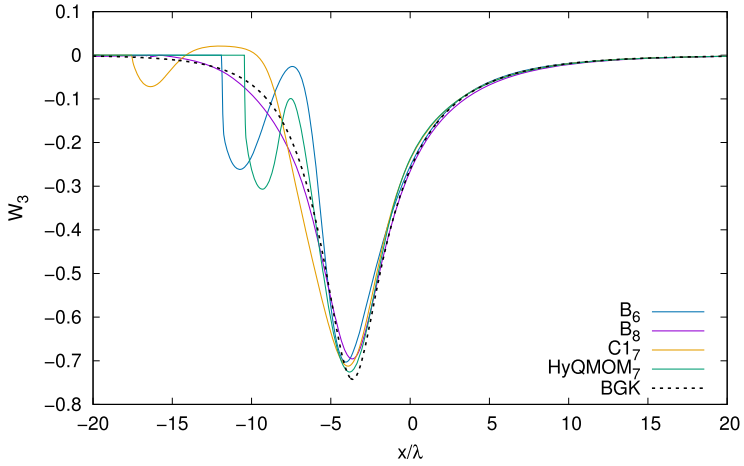

(b) Non dimensional heat flux, higher-order closures

Fig. 10. Predicted normalized heat flux across a Ma = 2, 1-D stationary shock wave as determined by quadrature-based moment models and direct numerical solutions of the BGK kinetic equation: (a) lower-order closures, (b) higher-order closures.

Appendix A. Quadrature-based closure from eigenvalue construction, 3-moment example

In order to illustrate the new method presented in this work, one can consider the Euler equations as an example, since the form of both the closing flux and the wave speeds are known. The flux Jacobian of any 3-moment system can be represented as

$$\frac{\mathrm{d}\boldsymbol{F}}{\mathrm{d}\boldsymbol{U}} = \begin{bmatrix} 0 & 1 & 0 \\ 0 & 0 & 1 \\ \lambda_0\lambda_1\lambda_2 & -(\lambda_0\lambda_1+\lambda_0\lambda_2+\lambda_1\lambda_2) & \lambda_0+\lambda_1+\lambda_2 \end{bmatrix}, \tag{A.1}$$

with the closing flux given by,

$$U_{n+1} = U_0\,(\lambda_0\lambda_1\lambda_2) - U_1\,(\lambda_0\lambda_1+\lambda_0\lambda_2+\lambda_1\lambda_2) + U_2\,(\lambda_0+\lambda_1+\lambda_2)\,. \tag{A.2}$$

The vector $\left(\frac{\partial U_{n+1}}{\partial \lambda}\right)_U$ can be computed easily,

$$\left(\frac{\partial U_{n+1}}{\partial \lambda}\right)_U = \begin{bmatrix} U_0\;\lambda_1\lambda_2 - U_1\;(\lambda_1+\lambda_2)+U_2 \\ U_0\;\lambda_0\lambda_2 - U_1\;(\lambda_0+\lambda_2)+U_2 \\ U_0\;\lambda_0\lambda_1 - U_1\;(\lambda_0+\lambda_1)+U_2 \end{bmatrix}^{\mathrm{T}}. \tag{A.3}$$

In general the matrix $\left(\frac{\partial \lambda}{\partial \boldsymbol{U}}\right)$ is not known since this would require one to know the exact form of the λs. However, by assuming that the wave speeds are Galilean invariant and scale correctly with the temperature, a general form can be assumed,

69

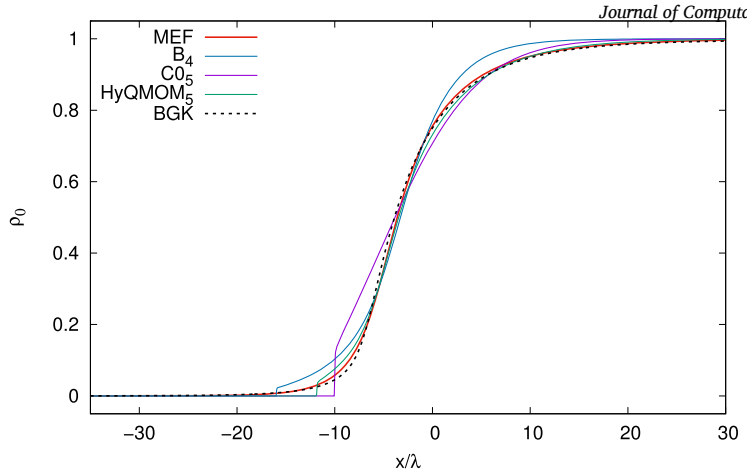

(a) Normalized density, lower-order closures

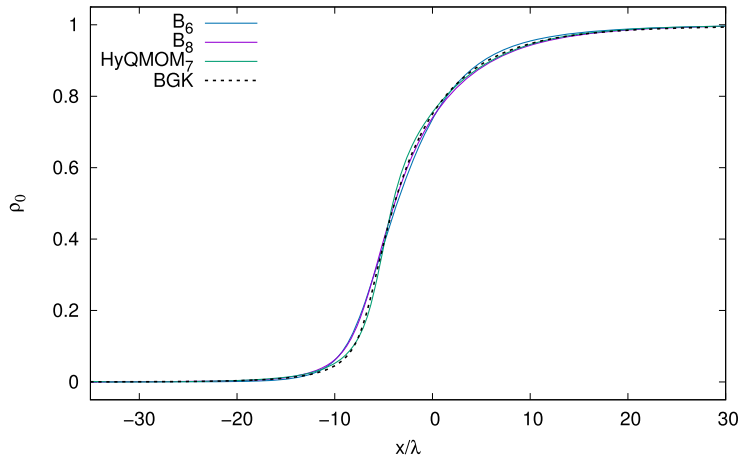

(b) Normalized density, higher-order closures

Fig. 11. Predicted normalized density across a Ma = 4, 1-D stationary shock wave as determined by quadrature based-moment models and direct numerical solutions of the BGK kinetic equation: (a) lower-order closures, (b) higher-order closures.

$$\lambda_i = u + \sqrt{\theta} f_i(W_3, W_4, \cdots, W_n), \tag{A.4}$$

where the f_i are unknown functions of the normalized moments. One can rewrite Eq. (27) in terms of the primitive and normalized moments,

$$\left(\frac{\partial \boldsymbol{\lambda}}{\partial \boldsymbol{U}}\right) = \left(\frac{\partial \boldsymbol{\lambda}}{\partial \boldsymbol{Y}}\right)\left(\frac{\partial \boldsymbol{U}}{\partial \boldsymbol{Y}}\right)^{-1}. \tag{A.5}$$

This leads to,

$$\left(\frac{\partial U_{n+1}}{\partial \boldsymbol{\lambda}}\right)_U \left(\frac{\partial \boldsymbol{\lambda}}{\partial \boldsymbol{Y}}\right) = 0, \tag{A.6}$$

where $\boldsymbol{Y} = [\rho, u, \theta, W_3, W_4, \cdots, W_n]^{\mathrm{T}}$. By taking the Jacobian between $\boldsymbol{Y}$ and $\boldsymbol{\lambda}$ one can show that the three first columns of $\left(\frac{\partial \boldsymbol{\lambda}}{\partial \boldsymbol{Y}}\right)$ are always,

$$\left(\frac{\partial \boldsymbol{\lambda}}{\partial \boldsymbol{Y}}\right) = \begin{bmatrix} 0 & 1 & \frac{f_0}{2\sqrt{\theta}} & \cdots \\ 0 & 1 & \frac{f_1}{2\sqrt{\theta}} & \cdots \\ 0 & 1 & \frac{f_2}{2\sqrt{\theta}} & \cdots \\ \vdots & \vdots & \vdots & \cdots \\ 0 & 1 & \frac{f_n}{2\sqrt{\theta}} & \cdots \end{bmatrix} \tag{A.7}$$

70

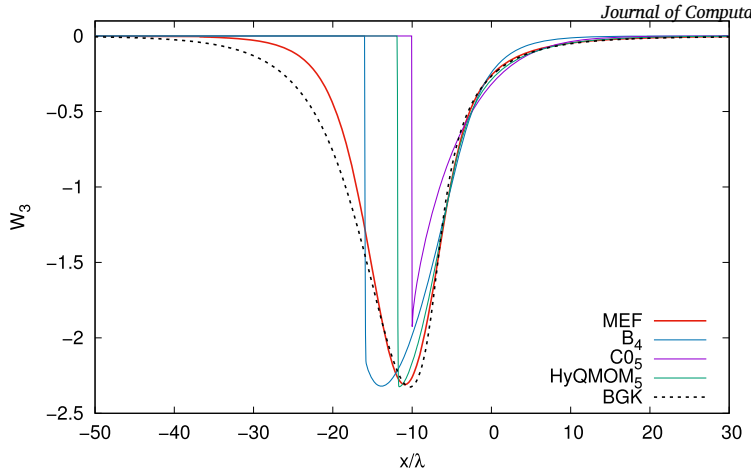

(a) Normalized heat flux, lower-order closures

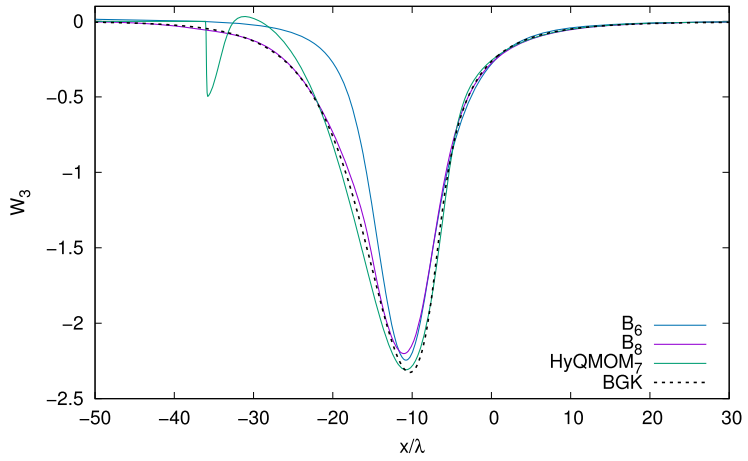

(b) Normalized heat flux, higher-order closures

Fig. 12. Predicted normalized heat flux across a Ma = 4, 1-D stationary shock wave as determined by quadrature-based moment models and direct numerical solutions of the BGK kinetic equation: (a) lower-order closures, (b) higher-order closures.

Using a simple change of variable, one can see that the first three columns of the following matrix span the same space,

$$\begin{bmatrix} 0 & 1 & \lambda_0 & \cdots \\ 0 & 1 & \lambda_1 & \cdots \\ 0 & 1 & \lambda_2 & \cdots \\ \vdots & \vdots & \vdots & \cdots \\ 0 & 1 & \lambda_n & \cdots \end{bmatrix} \tag{A.8}$$

Going back to the 3-moments case, this matrix simplifies to,

$$\begin{bmatrix} 0 & 1 & \lambda_0 \\ 0 & 1 & \lambda_1 \\ 0 & 1 & \lambda_2 \end{bmatrix}, \tag{A.9}$$

providing two equations that must be satisfied,

$$\left(\frac{\partial U_{n+1}}{\partial \lambda}\right)_U \cdot \mathbf{1} = 0 \qquad \left(\frac{\partial U_{n+1}}{\partial \lambda}\right)_U \cdot \lambda = 0\,. \tag{A.10}$$

Only using these two equations an infinite number of solutions can be found. However, assuming that no direction is preferred, a third equation needs to be considered, $\frac{\partial U_{n+1}}{\partial \lambda_0} = \frac{\partial U_{n+1}}{\partial \lambda_2}$, providing reflective symmetry in the x direction. This yields a unique real solution to the 3-moments system,

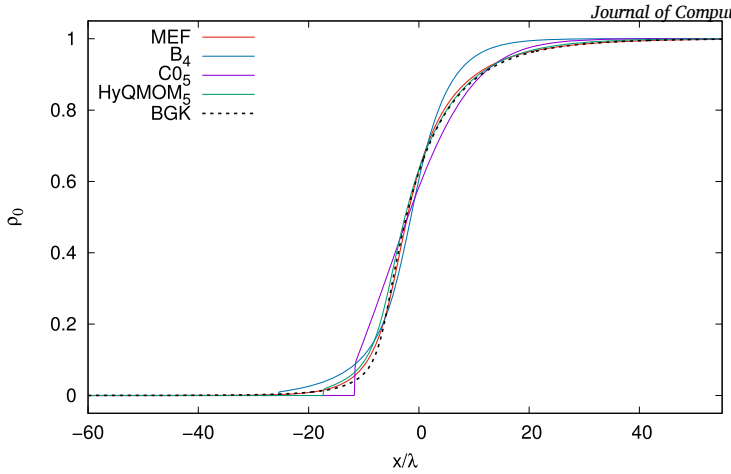

(a) Normalized density, lower-order closures

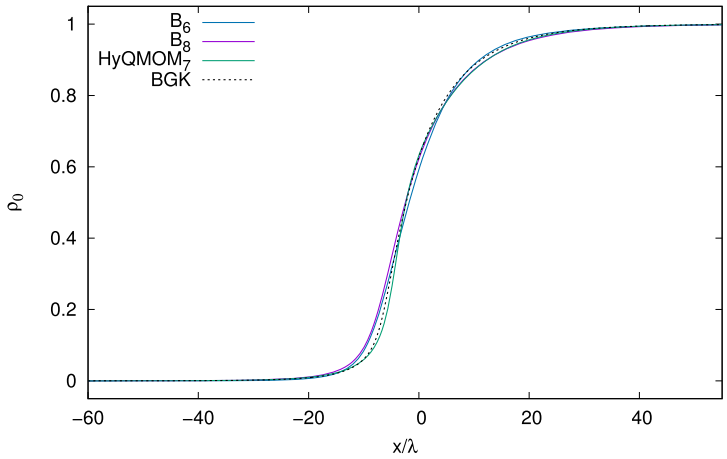

(b) Normalized density, higher-order closures

Fig. 13. Predicted normalized density across a Ma = 6, 1-D stationary shock wave as determined by quadrature-based moment models and direct numerical solutions of the BGK kinetic equation: (a) lower-order closures, (b) higher-order closures.

$$\lambda_0 = u - \sqrt{\theta}\,\sqrt{3} \qquad \lambda_1 = u \qquad \lambda_2 = u + \sqrt{\theta}\,\sqrt{3} \tag{A.11}$$

In order to use this technique for higher order moment systems further information is required. This information can come from a set of relations for the entries of $\left(\frac{\partial U_{n+1}}{\partial \lambda}\right)$, or by picking the general form of the wave speeds thus providing the entries of $\left(\frac{\partial \lambda}{\partial \boldsymbol{Y}}\right)$. Another important takeaway from this analysis is that Eq. (A.10) provides necessary constraints for the systems wave speeds to be Galilean invariant and scale correctly with the temperature.

Appendix B. Galilean invariance and correct temperature scaling, 3-moment example

Going back to the 3-moments case presented in Appendix A, the associated characteristic polynomial in terms of the wave speeds is given by,

$$P_{n+1} = v^3 - (\lambda_0+\lambda_1+\lambda_2)v^2 + (\lambda_0\lambda_1+\lambda_0\lambda_2+\lambda_1\lambda_2)v - \lambda_0\lambda_1\lambda_2\,, \tag{B.1}$$

leading to,

$$\left\langle P'_{n+1}\right\rangle = 3U_2 - 2(\lambda_0+\lambda_1+\lambda_2)U_1 + (\lambda_0\lambda_1+\lambda_0\lambda_2+\lambda_1\lambda_2)U_0 = 0$$
$$\left\langle vP'_{n+1}\right\rangle = (\lambda_0+\lambda_1+\lambda_2)U_2 - 2(\lambda_0\lambda_1+\lambda_0\lambda_2+\lambda_1\lambda_2)U_1 + 3\lambda_0\lambda_1\lambda_2\,U_0 = 0\,,$$

which, using Eq. (A.3), can be shown to be exactly

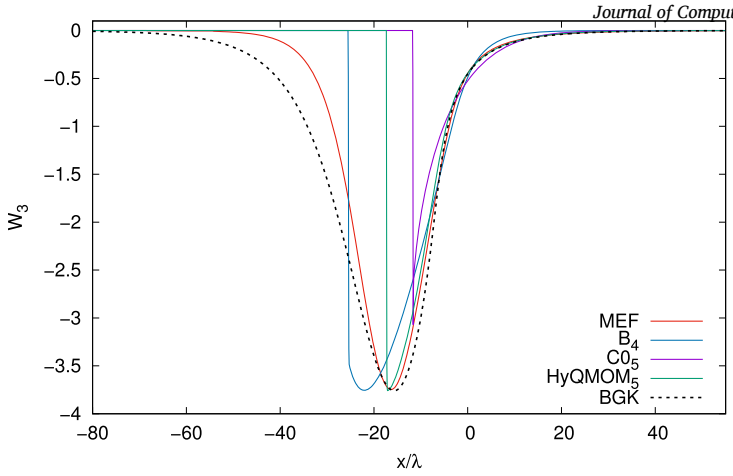

(a) Normalized heat flux, lower-order closures

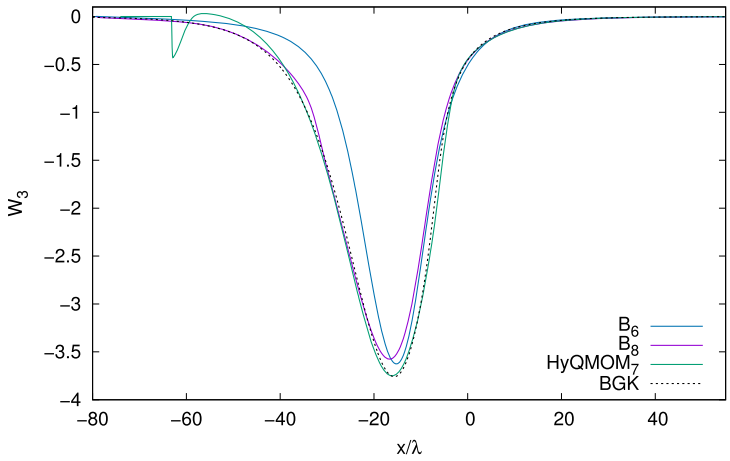

(b) Normalized heat flux, higher-order closures

Fig. 14. Predicted normalized heat flux across a Ma = 6, 1-D stationary shock wave as determined by quadrature-based moment models and direct numerical solutions of the BGK kinetic equation: (a) lower-order closures, (b) higher-order closures.

$$\left(\frac{\partial U_{n+1}}{\partial \lambda}\right)_U \cdot \mathbf{1} = 0 \qquad \left(\frac{\partial U_{n+1}}{\partial \lambda}\right)_U \cdot \lambda = 0\,. \tag{B.2}$$

Even if no formal proof is presented, this condition is believed to holds for any number of moments.

Appendix C. Derivation of the 4-moment system using the new approach

Here the proposed technique is derived for the 4-moment system. First, the sequence of orthogonal polynomials are first built until P_4 using the recurrence relations,

$$\begin{aligned}
P_0 =& 0\\
P_1 =& (v - a_0)\\
P_2 =& v^2 - (a_1 + a_0)v + a_1a_0 - b_1\\
P_3 =& v^3 - (a_2 + a_1 + a_0)v^2 + (-a_2(-a_1 - a_0) + a_1a_0 - b_1 - b_2)v - a_2(a_1a_0 - b_1) + b_2a_0\\
P_4 =& v^4 - (a_0 + a_1 + a_2 + a_3)v^3 + (a_0a_1 + a_0a_2 + a_0a_3 + a_1a_2 + a_1a_3 + a_2a_3 - b_1 - b_2 - b_3)v^2\\
&+ (-a_0a_1a_2 - a_0a_1a_3 - a_0a_2 * a_3 - a_1a_2a_3 + a_0b_2 + a_0b_3 + a_1b_3 + a_2b_1 + a_3b_1 + a_3b_2)v\\
&+ a_0a_1a_2a_3 - a_0a_1b_3 - a_0a_3b_2 - a_2a_3b_1 + b_1b_3
\end{aligned}$$

where the coefficient of the resulting characteristic polynomial (polynomial of the flux Jacobian) are,

$$
\begin{aligned}
A_0 =& a_0a_1a_2a_3 - a_0a_1b_3 - a_0a_3b_2 - a_2a_3b_1 + b_1b_3 \\
A_1 =& -a_0a_1a_2 - a_0a_1a_3 - a_0a_2a_3 - a_1a_2a_3 + a_0b_2 + a_0b_3 + a_1b_3 + a_2b_1 + a_3b_1 + a_3b_2 \\
A_2 =& a_0a_1 + a_0a_2 + a_0a_3 + a_1a_2 + a_1a_3 + a_2a_3 - b_1 - b_2 - b_3 \\
A_3 =& a_0 + a_1 + a_2 + a_3 .
\end{aligned}
$$

The first three recurrence coefficients $a_0 = U_1/U_0$, $b_1 = U_2/U_0 - U_1^2/U_0^2$ and $a_1 = (U_0^2U_3 - 2U_0U_1U_2 + U_1^3)/(U_0(U_0U_2 - U_1^2))$ can be computed directly using Eq. (31). The higher order coefficients contain moments that are not part of the solution vector. Since the condition shown in Eq. (42) must be satisfied, it is then used to build the following system of equations,

$$
\begin{aligned}
U_0\frac{\partial A_0}{\partial U_0} + U_1\frac{\partial A_1}{\partial U_0} + U_2\frac{\partial A_2}{\partial U_0} + U_3\frac{\partial A_3}{\partial U_0} = 0, \\
U_0\frac{\partial A_0}{\partial U_1} + U_1\frac{\partial A_1}{\partial U_1} + U_2\frac{\partial A_2}{\partial U_1} + U_3\frac{\partial A_3}{\partial U_1} = 0, \\
U_0\frac{\partial A_0}{\partial U_2} + U_1\frac{\partial A_1}{\partial U_2} + U_2\frac{\partial A_2}{\partial U_2} + U_3\frac{\partial A_3}{\partial U_2} = 0, \\
U_0\frac{\partial A_0}{\partial U_3} + U_1\frac{\partial A_1}{\partial U_3} + U_2\frac{\partial A_2}{\partial U_3} + U_3\frac{\partial A_3}{\partial U_3} = 0.
\end{aligned}
$$

The first equation is always automatically satisfied by choosing the system to be function of the scaled moments, $\tilde{\boldsymbol{U}}$. This is necessary for the moment system to be first-order homogeneous. After substituting a_0, b_1 and a_1 the equations simplifies as,

$$
\begin{aligned}
&-\Bigg(a_3a_2\tilde{U_1}^3\tilde{U_2} - a_3a_2\tilde{U_1}^2\tilde{U_3} - a_3a_2\tilde{U_1}\tilde{U_2}^2 + 2a_3b_2\tilde{U_1}^2\tilde{U_2} + a_3a_2\tilde{U_2}\tilde{U_3} + a_3\tilde{U_1}\tilde{U_2}\tilde{U_3} \\
&+ a_2\tilde{U_1}\tilde{U_2}\tilde{U_3} + 2\tilde{U_1}^2\tilde{U_2}\tilde{U_3} - 3\frac{\partial b_2}{\partial\tilde{U_1}}\tilde{U_1}^4\tilde{U_2} - a_3b_2\tilde{U_1}^4 + 3\frac{\partial b_2}{\partial\tilde{U_1}}\tilde{U_1}^2\tilde{U_2}^2 - a_3\tilde{U_1}^3\tilde{U_3} + a_3\tilde{U_1}^2\tilde{U_2}^2 \\
&- b_3\tilde{U_1}^3\tilde{U_2} - a_2\tilde{U_1}^3\tilde{U_3} + a_2\tilde{U_1}^2\tilde{U_2}^2 - 2b_2\tilde{U_1}^3\tilde{U_2} - a_3b_2\tilde{U_2}^2 + b_3\tilde{U_1}^2\tilde{U_3} + b_3\tilde{U_1}\tilde{U_2}^2 + b_2\tilde{U_1}\tilde{U_2}^2 - b_3\tilde{U_2}\tilde{U_3} \\
&- 2\tilde{U_1}\tilde{U_2}^3 - 2\tilde{U_1}\tilde{U_3}^2 + 2\tilde{U_2}^2\tilde{U_3} + \frac{\partial b_2}{\partial\tilde{U_1}}\tilde{U_1}^6 + b_2\tilde{U_1}^5 - \frac{\partial b_2}{\partial\tilde{U_1}}\tilde{U_2}^3 - a_3\tilde{U_2}^3 - a_2\tilde{U_2}^3\Bigg)\Big/\Big(\tilde{U_1}^2 - \tilde{U_2}\Big)^2 = 0,
\end{aligned}
$$

$$
\begin{aligned}
&-\Bigg(\frac{\partial b_2}{\partial\tilde{U_2}}\tilde{U_1}^6 - 3\frac{\partial b_2}{\partial\tilde{U_2}}\tilde{U_1}^4\tilde{U_2} - a_3a_2\tilde{U_1}^4 + 3\frac{\partial b_2}{\partial\tilde{U_2}}\tilde{U_1}^2\tilde{U_2}^2 + 2a_3a_2\tilde{U_1}^2\tilde{U_2} - a_3\tilde{U_1}^3\tilde{U_2} + b_3\tilde{U_1}^4 - a_2\tilde{U_1}^3\tilde{U_2} \\
&- \frac{\partial b_2}{\partial\tilde{U_2}}\tilde{U_2}^3 - a_3a_2\tilde{U_2}^2 + a_3\tilde{U_1}^2\tilde{U_3} + a_3\tilde{U_1}\tilde{U_2}^2 - 2b_3\tilde{U_1}^2\tilde{U_2} + a_2\tilde{U_1}^2\tilde{U_3} + a_2\tilde{U_1}\tilde{U_2}^2 - \tilde{U_1}^3\tilde{U_3} + 2\tilde{U_1}^2\tilde{U_2}^2 \\
&- a_3\tilde{U_2}\tilde{U_3} + b_3\tilde{U_2}^2 - a_2\tilde{U_2}\tilde{U_3} - \tilde{U_1}\tilde{U_2}\tilde{U_3} - \tilde{U_2}^3 + \tilde{U_3}^2\Bigg)\Big/\Big(\tilde{U_1}^2 - \tilde{U_2}\Big)^2 = 0,
\end{aligned}
$$

$$
-\Bigg(\frac{\partial b_2}{\partial\tilde{U_3}}\tilde{U_1}^4 - 2\frac{\partial b_2}{\partial\tilde{U_3}}\tilde{U_1}^2\tilde{U_2} + \frac{\partial b_2}{\partial\tilde{U_3}}\tilde{U_2}^2 + a_3\tilde{U_1}^2 + a_2\tilde{U_1}^2 - a_3\tilde{U_2} - a_2\tilde{U_2} - \tilde{U_1}\tilde{U_2} + \tilde{U_3}\Bigg)\Big/\Big(\tilde{U_1}^2 - \tilde{U_2}\Big) = 0.
$$

One can see that the system only depends on the choice of the closing coefficient, b_2, and its derivatives, all other derivatives simplifies in the process. This allows for the higher-order coefficients to be solved algebraically,

$$
\begin{aligned}
a_2 =& \Bigg(-\frac{\partial b_2}{\partial\tilde{U_3}}b_2\tilde{U_1}^4 - \frac{\partial b_2}{\partial\tilde{U_1}}\tilde{U_1}^4 - \frac{\partial b_2}{\partial\tilde{U_2}}\tilde{U_1}^3\tilde{U_2} + 2\frac{\partial b_2}{\partial\tilde{U_3}}b_2\tilde{U_1}^2\tilde{U_2} - \frac{\partial b_2}{\partial\tilde{U_3}}\tilde{U_1}^3\tilde{U_3} + 2\frac{\partial b_2}{\partial\tilde{U_1}}\tilde{U_1}^2\tilde{U_2} + \frac{\partial b_2}{\partial\tilde{U_2}}\tilde{U_1}^2\tilde{U_3} \\
&+ \frac{\partial b_2}{\partial\tilde{U_2}}\tilde{U_1}\tilde{U_2}^2 - \frac{\partial b_2}{\partial\tilde{U_3}}b_2\tilde{U_2}^2 + 3\frac{\partial b_2}{\partial\tilde{U_3}}\tilde{U_1}\tilde{U_2}\tilde{U_3} - \frac{\partial b_2}{\partial\tilde{U_3}}\tilde{U_2}^3 - b_2\tilde{U_1}^3 - \frac{\partial b_2}{\partial\tilde{U_1}}\tilde{U_2}^2 - \frac{\partial b_2}{\partial\tilde{U_2}}\tilde{U_2}\tilde{U_3} \\
&- \frac{\partial b_2}{\partial\tilde{U_3}}\tilde{U_3}^2 + 2b_2\tilde{U_1}\tilde{U_2} - b_2\tilde{U_3}\Bigg)\Big/\Big(b_2(\tilde{U_1}^2 - \tilde{U_2})\Big), \\
a_3 =& \Bigg((\tilde{U_1}^2 - \tilde{U_2})(\tilde{U_1}\tilde{U_2} - \tilde{U_3})\frac{\partial b_2}{\partial\tilde{U_2}} + (\tilde{U_1}^3\tilde{U_3} - 3\tilde{U_1}\tilde{U_2}\tilde{U_3} + \tilde{U_2}^3 + \tilde{U_3}^2)\frac{\partial b_2}{\partial\tilde{U_3}} \\
&+ ((\tilde{U_1}^2 - \tilde{U_2})\frac{\partial b_2}{\partial\tilde{U_1}} + b_2\tilde{U_1})(\tilde{U_1}^2 - \tilde{U_2})\Bigg)\Big/\Big(b_2(\tilde{U_1}^2 - \tilde{U_2})\Big), \\
b_3 =& \Bigg(-((\tilde{U_1}^2 - \tilde{U_2})^2b_2 + \tilde{U_1}^3\tilde{U_3} - 3\tilde{U_1}\tilde{U_2}\tilde{U_3} + \tilde{U_2}^3 + \tilde{U_3}^2)(\tilde{U_1}^3\tilde{U_3} - 3\tilde{U_1}\tilde{U_2}\tilde{U_3} + \tilde{U_2}^3 + \tilde{U_3}^2)\frac{\partial b_2}{\partial\tilde{U_3}}^2 \\
&+ (-(\tilde{U_1}\tilde{U_2} - \tilde{U_3})(\tilde{U_1}^2 - \tilde{U_2})((\tilde{U_1}^2 - \tilde{U_2})^2b_2 + 2\tilde{U_1}^3\tilde{U_3} - 6\tilde{U_1}\tilde{U_2}\tilde{U_3} + 2\tilde{U_2}^3 + 2\tilde{U_3}^2)\frac{\partial b_2}{\partial\tilde{U_2}}
\end{aligned}
$$

74

$$
\begin{aligned}
&- (\tilde{U_1}^2 - \tilde{U_2})^2((\tilde{U_1}^2 - \tilde{U_2})^2 b_2 + 2\tilde{U_1}^3\tilde{U_3} - 6\tilde{U_1}\tilde{U_2}\tilde{U_3} + 2\tilde{U_2}^3 + 2\tilde{U_3}^2)\frac{\partial b_2}{\partial \tilde{U_1}} \\
&- b_2((\tilde{U_1}^2 - \tilde{U_2})^2(\tilde{U_1}^3 - \tilde{U_3})b_2 + (2(\tilde{U_1}^3 - 1.5\tilde{U_1}\tilde{U_2} + 0.5\tilde{U_3}))(\tilde{U_1}^3\tilde{U_3} - 3\tilde{U_1}\tilde{U_2}\tilde{U_3} + \tilde{U_2}^3 + \tilde{U_3}^2)))\frac{\partial b_2}{\partial \tilde{U_3}} \\
&- ((\tilde{U_1}^2 - \tilde{U_2})(\tilde{U_1}\tilde{U_2} - \tilde{U_3})^2\frac{\partial b_2}{\partial \tilde{U_2}}^2 + (2(\tilde{U_1}^2 - \tilde{U_2})^2(\tilde{U_1}\tilde{U_2} - \tilde{U_3})\frac{\partial b_2}{\partial \tilde{U_1}} \\
&+ (2(0.5(\tilde{U_1}^2 - \tilde{U_2})^2 b_2 + (\tilde{U_1}\tilde{U_2} - \tilde{U_3})(\tilde{U_1}^3 - 1.5\tilde{U_1}\tilde{U_2} + 0.5\tilde{U_3})))b_2)\frac{\partial b_2}{\partial \tilde{U_2}} \\
&+ ((\tilde{U_1}^2 - \tilde{U_2})^2\frac{\partial b_2}{\partial \tilde{U_1}}^2 + (2(\tilde{U_1}^3 - 1.5\tilde{U_1}\tilde{U_2} + 0.5\tilde{U_3}))b_2\frac{\partial b_2}{\partial \tilde{U_1}} \\
&+ b_2^2(\tilde{U_1}^2 - \tilde{U_2}))(\tilde{U_1}^2 - \tilde{U_2}))(\tilde{U_1}^2 - \tilde{U_2})\Big)\Big/\Big(b_2^2(\tilde{U_1}^2 - \tilde{U_2})^2\Big).
\end{aligned}
$$

The resulting relations are significantly larger than ones obtained for the 3-moment system. However, the process is exactly the same. The closing coefficient, b_2 need to be chosen such that the coefficients a_2 and a_3 remain real valued and b_3 remains positive. Once b_2 is chosen and the derivatives are evaluated, the system, can be normalized ($\tilde{U_1} = 0$ and $\tilde{U_2} = 1$). An infinite number of closures can be found this way, but in this work, the closing coefficient was set to $b_2 = 2b_1 + (a_1 - a_0)^2$. The higher order recurrence coefficients are found as,

$$
a_2 = \frac{W_3(3W_3^2 + 4)}{W_3^2 + 2} \qquad a_3 = \frac{2W_3}{W_3^2 + 2} \qquad b_3 = \frac{9W_3^4 + 20W_3^2 + 12}{(W_3^2 + 2)^2}, \tag{C.1}
$$

fulfilling the requirements of Favard theorem. The associated closing flux can easily be found using the definition of b_2,

$$
b_2 = \frac{\langle P_2^2 \rangle}{\langle P_1^2 \rangle} = 2b_1 + (a_1 - a_0)^2,
$$

allowing to solve for $W_4 = 2W_3^2 + 3$. Furthermore the resulting characteristic polynomial can be shown to respect Eq. (32).

Data availability

Data will be made available on request.

References

[1] G.A. Bird, Molecular Gas Dynamics and the Direct Simulation of Gas Flows, Clarendon Press, Oxford, 1994.
[2] Q. Sun, I.D. Boyd, A direct simulation method for subsonic, microscale gas flow, J. Comput. Phys. 179 (2002) 400–425.
[3] A.V. Bobylev, The Chapman-Enskog and Grad methods for solving the Boltzmann equation, Sov. Phys. Dokl. 27 (1) (1982) 29–31.
[4] H. Grad, On the kinetic theory of rarefied gases, Commun. Pure Appl. Math. 2 (1949) 331–407.
[5] I. Müller, T. Ruggeri, Rational Extended Thermodynamics, Springer-Verlag, New York, 1998.
[6] S.L. Brown, P.L. Roe, C.P.T. Groth, Numerical solution of a 10-moment model for nonequilibrium gasdynamics, Paper 95-1677, AIAA, June 1995.
[7] M. Torrilhon, Modeling nonequilibrium gas flow based on moment equations, Annu. Rev. Fluid Mech. 48 (2016) 429–458.
[8] H. Struchtrup, M. Torrilhon, H theorem, regularization, and boundary conditions for the linearized 13 moment equations, Phys. Rev. Lett. 99 (2007) 014502.
[9] H. Struchtrup, T. Thatcher, Bulk equations and Knudsen layers for the regularized 13 moment equations, Contin. Mech. Thermodyn. 19 (2007) 177–189.
[10] Z. Cai, Y. Fan, R. Li, Globally hyperbolic regularization of Grad's moment system in one dimensional space, Commun. Math. Sci. 11 (2) (2013) 547–571.
[11] Z. Cai, Y. Fan, R. Li, Globally hyperbolic regularization of Grad's moment system, Commun. Pure Appl. Math. 67 (3) (2014) 464–514.
[12] W. Dreyer, Maximization of the entropy in non-equilibrium, J. Phys. A, Math. Gen. 20 (1987) 6505–6517.
[13] I. Müller, T. Ruggeri, Extended Thermodynamics, Springer-Verlag, New York, 1993.
[14] C.D. Levermore, Moment closure hierarchies for kinetic theories, J. Stat. Phys. 83 (1996) 1021–1065.
[15] J.G. McDonald, M. Torrilhon, Affordable robust moment closures for CFD based on the maximum-entropy hierarchy, J. Comput. Phys. 251 (2013) 500–523.
[16] M. Junk, Domain of definition of Levermore's five-moment system, J. Stat. Phys. 93 (5/6) (1998) 1143–1167.
[17] F. Giroux, J.G. McDonald, An approximation for the twenty-one-moment maximum-entropy model of rarefied gas dynamics, Int. J. Comput. Fluid Dyn. 35 (8) (2021) 632–652.
[18] R. McGraw, Description of aerosol dynamics by the quadrature method of moments, Aerosol Sci. Technol. 27 (2) (1997) 255–265.
[19] R.O. Fox, A quadrature based third-order moment method for dilute gas-particle flows, J. Comput. Phys. 227 (2008) 6313–6350.
[20] R.O. Fox, F. Laurent, Hyperbolic quadrature method of moments for the one-dimensional kinetic equation, SIAM J. Appl. Math. 82 (2) (2022) 750–771.
[21] R.O. Fox, F. Laurent, A. Passalacqua, The generalized quadrature method of moments, J. Aerosol Sci. 167 (2023).
[22] R.O. Fox, Higher-order quadrature-based moment methods for kinetic equations, J. Comput. Phys. 228 (2009) 7771–7791.
[23] H.L. Hamburger, Hermitian transformations of deficiency-index (1, 1), jacobian matrices, and undetermined moment problems, Am. J. Math. 66 (1944) 489–552.
[24] P.L. Bhatnagar, E.P. Gross, M. Krook, A model for collision processes in gases. I. small amplitude processes in charged and neutral one-component systems, Phys. Rev. 94 (3) (1954) 511–525.
[25] J.G. McDonald, C.P.T. Groth, Towards realizable hyperbolic moment closures for viscous heat-conducting gas flows based on a maximum-entropy distribution, Contin. Mech. Thermodyn. 25 (2013) 573–603.
[26] L. Mieussens, Discrete velocity model and implicit scheme for the BGK equation of rarefied gas dynamics, Math. Models Methods Appl. Sci. 10 (8) (2000) 1121–1149.
[27] A. Harten, P.D. Lax, B. van Leer, On upstream differencing and Godunov-type schemes for hyperbolic conservation laws, SIAM Rev. 25 (1) (1983) 35–61.

Chapter 5

Third Journal Publication: Applications of Orthogonal-Polynomial-Based One-Dimensional Moment Closures to Plasma Flows

Following the success of the new hierarchy in predicting non-equilibrium gas flows, this third paper investigates the applicability of these new moment closures to plasma flows. Plasma are notoriously difficult to model accurately using fluid models [52, 53, 54] especially when dealing with situations where collisional effects are small or negligible. This study is primarily focused on low-temperature plasma flows applications such as Hall thrusters discharges. To this effect, two canonical plasma problems featuring both collisional and collisionless regimes are used to access the proposed closures capabilities and limitations. First, ions in a stationary electric potential are considered, followed by linear Landau damping calculations. The following manuscript was submitted to a peer-reviewed journal but is not yet published.

Applications of Orthogonal-Polynomial-Based One-Dimensional Moment Closures to Plasma Flows

William Morin and James G. M^{c}Donald

[a]*Department of Mechanical Engineering, University of Ottawa, 161 Louis-Pasteur, Ottawa, K1N 6N5, ON, Canada*

Abstract

The applicability of a novel hierarchy of orthogonal-polynomial-based moment closures (OPMC) to plasma physics is investigated. Direct discretization of the Vlasov-Poisson-BGK system of equations is often prohibitively expensive for many practical problems. The orthogonal-polynomial-based moment closures, recently introduced by Morin and M^{c}Donald, are a computationally advantageous alternative to direct discretization or Lagrangian particle approaches, such as Direct Simulation Monte Carlo (DSMC). This is because they are able to provide a noise-free solutions without excessive computational cost. Numerical solutions of two canonical plasma physics problems are investigated to assess the applicability and challenges of this moment-closure technique. Good agreement could be observed for cases in the transition regime, where collisional effects are of moderate importance. However, for the collision-less cases, the proposed closures were only producing sensible approximations at relatively early times. Furthermore, distribution functions predicted by the Vlasov-Poisson-BGK system are compared to the closures associated quadrature-based distribution functions demonstrating that these methods can be seen as discrete velocity schemes with a velocity grid that automatically adapts to the local flow state.

Keywords:
hyperbolic moment closures, kinetic theory of gases, quadrature-based method of moments

1. Introduction

The development of models that accurately predict non-equilibrium phenomena, such as supersonic gas flows or plasma flows for a wide range of Knudsen number, has proven difficult. Traditional methods, typically involving some equilibrium assumption, such as the Navier-Stokes equations often fail to reliably capture these phenomena accurately.

Kinetic theory commonly describes the motion of large collections of classical gas particles through its velocity distribution function (VDF). The accurate computation of the time evolution of this distribution function through the Boltzmann equation or the Vlasov-Poisson system of equations enables the study of numerous physical phenomena ranging from supersonic or rarefied gas flows [1, 2, 3], plasma physics [4, 5, 6, 7], quantum hydrodynamics [8, 9] and others [10, 11]. Due to the high number of independent variables required to describe these kinetic equations, direct discretization is prohibitively expensive for most problems. Lagrangian particle approaches such as Direct Simulation Monte Carlo (DSMC) can also be computationally intensive while being subject to statistical noise [12]. The cost linked to stochastic particle methodologies becomes particularly prohibitive when aiming for time-accurate computations or low speed flow [13]. The use of moment methods for the prediction of non-equilibrium flows have been shown to offer some modeling and numerical advantages over other methods [1, 14].

Moment closure was found to be a promising method for simplifying kinetic equations into fluid models [15, 16, 17, 18]. The resulting first-order balance laws provide a stable hyperbolic treatment of local thermal non-equilibrium effects through their inclusion in the solution vector. Moment closures also have the potential for more convenient numerical solutions than traditional fluid-dynamic equations, (e.g., the Navier–Stokes equations) which require the evaluation of second order derivatives. Only computing first derivatives can allow for an extra order of spatial accuracy to be obtained for a given stencil while making numerical solutions of system of moment equations considerably less sensitive to grid irregularities [19]. Furthermore, as opposed to typical Lagrangian approaches, moment closures provide noise-free approximations to the Boltzmann equation or Vlasov-Poisson system of equations.

Traditional moment closures do, unfortunately, also suffer from numerical and modeling issues. The original hierarchy proposed by Grad [1] was found to have a restrictive region of hyperbolicity. This is due to the fact that the flux Jacobian can develop complex eigenvalues for moderate departures from equilibrium [20]. The Grad closures are built using an expansion of the equilibrium distribution (Maxwellian) in Hermite polynomials. Due to the polynomial nature of the resulting VDF, this method is not guaranteed to predict strictly positive distribution functions. Other authors have proposed regularized moment systems to extend the robustness of the closures, consequently adding non-conservative terms into the moment system [20, 21]. Thus, these closure sacrifice balance-law form.

The maximum-entropy hierarchy of moment closure, originally proposed by Dreyer[22], Muller & Ruggeri [23] and Levermore [24] has gained in popularity in the past decades. The resulting moment system was shown to produce accurate predictions of non-equilibrium flows, while guaranteeing global hyperbolicity [3]. However, as shown by Junk [25], there exists flow states for which a maximum-entropy VDF cannot be constructed. Moreover, for closure of sufficiently high order to include a treatment for heat transfer, it is not possible to write the closing fluxes in closed-form, thus requiring approximations, which are currently only available for a limited number of moments [3, 26]. Quadrature based methods, on the other hand, have been shown to offer more flexibility in producing stable hyperbolic moment equations while yielding a system of hyperbolic balance-laws. First introduced by McGraw [27] in the context of aerosol dynamics description, Fox developed the QMOM hierarchy [28] and later with the contribution of Laurent, the HyQMOM hierarchy [29] providing hyperbolic stable moment closure models for one-dimensional gases, though only for closures with a odd number of moments.

1.1. Scope of study

More recently, Morin and M^{c}Donald proposed a new globally hyperbolic even-order closures hierarchy [30]. These new closures were shown to provide accurate approximations for non-equilibrium gas flows. However, plasmas are notoriously difficult to model using moment methods. Investigation into the robustness of various moment methods was recently conducted outlining the applicability of these closures to plasma physics [31, 32, 7, 33]. Similarly, this work explores the robustness of the new closures. Primarily focusing to low-temperature plasma flows applications, such as could be encountered in Hall thrusters discharges. Canonical plasma problems featuring both collisional and collisionless regimes are used to access each model's capabilities and limitations. Furthermore, it is demonstrated that these methods can be seen as discrete velocity schemes with a velocity grid that automatically adapts to the local flow state.

2. Moment closures

Moment closures follow from the field of gaskinetic theory. In this theory, a monatomic gas is described by a probability density function, $\mathcal{F}(x_i, v_i, t)$, that describes the probability of finding a gas particle at a

given position, x_i , with a velocity, v_i, at a time, t. In most cases, only a small number of macroscopic properties are of interest and not all the information contained in the distribution function is necessary. These macroscopic properties can be obtained by taking moments of the distribution function. The present work only consider a one-dimensional VDF. That is, $\mathcal{F}(x, v, t)$, is defined for $(x, v, t) \in \mathbb{R} \times \mathbb{R} \times \mathbb{R}^+$. For a one-dimensional treatment, the following are examples of moments of the distribution function yielding macroscopic properties of interest:

$$\rho = \int m\mathcal{F}\,\mathrm{d}v = \langle m\mathcal{F}\rangle\ , \qquad \rho u = \langle mv\mathcal{F}\rangle\ ,$$
$$\rho\theta = \left\langle mc^2\mathcal{F}\right\rangle\ , \qquad Q = \left\langle mc^3\mathcal{F}\right\rangle\ ,$$
$$r = \left\langle mc^4\mathcal{F}\right\rangle\ , \qquad s = \left\langle mc^5\mathcal{F}\right\rangle\ .$$

The notation, $\langle\cdot\rangle$, is used to denote the integral over all velocity space, m is the mass of one particle, ρ is the mass density, u is the bulk velocity, $c = v - u$ is the peculiar component of the particle velocity, θ is the temperature, and Q is the heat-flux. The macroscopic quantities r and s are associated with the fourth- and fifth-order moment. Moment of the full particle velocity, often called convective moments, are denoted by U_n,

$$U_n = \langle mv^n\mathcal{F}\rangle\ , \tag{1}$$

with $n \in \mathbb{N}$. A vector of such moments can be defined as, $\boldsymbol{U} = [U_0, U_1, \cdots, U_n]^{\mathrm{T}}$. The normalized moments, W_n, are constructed by shifting the probability distribution function in velocity space resulting in a zero bulk velocity, followed by a non-dimensionalization such that $\rho = 1$ and $\theta = 1$,

$$W_n = \frac{1}{\rho}\left(\frac{1}{\theta}\right)^{n/2}\langle mc^n\mathcal{F}\rangle \quad \text{for} \quad n > 2 \in \mathbb{N}\,. \tag{2}$$

The resulting normalized moment vector has the form $\boldsymbol{\mathcal{W}}_n = [1, 0, 1, W_3 \cdots, W_n]^{\mathrm{T}}$.

2.1. The Vlasov-Poisson-BGK system

Plasma are multi-component collections of charged and neutral particles which typically behave quite differently than gases. For plasma flows, the movement of electrically charged particles, such as electron and ions, induces electromagnetic fields which affect the fluid flow as a whole. Furthermore, at high temperatures, some particles have enough energy to ionize neutral particles through collisions.

In this work two different canonical idealized plasma problems are considered. First, a single ion species subjected to an imposed electric field is studied. The evolution of such a kinetic system is governed by the Vlasov-BGK equation,

$$\frac{\partial\mathcal{F}}{\partial t} + v\frac{\partial\mathcal{F}}{\partial x} - \frac{q}{m}E\frac{\partial\,\mathcal{F}}{\partial v} = \frac{\delta\mathcal{F}}{\delta t}\,, \tag{3}$$

where q is the electric charge of the particles, E is the imposed electric field and $\frac{\delta\mathcal{F}}{\delta t}$ represent the collision operator. The second term of Eq. (3) represents the convective contribution to the time evolution, while the third term describes the acceleration effects on the charged particles due to the electric field. For this study, it is assumed that the collective motion of the charges does not generate a significant magnetic field. The second case assumes a fully ionized plasma consisting of only two species (electron and ions). In the limit of small electron to ions mass ratio the two-component kinetic plasma equations describing the time

evolution of the electron VDF can be reduced to,

$$\frac{\partial \mathcal{F}_e}{\partial t} + v\frac{\partial \mathcal{F}_e}{\partial x} - \frac{q}{m}E\frac{\partial\, \mathcal{F}_e}{\partial v} = \frac{\delta \mathcal{F}_e}{\delta t}\,. \tag{4}$$

$$\frac{\partial^2 \Phi}{\partial^2 x} = -\frac{1}{\epsilon_0}\left(e\rho_e - q_i\rho_i\right)\,, \tag{5}$$

where e is the fundamental charge, q_i is the ion charge and Φ is the electric potential with $E = -\frac{\partial \Phi}{\partial x}$. The electrons are assumed to exist within a uniform background of positively charged ions. This Vlasov-Poisson system has become a benchmark to study the accuracy of different closures, since the evolution of $\mathcal{F}_e$ can develop fine-scale structure that are difficult to numerically capture [34]. This system also exhibits non-collisional damping, typically referred to as Landau damping, which has proved challenging to compute accurately [32, 31].

In this work the simple BGK relaxation-time collision operator [35] is used to close the right hand-side of Eqs. (4) and (3),

$$\frac{\delta \mathcal{F}}{\delta t} = -\frac{\mathcal{F} - \mathcal{M}}{\tau}\,, \tag{6}$$

where τ is the characteristic relaxiation time and $\mathcal{M}$ is the local equilibrium distribution (Maxwellian),

$$\mathcal{M} = \frac{\rho}{m}\left(\frac{1}{2\pi\theta}\right)^{\frac{3}{2}}\exp\left(\frac{1}{2\theta}c^2\right)\,. \tag{7}$$

In order to obtain a set of PDEs describing the evolution of the properties of interest, velocity moments of the Vlasov-BGK equation are taken,

$$\frac{\partial}{\partial t}\left\langle m\boldsymbol{\mathcal{W}}\mathcal{F}\right\rangle + \frac{\partial}{\partial x}\left\langle mv\boldsymbol{\mathcal{W}}\mathcal{F}\right\rangle - \left\langle \frac{q}{m}E\ \boldsymbol{\mathcal{W}}\frac{\partial \mathcal{F}}{\partial v}\right\rangle = \left\langle m\boldsymbol{\mathcal{W}}\frac{\delta \mathcal{F}}{\delta t}\right\rangle\,, \tag{8}$$

$$\frac{\partial}{\partial t}\left\langle m\boldsymbol{\mathcal{W}}\mathcal{F}\right\rangle + \frac{\partial}{\partial x}\left\langle mv\boldsymbol{\mathcal{W}}\mathcal{F}\right\rangle = -\left\langle \frac{q}{m}E\ \mathcal{F}\ \frac{\partial \boldsymbol{\mathcal{W}}}{\partial v}\right\rangle + \left\langle m\boldsymbol{\mathcal{W}}\frac{\delta \mathcal{F}}{\delta t}\right\rangle\,, \tag{9}$$

where, $\boldsymbol{\mathcal{W}}$ is a vector of velocity momonials, $\boldsymbol{\mathcal{W}} = [1, v, v^2, \cdots, v^n]^{\mathrm{T}}$. This allows one to write the equation as,

$$\frac{\partial \boldsymbol{U}}{\partial t} + \frac{\partial \boldsymbol{F}}{\partial x} = -\boldsymbol{S} + \boldsymbol{C}_{\mathrm{BGK}}\,, \tag{10}$$

where $\boldsymbol{U}$ is the solution vector containing the moment of interest, $\boldsymbol{F}$ is the flux vector, $\boldsymbol{S}$ is a source vector accounting for the particles acceleration due to the electric field and $\boldsymbol{C}_{\mathrm{BGK}}$ is the source vector adding the effect of inter-partical collisions. This system of equations can be represented in vector form as,

$$\boldsymbol{U} = \begin{bmatrix} U_0 \\ U_1 \\ U_2 \\ U_3 \\ \vdots \\ U_n \end{bmatrix} \qquad \boldsymbol{F} = \begin{bmatrix} U_1 \\ U_2 \\ U_3 \\ U_4 \\ \vdots \\ U_{n+1} \end{bmatrix} \qquad \boldsymbol{S} = \begin{bmatrix} 0 \\ \left(\frac{q}{m}E\right)\ U_0 \\ 2\left(\frac{q}{m}E\right)\ U_1 \\ 3\left(\frac{q}{m}E\right)\ U_2 \\ \vdots \\ n\left(\frac{q}{m}E\right)\ U_{n-1} \end{bmatrix} \qquad \boldsymbol{C}_{\mathrm{BGK}} = \begin{bmatrix} -(U_0 - M_0)/\tau \\ -(U_1 - M_1)/\tau \\ -(U_2 - M_2)/\tau \\ -(U_3 - M_3)/\tau \\ \vdots \\ -(U_n - M_n)/\tau \end{bmatrix}\,, \tag{11}$$

where, M_n are the moment of the Maxwellian distribution. Unfortunately, this method does not lead to a closed set of equations, since the time evolution of a given moment always depend on the spacial divergence of a moment that is one order higher. Consequently, the last entry of the flux vector, U_{n+1}, unknown.

A popular technique to close the system is to prescribe a form for the VDF. This technique has been particularity successful and is at the center of many moment-closure hierarchies. The assumed distribution function, $\mathcal{F}$, should contain the same number of free parameters as there are moments of interest. The value of these parameters is chosen to maintain agreement with the macroscopic properties (moments). It is then possible to express the closing flux, U_{n+1}, as a function of the known moments by integrating the assumed distribution function, which is now known.

2.2. Quadrature based moment closures

As mentioned in the previous section, many strategies for the construction of the VDF have been studied in the past decades. Some distribution function are obtained using expansions around the Maxwellian while others are formed by solving an entropy maximization problem. However, it can be shown that every hyperbolic one-dimensional closure can be represented as quadrature-based method where the associated VDF is as a weighted sum of Dirac deltas [36],

$$\mathcal{F} = \sum_{i=0}^{n} \mathfrak{W}_i \delta(v - \lambda_i)\,. \tag{12}$$

The λ_i are the positions of each quadrature point and $\mathfrak{W}_i$ are the associated weights. The weights can be calculated from known moments through,

$$\boldsymbol{V}\boldsymbol{\mathfrak{W}} = \boldsymbol{U}\,, \tag{13}$$

while the flux is computed as,

$$\boldsymbol{F} = \boldsymbol{V}\boldsymbol{\Omega}\boldsymbol{\mathfrak{W}} = \boldsymbol{V}\boldsymbol{\Omega}\boldsymbol{V}^{-1}\boldsymbol{U} \tag{14}$$

with

$$\boldsymbol{V} = \begin{bmatrix} 1 & 1 & 1 & \cdots & 1 \\ \lambda_0 & \lambda_1 & \lambda_2 & \cdots & \lambda_n \\ \lambda_0^2 & \lambda_1^2 & \lambda_2^2 & \cdots & \lambda_n^2 \\ \vdots & & \cdots & & \vdots \\ \lambda_0^n & \lambda_1^n & \lambda_2^n & \cdots & \lambda_n^n \end{bmatrix}, \qquad \boldsymbol{\Omega} = \begin{bmatrix} \lambda_0 & 0 & 0 & \cdots & 0 \\ 0 & \lambda_1 & 0 & \cdots & 0 \\ \vdots & 0 & \ddots & 0 & \vdots \\ 0 & \cdots & 0 & \lambda_{n-1} & 0 \\ 0 & \cdots & 0 & 0 & \lambda_n \end{bmatrix}. \tag{15}$$

For the resulting closure to be hyperbolic, the flux Jacobian needs to have real eigenvalues and the quadrature point positions, λ_i, are also required to be the system wave speeds [30]. This second requirement allows the flux Jacobin to be expressed as

$$\frac{d\boldsymbol{F}}{d\boldsymbol{U}} = \boldsymbol{V}\,\boldsymbol{\Omega}\,\boldsymbol{V}^{-1}\,. \tag{16}$$

3. Orthogonal-polynomial-based closure

In this section, the construction of a orthogonal-polynomial-based closure hierarchy is briefly reviewed. This hierarchy, recently introduced by Morin & M$^{\text{c}}$Donald [30], was shown to be a good addition to the well known HyQMOM hierarchy of odd-order closures, as it provides the even-order closures. The resulting closures were shown to produce reliable, strongly hyperbolic moment systems that have produced accurate solutions for traditional gas-flow problems, both in and out of local equilibrium.

3.1. Closure construction using orthogonal polynomials

Orthogonal polynomials of a single variable defined by moment of a non-negative distribution function have the following properties. Applying the Gram-Schmidt process to the momomials, allows orthogonal polynomials, P_n, to be written in terms of the moments of the distribution,

$$P_n = \det \begin{bmatrix} U_0 & U_1 & U_2 & \cdots & U_n \\ U_1 & U_2 & U_3 & \cdots & U_{n+1} \\ \vdots & \vdots & \vdots & \ddots & \vdots \\ U_{n-1} & U_n & U_{n+1} & \cdots & U_{2n-1} \\ 1 & v & v^2 & \cdots & v^n \end{bmatrix} , \tag{17}$$

where the system of polynomials that are always orthogonal to each other, i.e., $\langle P_n P_m \rangle = \langle P_n^2 \rangle \ \delta_{nm}$. The resulting polynomials are known to also satisfy the three-term recurrence relation, allowing one to build them sequentially,

$$P_{n+1} = (1 - a_n)P_n - b_n P_{n-1} , \tag{18}$$

with, $P_0 = 1$ and

$$a_n = \frac{\langle v P_n^2 \rangle}{\langle P_n^2 \rangle} , \qquad\qquad b_n = \frac{\langle P_n^2 \rangle}{\langle P_{n-1}^2 \rangle} . \tag{19}$$

Using this technique, the nature of the polynomial roots can determined. Following Favard's theorem, the roots of P_{n+1} are guarantied to be real and distinct if the recurrence coefficients a_n are real-valued functions of the known moments and the b_n are strictly positive.

Using this recurrence relation, the flux Jacobain characteristic polynomial can be built from the monic polynomials up to the $n+1$ order. The first recurrence coefficients of the series can be easily calculated in terms of normalized moments, $\boldsymbol{W} = [1, 0, 1, W_3, W_4, \cdots, W_n]^{\mathrm{T}}$ as,

$$\begin{aligned} a_0 &= \left\langle v P_0^2 / P_0^2 \right\rangle = 0 \\ a_1 &= W_3 & b_1 &= 1 \\ a_2 &= \frac{W_3^3 - 2W_3 W_4 + W_5}{W_4 - W_3^2 - 1} & b_2 &= W_4 - W_3^2 - 1 \\ &\vdots & &\vdots \\ a_n &= \left\langle v P_n^2 / P_n^2 \right\rangle & b_n &= \left\langle P_n^2 / P_{n-1}^2 \right\rangle . \end{aligned}$$

However, the closing flux cannot be calculated directly by taking moments of the resulting polynomial, since it contains higher-order moments that are not part of the solution vector. In order to close the system, one needs to choose the form of this closing flux such that all the recurrence coefficients fulfill the requirements of Favard's theorem. The closing flux, U_{n+1}, is always completely determined by choosing the form of the closure coefficient. The term "closure coefficient" does not refer to the highest-order recurrence coefficient of the characteristic polynomial, but rather to the first coefficient containing the closing flux. For even moment systems (system containing an even number of entries in the solution vector), the associated closure coefficient is always given by $b_{(n+1)/2}$. Similarly, for odd moment systems, the closure coefficient is given by $a_{n/2}$. All higher recurrence coefficients become fixed after this choice as there is a one to one relation between the closure coefficient and the closing flux. However, choosing the closing coefficient such that Favards theorem is fulfilled is not trivial.

3.2. OPMC-B hierarchy

Following the technique shown above, the orthogonal polynomial-based closures are constructed, providing a strongly hyperbolic and Galilean invariant even-moment hierarchy [30].

The first member of this hierarchy is the 4-moment closure, denoted B_4, the closing coefficient is taken to be

$$b_2 = \beta_1 b_1 + \beta_2 (a_1 - a_0)^2 \,. \tag{20}$$

The constant $\beta_1 = 2$ was chosen in order to recover the equilibrium moment state while $\beta_2 = 1$ is necessary fulfill the requirement of Favard's theorem. The corresponding closing flux is,

$$W_4 = 2W_3^2 + 3 \,. \tag{21}$$

For this closure, the higher-order recurrence coefficients are found as,

$$a_3 = \frac{2W_3}{W_3^2 + 2} \qquad\qquad b_3 = \frac{9W_3^4 + 20W_3^2 + 12}{(W_3^2 + 2)^2} \,, \tag{22}$$

where a_3 is a real function and b_3 is always positive. Similarly, the 6-moment closure B_6 is obtained by setting the closing coefficient to be,

$$b_3 = \beta_3 (b_1 + b_2) + \beta_4 \left[(a_2 - a_0)^2 + (a_2 - a_1)^2 \right] \,, \tag{23}$$

where, the constants are set to $\beta_3 = 1$ and $\beta_4 = \frac{1}{2}$ in order to recover equilibrium and maintain hyperbolicity. The resulting closing flux is given by,

$$\begin{aligned} W_6 = &- \frac{1}{2} \frac{3W_3^6 - 10W_3^4 W_4 - 2W_3^4 + 6W_3^3 W_5 + 7W_3^2 W_4^2 + 8W_3^2 W_4}{W_3^2 - W_4 + 1} \\ &+ \frac{1}{2} \frac{14W_3 W_4 W_5 + 4W_4^3 - W_3^2 - 2W_3 W_5 - 6W_4^2 + 4W_5^2 + 2W_4}{W_3^2 - W_4 + 1} \,. \end{aligned}$$

The higher-order recurrence coefficients a_4, a_5, b_4 and b_5 are too large to be displayed here. However, extensive numerical experimentation shows that the resulting closure is strongly hyperbolic [30] as the b_4 and b_5 remain positive throughout the realizability domain and the a_4, a_5 are real valued functions.

The next member of this hierarchy, the 8-moment system, denoted B_8, is found by setting,

$$b_4 = \frac{2}{3}(b_1 + b_2 + b_3) + \frac{1}{3} \left[(a_3 - a_0)^2 + (a_3 - a_1)^2 + (a_3 - a_2)^2 \right] \,. \tag{24}$$

Again, the hyperbolicity of the 8-moment system have been investigated numerically. Following this pattern, a general form for the closing coefficient, $b_{(n+1)/2}$, can be expressed as,

$$b_{(n+1)/2} = \frac{4}{(n-1)} \sum_{k=1}^{(n-1)/2} b_k + \frac{2}{(n-1)} \sum_{l=0}^{(n-3)/2} (a_{(n-1)/2} - a_l)^2 \tag{25}$$

allowing the computation of a closing flux, U_{n+1} of any even-order moment.

4. Numerical results

In order to investigate the applicability of the proposed closures to plasma physics, classical cases of ions in a stationary wave and linear Landau damping are studied. Comparisons are made between the moment models and the direct numerical solution of the Vlasov-Poisson-BGK system using a discrete-velocity method. An upwind Godunov-type finite-volume scheme with HLL flux function [37] is used for the numerical solution of the moment equations. Wave speeds are determined by numerically computing the eigenvalues of the flux Jacobian. A first-order-accurate time-marching scheme is used that treats the hyperbolic left-hand side of the moment equations explicitly while employing a point-implicit treatment for the stiff right-hand side [36].

4.1. Numerical solutions of ions in a stationary wave

A periodic system with an imposed sinusoidal longitudinal electric field is considered. The strongly non-equilibrium kinetic solution of such problems consist in a progressive rolling up (in phase space) of the initial distribution function, leading to the development of filamentation. This problem has been studied extensively, and analytical kinetic solutions are available [38, 34]. In this section, investigation into the accuracy of the different moment closures is conducted for the original collision-less case along with cases in the transition regime.

The time evolution of the moment method is computed on a periodic one-dimensional domain. Ions are initially uniformly distributed in the spacial domain, following a 1D1V Maxwellian with zero average velocity and a initial non-dimensional temperature, $\hat{W}_2/\hat{W}_0 = 1$. Here, the symbols documented with a hat signify the initial value. The imposed electric potential is given by,

$$\Phi = V_0 \cos(kx)\,, \tag{26}$$

where the wave number, k, was chosen to have four peaks through the spacial domain, $k = 2N\pi/L$ with $N = 4$ and $L = 3$. The corresponding electric field is,

$$E = kV_0 \sin(kx)\,. \tag{27}$$

For all cases, the electric potential amplitude is prescribed to be $V_0 = 5\hat{W}_2/\hat{W}_0$. Since the initial ion temperature is fixed, the potential amplitude completely determines the problem dynamics. The ions with initial energy lower than V_0 will be trapped within one trough of the electric field profile. However, the ions with initial energy larger than the electric potential amplitude will be perturbed but still escape the electric barrier [34]. All moment solutions are computed on a grid of 7500 equal-sized cells, while the kinetic solutions are computed using 2500×2500 grid cells in physical and velocity space. All computations are non-dimensionalized such that $\hat{\rho} = 1$, $\hat{\theta} = 1$ and $L = 3$. The Knudsen number, $\mathrm{Kn} = \frac{\lambda}{l}$, is proportional to the collision time scale, τ. In all calculation the characteristic length scale is set to $l = 1$ m. Following the expression for hard-sphere collisional processes given by Bird [12], combined with the relation provided by the BGK collision operator linking the relaxation time and fluid properties, the mean free path is estimated as

$$\lambda = \frac{16\tau}{5}\sqrt{\frac{\hat{\theta}}{2\pi}}\,. \tag{28}$$

Figure 1, shows the predicted density and normalized heat flux as determined by the moment models for the collisionless case as compared to the kinetic solution for two different non-dimensional times. One

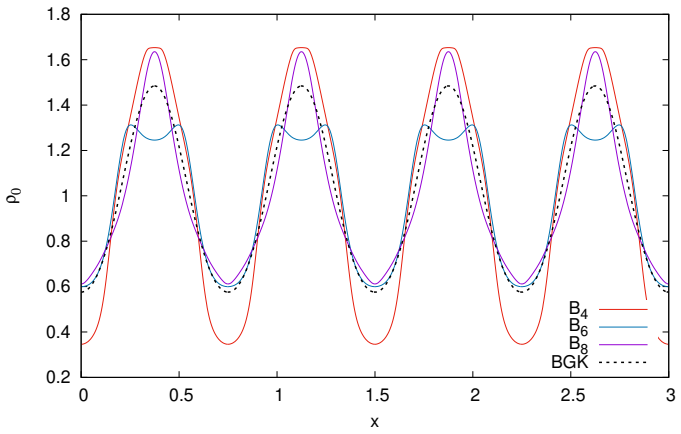

(a) density, $t = 0.35$

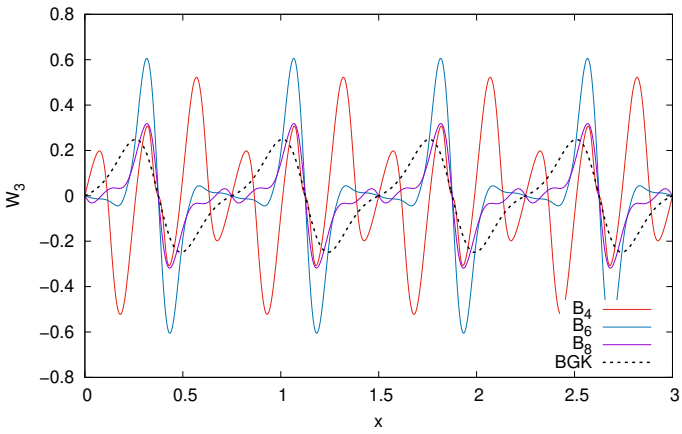

(b) normalized heat flux, $t = 0.35$

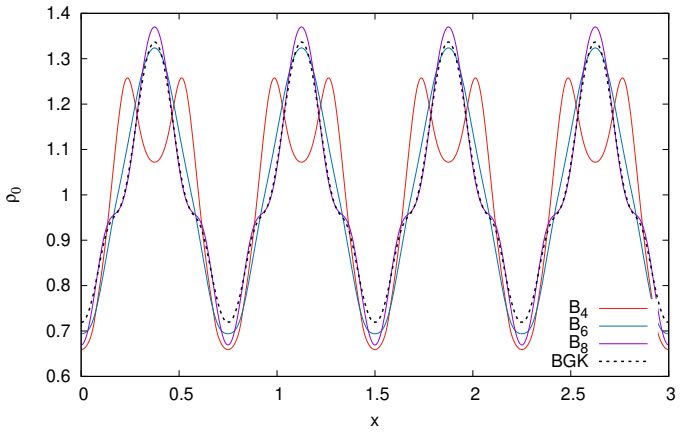

(c) density, $t = 0.75$

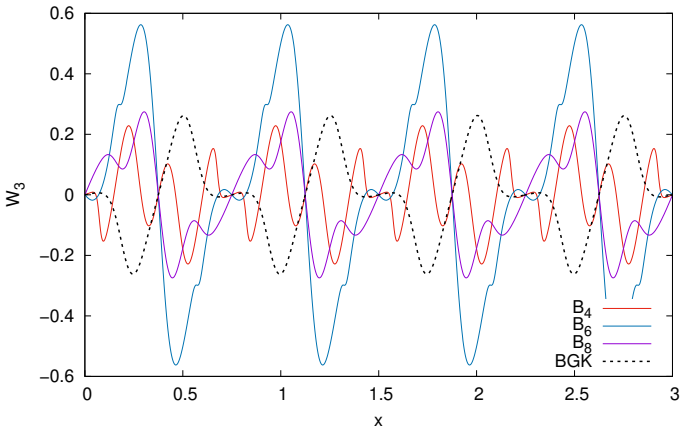

(d) normalized heat flux, $t = 0.75$

Figure 1: Predicted density and normalized heat flux of ions in the free molecular regime as determined by the moment models and direct numerical solutions of the Vlasov kinetic equation.

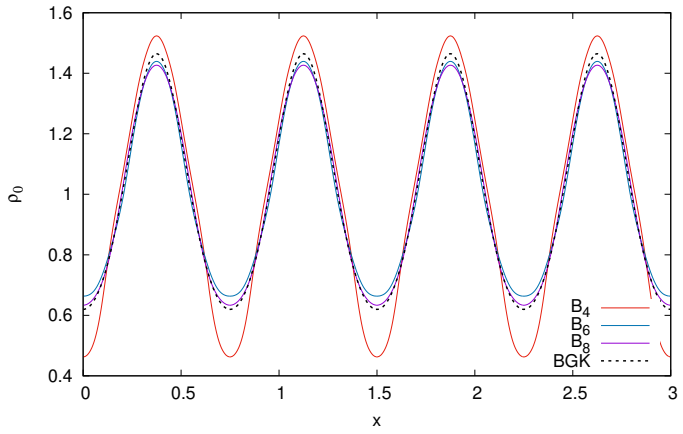

(a) density, $t = 0.35$

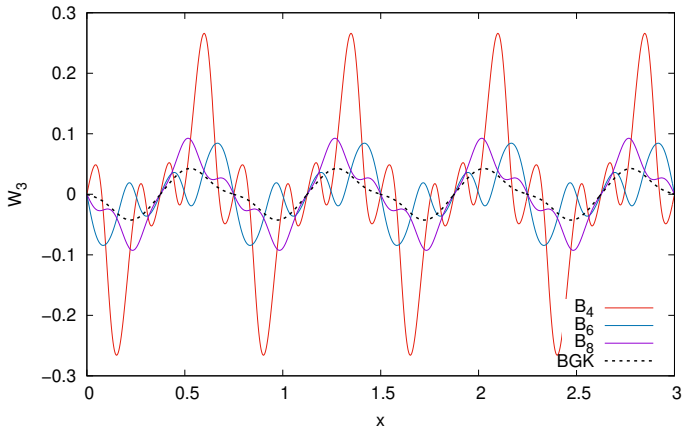

(b) normalized heat flux, $t = 0.35$

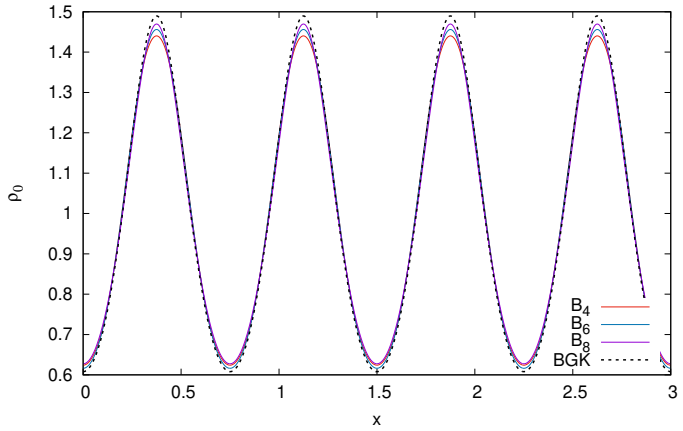

(c) density, $t = 0.75$

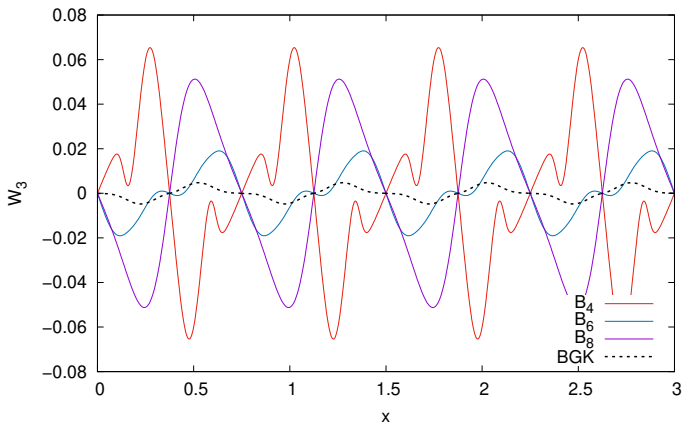

(d) normalized heat flux, $t = 0.75$

Figure 2: Predicted density and normalized heat flux of ions in the transition regime, $Kn = 1$, as determined by the moment models and direct numerical solutions of the Vlasov kinetic equation.

can see that the density is, to some degree, correctly predicted by the 8th-order closure, especially at later time. However, moment methods struggle to accurately capture the plasma behavior in this free-molecular regime. This is most apparent when looking at the heat flux.

Figure 2, 3 and 4 show the moment solutions for decreasing Knudsen number. As expected, moment closures provide far better approximation in the transition regime. However, as one can see, for the case where Kn = 1, the models still fail to approximate the heat flux accurately, thus posing a limit on the applicability of these closures.

In order to provide a better understanding of the physical validity of the moment models, phase-space distributions predicted by the Vlasov-BGK equation are compared to the corresponding quadrature-based VDF representation associated with each closures. In this representation, the distribution function is approximated using Eq. (12). The black lines correspond to the system wave speeds, while the line thickness represents the weight of each quadrature point, following Eq. (14). Figures 5 and 6 show the phase-space distributions at $t = 0.35$ for the free-molecular and transition regimes, respectively. In accordance with

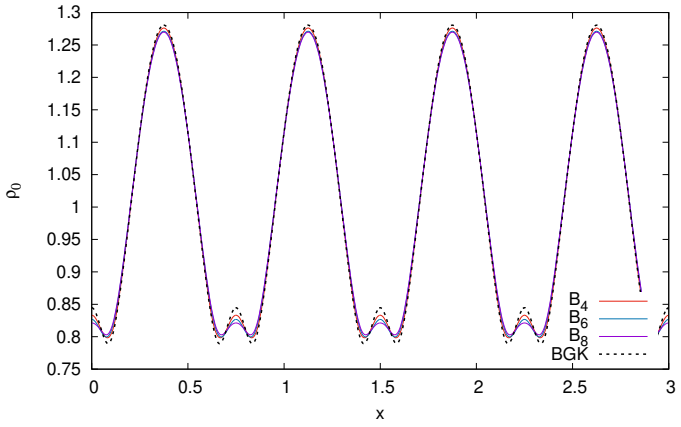

(a) density, $t = 0.35$

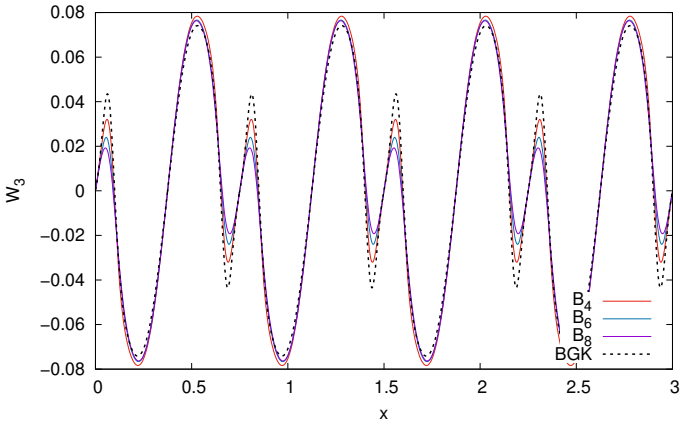

(b) normalized heat flux, $t = 0.35$

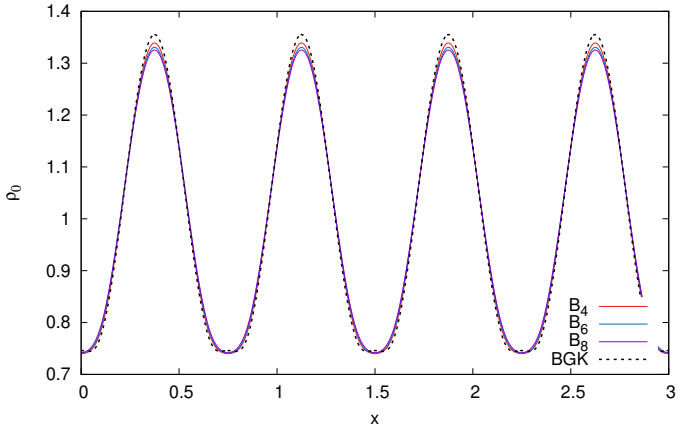

(c) density, $t = 0.75$

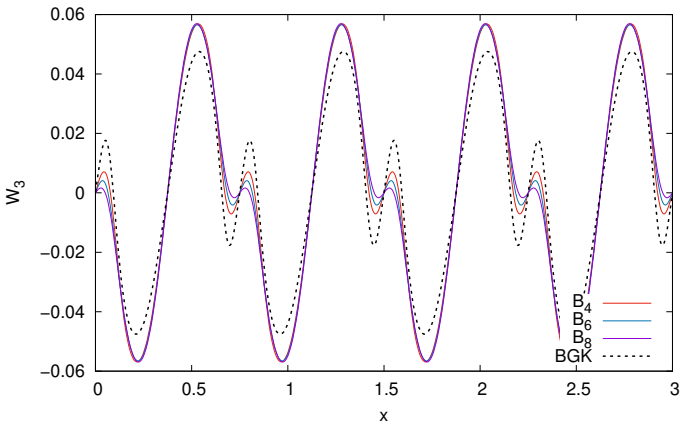

(d) normalized heat flux, $t = 0.75$

Figure 3: Predicted density and normalized heat flux of ions in the transition regime, $Kn = 0.1$, as determined by the moment models and direct numerical solutions of the Vlasov kinetic equation.

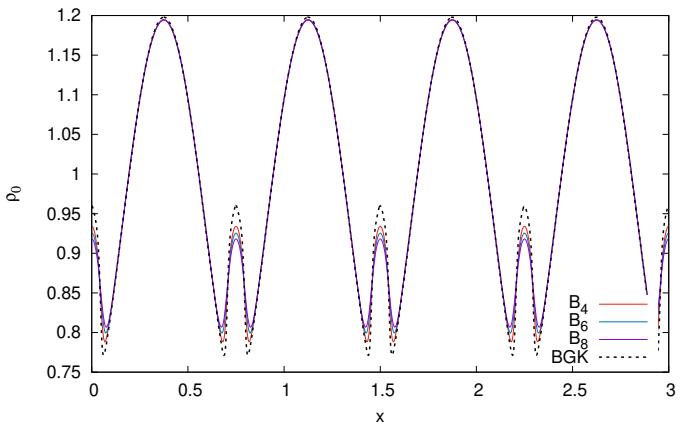

(a) density, $t = 0.35$

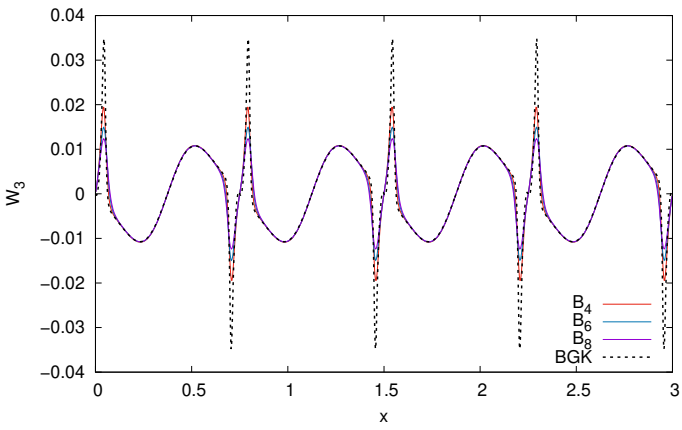

(b) normalized heat flux, $t = 0.35$

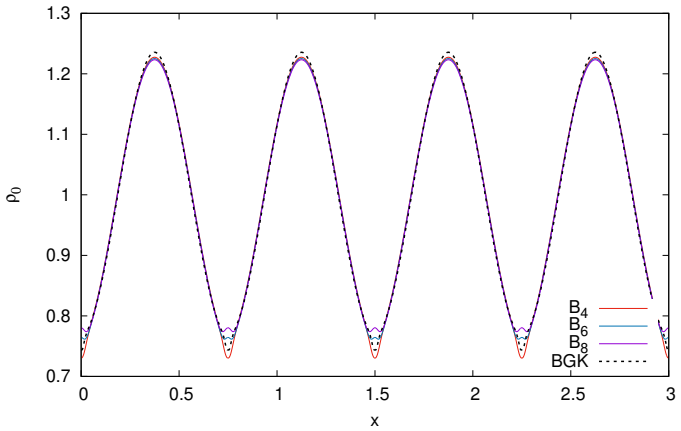

(c) density, $t = 0.75$

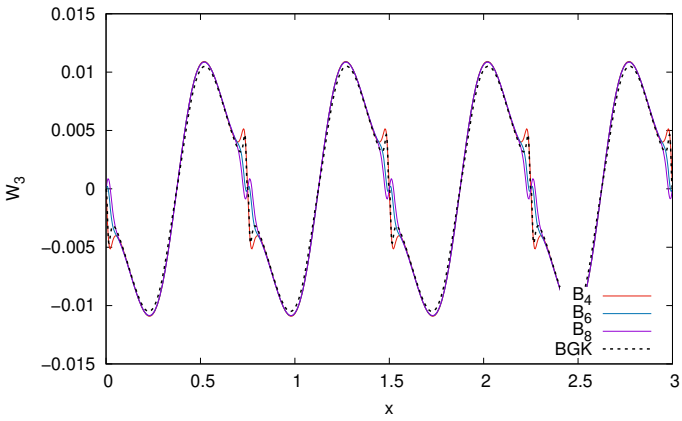

(d) normalized heat flux, $t = 0.75$

Figure 4: Predicted density and normalized heat flux of ions in the transition regime, $Kn = 0.01$, as determined by the moment models and direct numerical solutions of the Vlasov kinetic equation.

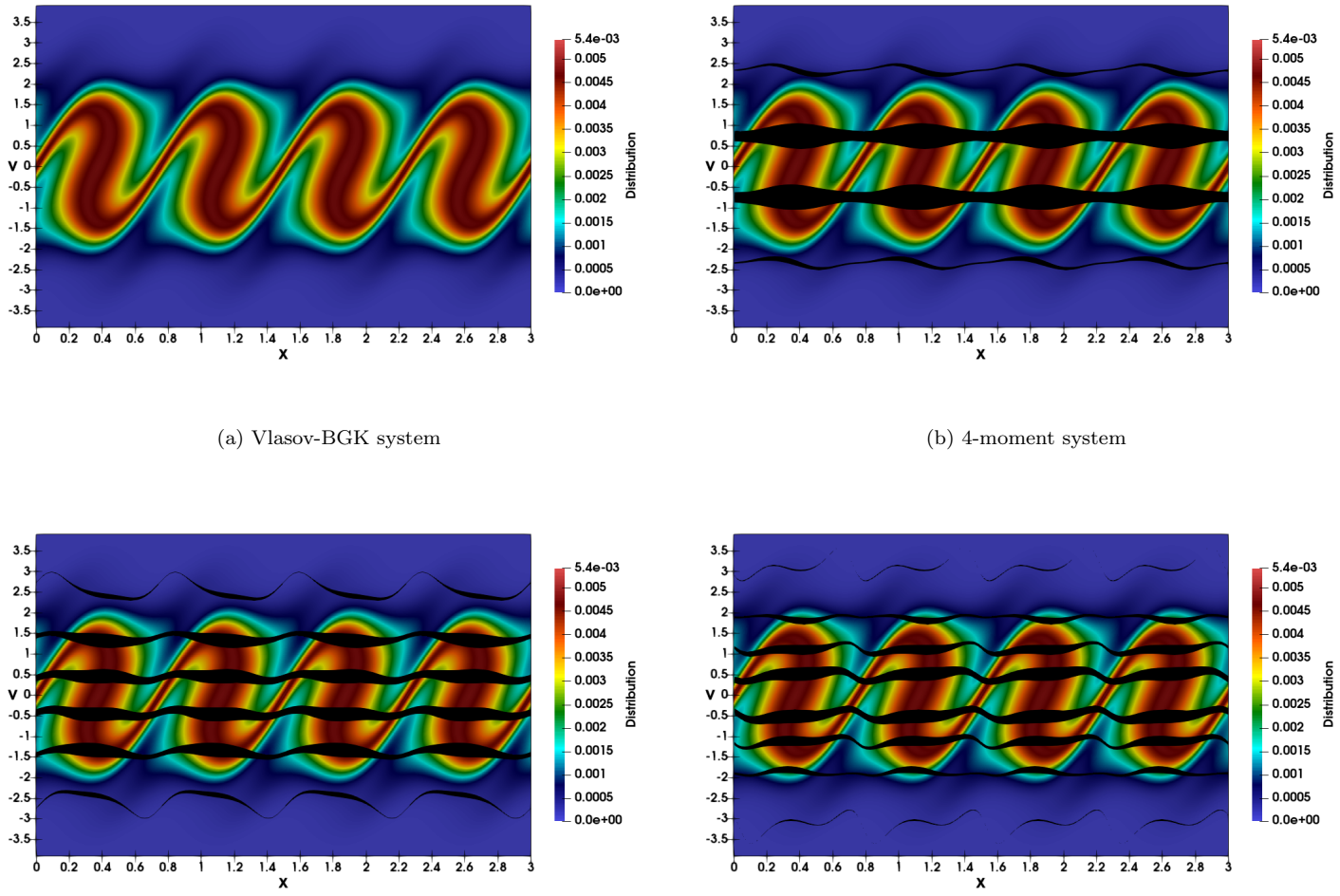

(a) Vlasov-BGK system

(b) 4-moment system

(c) 6-moment system

(d) 8-moment system

Figure 5: Phase space distribution of ions in the free-molecular regime as determined by the moment models and direct numerical solutions of the Vlasov kinetic equation at time $t = 0.35$.

the results previously presented for the moments, the free-molecular case is difficult to capture accurately. However, one can clearly see that the wave speeds (black lines) are trying to represent the correct distribution by getting thicker in the center, representing a higher particle density. However, the profile of the true VDF is too complex to be well represented by such a small number of quadrature points, even if they are well placed. Improvement can be observe for the higher-order method, however, many more moments would be required to correctly approximate the real distribution. On the other hand, excellent agreement can be observed in the transition regime where the wave speeds of all moment methods closely follow the Vlasov-BGK distribution. The approximation improves with increasing number of moments, as it allows for a more complete coverage of phase space. These results suggest that the presented closures can be interpreted as an adaptive discrete-velocity method where the velocities constantly evolves with the flow state.

It has previously been shown that moment-closures are intimately related to optimal quadrature-based

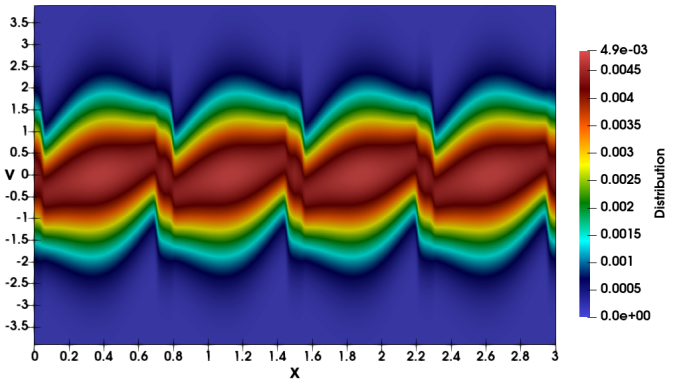

(a) Vlasov-BGK system

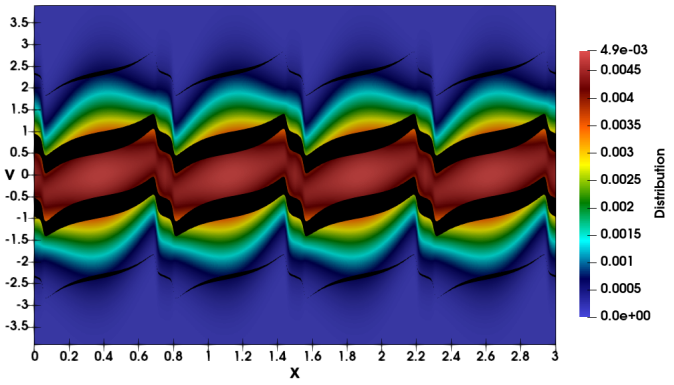

(b) 4-moment system

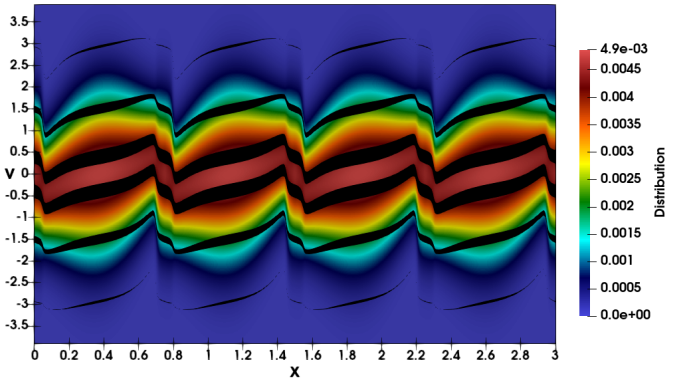

(c) 6-moment system

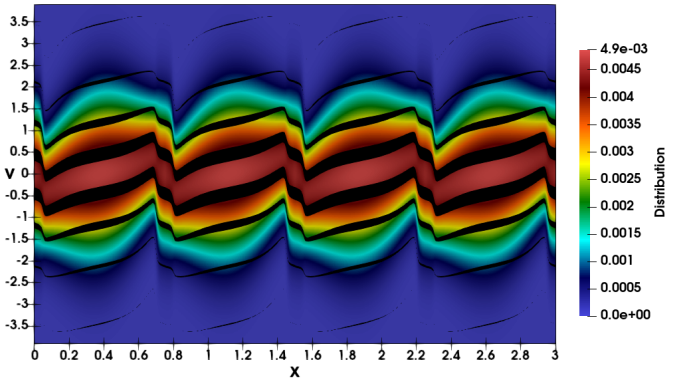

(d) 8-moment system

Figure 6: Phase space distribution of ions in the transition regime, Kn = 0.01, as determined by the moment models and direct numerical solutions of the Vlasov kinetic equation at time $t = 0.35$.

representations of the distribution function [36]. The system wave speeds of an n-moment system are the quadrature points that give exact agreement with the first $2n$ moments of the distribution. It is therefore possible to interpret moment methods as an adaptive discrete-velocity scheme in which velocity discretization points automatically adjust to the local gas state. Figure 6 shows how the discrete representation of the distribution function predicted by the moment method closely follows the true distribution. It is for this reason that moment methods can provide accurate results using far fewer unknowns that a direct scheme using a fixed mesh in velocity space.

4.2. Numerical approximations of the Vlasov-Poisson-BGK system

Landau damping refers to the non-collisional damping of plasma oscillations. These so called Langmuir waves, consisting of rapid oscillations of the electron density field, typically cannot be treated by simply considering collisions between charged particles. In this section a fully ionized plasma, where electrons are initially at thermodynamic equilibrium with a non-dimensional temperature $\hat{\theta}_e = 1$ is considered. The electrons are within a uniform positive ions background with $\rho_i = 1$. The spacial domain is periodic with a length $[-2\pi, 2\pi]$. The kinetic solutions are computed using 2500×2500 grid cells in physical and velocity space while the moment solutions are computed using a grid of 5000 equal-sized cells. The electric field, E, is obtained by solving a Poisson problem at each time step, as described by Eq. (4). The initial electron density is perturbed using a small perturbation $a = 0.001$. The associated VDF is,

$$\mathcal{F}_e = (1 + a\cos(kx))\mathcal{M}\,, \tag{29}$$

where the wave number is set to $k = 2\pi/L = 0.5$. This small density perturbation gives rise to an electrostatic field that periodically exchanges energy with the electrons. This electrostatic field, in turn decays through this collisionless process. This is a notoriously hard problem to accurately solve using moment methods [31, 32]. However, if a collision term is added, moment approximations of the discretized Vlasov-Poisson-BGK system improve. In this work, the simple BGK operator is again used. However, other operators, such as the Kirkwood or Lenard and Berstein operators have also been considered by other authors [39]. Figure 7 show the temporal evolution of the normalized L^2 norm of the electric field for different Knudsen numbers. Clearly, in the free-molecular case, the moment models only gives reasonable approximations over a short time interval. The 8-moment model seems to provide a slightly better approximation, but also diverges from the exact solution quickly. The case with $\mathrm{Kn} = 10$ yields barely noticeable improvements over the collisionless case. On the other hand, significant improvement can be observed once $\mathrm{Kn} = 1$, where the 8th-order closure, B_8, predicts almost perfectly the damping rate over the shown time period. Finally, for $\mathrm{Kn} = 0.1$, all approximations are in excellent agreement with the kinetic solution. Better approximations can probably be obtained by considering higher-order moment system.

5. Conclusions

In this work, the accuracy of the orthogonal polynomial based closures of Morin and M$^{\mathrm{c}}$Donald [30] for plasma physics was investigated for two canonical problems. Numerical solutions of ions inside imposed sinusoidal longitudinal electric field was first considered for the free-molecular and transition regimes. While the density field was well captured by the closures, the heat flux approximations were only accurate when considering a Knudsen number of the order of 10^{-1} or lower. The associated velocity distribution of each closures was also compared to the distribution predicted by the Vlasov-BGK system. This representation, reinforce the notion that quadrature-based closure can be seen as adaptive discrete velocity methods.

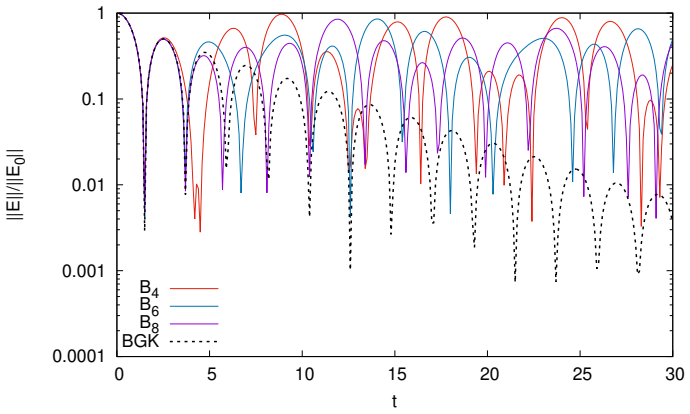

(a) Free molecular

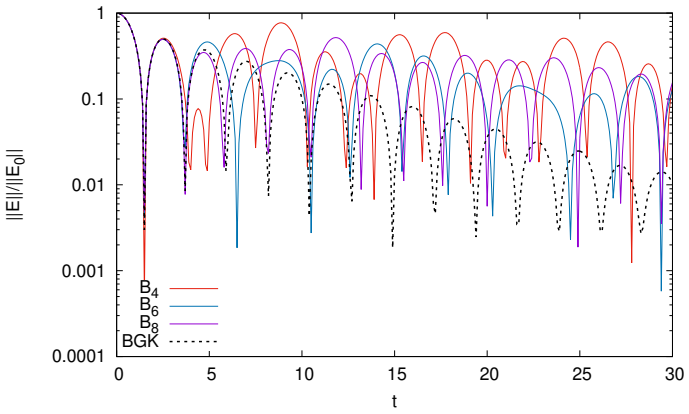

(b) $Kn = 10$

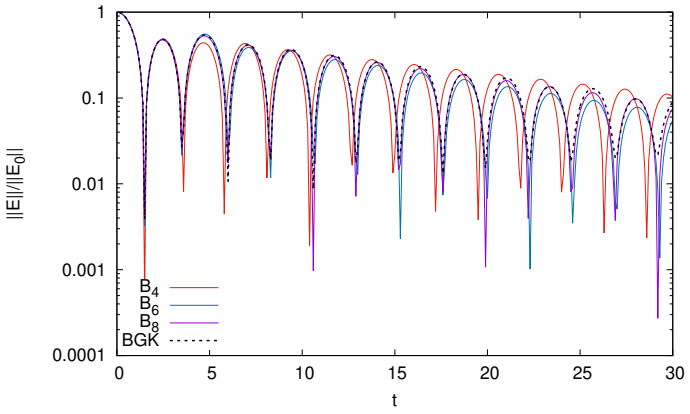

(c) $Kn = 1$

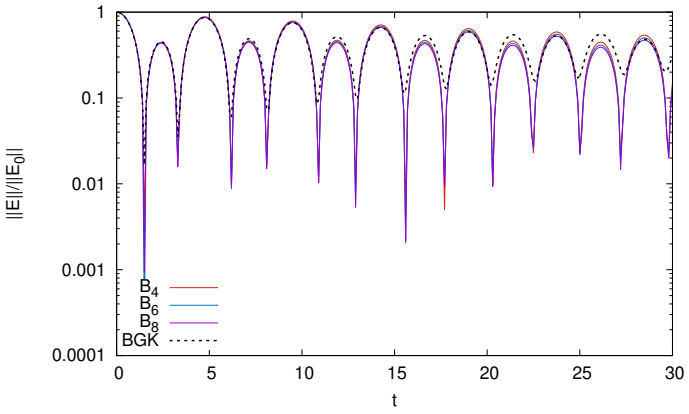

(d) $Kn = 0.1$

Figure 7: Electric field energy as a function of time for the Landau damping problem as computed by the the moment models and direct numerical solutions of the Vlasov-Poisson-BGK kinetic system.

Solutions of the Vlasov-Poisson-BGK system were also considered. Both collisional and collisionless cases were computed. As expected, when simulating Laudau damping, without any collisions, the moment methods yielded sensible approximation only for a short period of time. However, when considering a $\mathrm{Kn} = 1$ or less, the moment closures predict the damping rate very accurately.

Funding

This work was supported by the Natural Sciences and Engineering Research Council of Canada (Grant No. RGPIN-2020-06295). The authors are very grateful for the support.

References

[1] H. Grad, On the kinetic theory of rarefied gases, Communications on Pure and Applied Mathematics 2 (1949) 331–407.

[2] K. Xu, J.-C. Huang, A unified gas-kinetic scheme for continuum and rarefied flows, Journal of Computational Physics 229 (20) (2010) 7747–7764.

[3] J. G. McDonald, M. Torrilhon, Affordable robust moment closures for CFD based on the maximum-entropy hierarchy, Journal of Computational Physics 251 (2013) 500–523.

[4] L. D. Landau, The transport equation in the case of coulomb interactions, Collected papers of LD Landau (1936) 163–170.

[5] A. Lenard, On Bogoliubov's kinetic equation for a spatially homogeneous plasma, Annals of Physics 10 (3) (1960) 390–400.

[6] R. Balescu, Irreversible processes in ionized gases, The Physics of Fluids 3 (1) (1960) 52–63.

[7] S. Boccelli, F. Giroux, T. E. Magin, C. Groth, J. G. McDonald, A 14-moment maximum-entropy description of electrons in crossed electric and magnetic fields, Physics of Plasmas 27 (12) (2020).

[8] Z. Cai, Y. Fan, R. Li, T. Lu, Y. Wang, Quantum hydrodynamic model by moment closure of wigner equation, Journal of mathematical physics 53 (10) (2012).

[9] W. Morin, F. Giroux, J. G. McDonald, Application of approximate maximum-entropy moment closure to the wigner equation, Journal of Computational and Theoretical Transport 52 (5) (2023) 374–398.

[10] D. Lynden-Bell, Statistical mechanics of violent relaxation in stellar systems, Monthly Notices of the Royal Astronomical Society, Vol. 136, p. 101 136 (1967) 101.

[11] P.-H. Chavanis, Kinetic theory of spatially inhomogeneous stellar systems without collective effects, Astronomy & Astrophysics 556 (2013) A93.

[12] G. A. Bird, Molecular Gas Dynamics and the Direct Simulation of Gas Flows, Clarendon Press, Oxford, 1994.

[13] Q. Sun, I. D. Boyd, A direct simulation method for subsonic, microscale gas flow, Journal of Computational Physics 179 (2002) 400–425.

[14] I. Müller, T. Ruggeri, Rational Extended Thermodynamics, Springer-Verlag, New York, 1998.

[15] S. L. Brown, P. L. Roe, C. P. T. Groth, Numerical solution of a 10-moment model for nonequilibrium gasdynamics, Paper 95-1677, AIAA (June 1995).

[16] M. Torrilhon, Modeling nonequilibrium gas flow based on moment equations, Annual review of fluid mechanics 48 (2016) 429–458.

[17] H. Struchtrup, M. Torrilhon, H theorem, regularization, and boundary conditions for the linearized 13 moment equations, Physical Review Letters 99 (2007) 014502.

[18] H. Struchtrup, T. Thatcher, Bulk equations and Knudsen layers for the regularized 13 moment equations, Continuum Mechanics and Thermodynamics 19 (2007) 177–189.

[19] J. G. McDonald, C. P. T. Groth, Extended fluid-dynamic model for micron-scale flows based on Gaussian moment closure, Paper 2008-0691, AIAA (January 2008).

[20] Z. Cai, Y. Fan, R. Li, Globally hyperbolic regularization of Grad's moment system in one dimensional space, Communications in Mathematical Sciences 11 (2) (2013) 547–571.

[21] Z. Cai, Y. Fan, R. Li, Globally hyperbolic regularization of Grad's moment system, Communications on Pure and Applied Mathematics 67 (3) (2014) 464–514.

[22] W. Dreyer, Maximization of the entropy in non-equilibrium, Journal of Physics A: Mathematical and General 20 (1987) 6505–6517.

[23] I. Müller, T. Ruggeri, Extended Thermodynamics, Springer-Verlag, New York, 1993.

[24] C. D. Levermore, Moment closure hierarchies for kinetic theories, Journal of Statistical Physics 83 (1996) 1021–1065.

[25] M. Junk, Domain of definition of Levermore's five-moment system, Journal of Statistical Physics 93 (5/6) (1998) 1143–1167.

[26] F. Giroux, J. G. McDonald, An approximation for the twenty-one-moment maximum-entropy model of rarefied gas dynamics, International Journal of Computational Fluid Dynamics 35 (8) (2021) 632–652.

[27] R. McGraw, Description of aerosol dynamics by the quadrature method of moments, Aerosol Science and Technology 27 (2) (1997) 255–265.

[28] R. O. Fox, A quadrature based third-order moment method for dilute gas-particle flows, Journal of Computational Physics 227 (2008) 6313–6350.

[29] R. O. Fox, F. Laurent, Hyperbolic quadrature method of moments for the one-dimensional kinetic equation, SIAM Journal on Applied Mathematics 82 (2) (2022) 750–771.

[30] W. Morin, J. G. McDonald, Development of globally hyperbolic one-dimensional moment closures based on orthogonal polynomials, Journal of Computational Physics (2024) submitted.

[31] P.-Y. C. Taunay, M. E. Mueller, Quadrature-based moment methods for kinetic plasma simulations, Journal of Computational Physics 473 (2023) 111700.

[32] R. Schärer, Entropy-based moment closures for rarefied gases and plasmas, Ph.D. thesis, Dissertation, RWTH Aachen University, 2016 (2016).

[33] S. Boccelli, J. G. McDonald, T. E. Magin, 14-moment maximum-entropy modeling of collisionless ions for hall thruster discharges, Physics of Plasmas 29 (8) (2022).

[34] D. A. Silantyev, P. M. Lushnikov, H. A. Rose, Langmuir wave filamentation in the kinetic regime. i. filamentation instability of bernstein-greene-kruskal modes in multidimensional vlasov simulations, Physics of Plasmas 24 (4) (2017).

[35] P. L. Bhatnagar, E. P. Gross, M. Krook, A model for collision processes in gases. I. small amplitude processes in charged and neutral one-component systems, Physical Review 94 (3) (1954) 511–525.

[36] J. G. McDonald, C. P. T. Groth, Towards realizable hyperbolic moment closures for viscous heat-conducting gas flows based on a maximum-entropy distribution, Continuum Mechanics and Thermodynamics 25 (2013) 573–603.

[37] A. Harten, P. D. Lax, B. van Leer, On upstream differencing and Godunov-type schemes for hyperbolic conservation laws, SIAM Review 25 (1) (1983) 35–61.

[38] M. Berry, D. O'Dell, Ergodicity in wave-wave diffraction, Journal of Physics A: Mathematical and General 32 (19) (1999) 3571.

[39] J. T. Parker, P. J. Dellar, Fourier-Hermite spectral representation for the Vlasov-Poisson system in the weakly collisional limit, Journal of Plasma Physics 81 (2) (2015) 305810203.

Chapter 6

Conclusion

This study has been concerned with the application of hyperbolic moment closures to non-equilibrium gas flows, plasma flows, and quantum hydrodynamic systems. It has been demonstrated that moment closures offer many advantages over more traditional fluid models. The first work included in this thesis demonstrates that a closed-form moment closure offers promising alternatives to typical Wigner solvers. Using an approximation to the second one-dimensional member of the maximum-entropy moment closure hierarchy, the time evolution of a one-dimensional low-energy quantum wave-packet placed in different unbounded double-well potentials was computed and compared to the discretized solution of the Wigner equation. By comparing the probability density, the expected values for both the position and momentum, and the quasi-probability distributions, the general accuracy as well as the major challenges of this moment method were assessed. Even if good agreement was observed at early times, the low number of moments coupled with the inability of distribution functions from classical maximum-entropy closure to admit negative regions seems to limit its immediate applicability.

Following these conclusions, the need for higher-order moment-methods became the main motivation of the next work. Higher-order closures based on maximum-entropy approximations have proven difficult to obtain. The second paper presents a new method for the construction of quadrature-based globally hyperbolic closures, along with a new hierarchy of Galilean invariant models. The accuracy of the new closures was assessed by comparing numerical solutions of Riemann problems along with strong stationary shock wave calculations to discretized solutions of the Boltzmann' equation. In all cases, good agreement could be observed. As expected the closures' accuracy was found to increase rapidly with the number of moments.

The third and last work presented in this thesis investigates the applicability of the new moment hierarchy to plasma flows. This study is interested in low-temperature plasma applications. To this end, two canonical problems were considered. First, ions in a stationary electric potential at various Knudsen number was used to investigate the applicable range of these closures. Using this problem, it was also demonstrated that the moment models can be seen as discrete-velocity schemes, locally adapting to the flow state. Linear Landau damping was also studied in both the collisional and collisionless regimes. A good agreement could be observed for cases in the transition regime, $\mathrm{Kn} \leqq 1$. However, as expected, cases in the free-molecular regime were not well captured. The 8-order moment closure, B_8 could recover the density profile accurately, but not the heat-flux. Similarly, sensible approximations to the electric field energy were only observed at early times.

6.1 Suggestions and Future Work

This study clearly demonstrates the potential of quadrature-based moment closures for moderately rarefied gas and plasma flow prediction. However, the models introduced in this thesis are only defined for one-dimensional gases. Extending the proposed method to allow for the treatment of the full particle velocity is an important open problem. Furthermore, the presented models are constructed assuming monatomic gases with no internal degrees of freedom. Including a polyatomic treatment is paramount, since many engineering situations require the modeling of other energy modes (rotational and vibrational) to provide an accurate physical description. This is especially true when dealing with strong shock waves and reactive flows, which are highly non-equilibrium phenomena.

On a different note, the new hierarchy is yet to be tested for quantum hydrodynamics. The closures were constructed to conserve global hyperbolicity within the realizability domain of classical gases. Initial investigations suggested that the closures are not well suited for quantum hydrodynamics since the Wigner equation routinely predicts moments outside of this realizability boundary, resulting in lost of hyperbolicity. However, in order to circumvent this problem, the Husimi formalism could be used [55, 56]. This formulation results in positive distributions while yielding an equivalent description of quantum mechanics. It can be understood as the Weierstrass transform of the Wigner quasi-probability distribution producing a positive definite and bounded function. The introduction of the Husimi function along with the new higher-order closures could potentially yield accurate quantum hydrodynamic models.

Bibliography

[1] G. A. Bird. *Molecular Gas Dynamics and the Direct Simulation of Gas Flows*. Clarendon Press, Oxford, 1994.

[2] L. Mieussens. Discrete velocity model and implicit scheme for the BGK equation of rarefied gas dynamics. *Mathematical Models and Methods in Applied Sciences*, 10(8):1121–1149, 2000.

[3] P. Degond and C. Ringhofer. Quantum moment hydrodynamics and the entropy principle. *Journal of Statistical Physics*, 112(314):587–628, 2003.

[4] Florian Frommlet, Peter A Markowich, and Christian Ringhofer. A wignerfunction approach to phonon scattering. *VLSI Design*, 9(4):339–350, 1999.

[5] Zhenning Cai, Yuwei Fan, Ruo Li, Tiao Lu, and Yanli Wang. Quantum hydrodynamic model by moment closure of wigner equation. *Journal of mathematical physics*, 53(10), 2012.

[6] David K Ferry and Harold L Grubin. Modeling of quantum transport in semiconductor devices. In *Solid State Physics*, volume 49, pages 283–448. Elsevier, 1996.

[7] Carl L Gardner. The quantum hydrodynamic model for semiconductor devices. *SIAM Journal on Applied Mathematics*, 54(2):409–427, 1994.

[8] H. Grad. On the kinetic theory of rarefied gases. *Communications on Pure and Applied Mathematics*, 2:331–407, 1949.

[9] C. D. Levermore. Moment closure hierarchies for kinetic theories. *Journal of Statistical Physics*, 83:1021–1065, 1996.

[10] I. Müller and T. Ruggeri. *Extended Thermodynamics*. Springer-Verlag, New York, 1993.

[11] Zhenning Cai, Yuwei Fan, and Ruo Li. On hyperbolicity of 13-moment system. *Kinetic and Related Models*, 7(3):415–432, 2014.

[12] J. G. McDonald, J. S. Sachdev, and C. P. T. Groth. Gaussian moment closure for the modelling of continuum and micron-scale flows with moving boundaries. In H. Deconinck and E. Dick, editors, *Proceedings of the Fourth International Conference on Computational Fluid Dynamics, ICCFD, Ghent, Belgium, July 10–14, 2006*, pages 783–788, Heidelberg, 2009. Springer-Verlag.

[13] W. Dreyer. Maximization of the entropy in non-equilibrium. *Journal of Physics A: Mathematical and General*, 20:6505–6517, 1987.

[14] M. Junk. Domain of definition of Levermore's five-moment system. *Journal of Statistical Physics*, 93(5/6):1143–1167, 1998.

[15] M. Junk and A. Unterreiter. Maximum entropy moment systems and Galilean invariance. *Continuum Mechanics and Thermodynamics*, 14:563–576, 2002.

[16] H. Struchtrup and M. Torrilhon. Regularization of Grad's 13 moment equations: Derivation and linear analysis. *Physics of Fluids*, 15(9):2668–2680, 2003.

[17] Z. Cai, Y. Fan, and R. Li. Globally hyperbolic regularization of Grad's moment system in one dimensional space. *Communications in Mathematical Sciences*, 11(2):547–571, 2013.

[18] Z. Cai, Y. Fan, and R. Li. Globally hyperbolic regularization of Grad's moment system. *Communications on Pure and Applied Mathematics*, 67(3):464–514, 2014.

[19] R. O. Fox. Higher-order quadrature-based moment methods for kinetic equations. *Journal of Computational Physics*, 228:7771–7791, 2009.

[20] Rodney O Fox and Frédérique Laurent. Hyperbolic quadrature method of moments for the one-dimensional kinetic equation. *SIAM Journal on Applied Mathematics*, 82(2):750–771, 2022.

[21] Joseph Liouville. Note sur la théorie de la variation des constantes arbitraires. *Journal de mathématiques pures et appliquées*, 3:342–349, 1838.

[22] L. Boltzmann. Weitere studien über das wärmegleichgewicht unter gasmolekülen. *Sitz. Math.-Naturwiss. Cl. Akad. Wiss. Wien*, 66:275–370, 1872.

[23] J. C. Maxwell. On the dynamical theory of gases. *Philosophical Transactions of the Royal Society of London*, 157:49–88, 1867.

[24] Harold Grad. On boltzmann's h-theorem. *Journal of the Society for Industrial and Applied Mathematics*, 13(1):259–277, 1965.

[25] I. Müller. *Thermodynamics*. Pitman Publishing, Boston, 1985.

[26] H. Struchtrup. *Macroscopic Transport Equations for Rarefied Gas Flows*. Springer-Verlag, Berlin, 2005.

[27] T. I. Gombosi. *Gaskinetic Theory*. Cambridge University Press, Cambridge, 1994.

[28] P. L. Bhatnagar, E. P. Gross, and M. Krook. A model for collision processes in gases. I. small amplitude processes in charged and neutral one-component systems. *Physical Review*, 94(3):511–525, 1954.

[29] L. H. Holway, Jr. New statistical models for kinetic theory: Methods of construction. *Physics of Fluids*, 9(9):1658–1673, 1966.

[30] Fei Fei, Haihong Liu, Zhaohui Liu, and Jun Zhang. A benchmark study of kinetic models for shock waves. *AIAA Journal*, 58(6):2596–2608, 2020.

[31] I. Müller and T. Ruggeri. *Rational Extended Thermodynamics*. Springer-Verlag, New York, 1998.

[32] J. G. McDonald and M. Torrilhon. Affordable robust moment closures for CFD based on the maximum-entropy hierarchy. *Journal of Computational Physics*, 251:500–523, 2013.

[33] T. J. Barth. On discontinuous Galerkin approximations of boltzmann moment systems with Levermore closure. *Computer Methods in Applied Mechanics and Engineering*, 195:3311–3330, 2006.

[34] S. L. Brown. *Approximate Riemann Solvers for Moment Models of Dilute Gases*. PhD thesis, University of Michigan, 1996.

[35] S. L. Brown, P. L. Roe, and C. P. T. Groth. Numerical solution of a 10-moment model for nonequilibrium gasdynamics. Paper 95-1677, AIAA, June 1995.

[36] C. P. T. Groth and J. G. McDonald. Towards physically-realizable and hyperbolic moment closures for kinetic theory. *Continuum Mechanics and Thermodynamics*, 21(6):467–493, 2009.

[37] Y. Suzuki and B. van Leer. Application of the 10-moment model to MEMS flows. Paper 2005-1398, AIAA, January 2005.

[38] Fabien Giroux and James G McDonald. An approximation for the twenty-one-moment maximum-entropy model of rarefied gas dynamics. *International Journal of Computational Fluid Dynamics*, 35(8):632–652, 2021.

[39] M. R. A. Abdelmalik and E. H. van Brummelen. Moment closure approximations of the boltzmann equation based on φ-divergences. *Journal of Statistical Physics*, 164, 2015.

[40] C. Tsallis. *Introduction to Nonextensive Statistical Mechanics*. Springer, New York, 2009.

[41] Robert McGraw. Description of aerosol dynamics by the quadrature method of moments. *Aerosol Science and Technology*, 27(2):255–265, 1997.

[42] R. O. Fox. A quadrature based third-order moment method for dilute gas-particle flows. *Journal of Computational Physics*, 227:6313–6350, 2008.

[43] Daniele Marchisio and R. Fox. *Computational Models for Polydisperse Particulate and Multiphase Systems*. Cambridge University Press, Cambridge, 2013.

[44] C. Yuan and R.O. Fox. Conditional quadrature method of moments for kinetic equations. *Journal of Computational Physics*, 230(22):8216–8246, 2011.

[45] C. Yuan, F. Laurent, and R.O. Fox. An extended quadrature method of moments for population balance equations. *Journal of Aerosol Science*, 51:1–23, 2012.

[46] S. Chapman. On the kinetic theory of a gas. part II. – a composite monoatomic gas: Diffusion, viscosity, and thermal conduction. *Philosophical Transactions of the Royal Society of London A*, 217:115–116, 1916.

[47] D. Enskog. *Kinetishe Theorie der Vorgänge in Massing Verdumten Gasen*. PhD thesis, University of Upsala, 1917.

[48] Leopoldo S García-Colín, Rosa M Velasco, and Francisco J Uribe. Beyond the navier–stokes equations: burnett hydrodynamics. *Physics Reports*, 465(4):149–189, 2008.

[49] A. V. Bobylev. The Chapman-Enskog and Grad methods for solving the Boltzmann equation. *Soviet Physics Doklady*, 27(1):29–31, 1982.

[50] Leslie Colin Woods. *An introduction to the kinetic theory of gases and magnetoplasmas*. Oxford University Press, 1993.

[51] Josef Weinbub and DK Ferry. Recent advances in wigner function approaches. *Applied Physics Reviews*, 5(4), 2018.

[52] Pierre-Yves CR Taunay and Michael E Mueller. Quadrature-based moment methods for kinetic plasma simulations. *Journal of Computational Physics*, 473:111700, 2023.

[53] Roman Schärer. *Entropy-based moment closures for rarefied gases and plasmas*. PhD thesis, Dissertation, RWTH Aachen University, 2016, 2016.

[54] Stefano Boccelli, James G McDonald, and Thierry E Magin. 14-moment maximum-entropy modeling of collisionless ions for hall thruster discharges. *Physics of Plasmas*, 29(8), 2022.

[55] Ayumu Sugita and Hirokazu Aiba. Second moment of the husimi distribution as a measure of complexity of quantum states. *Phys. Rev. E*, 65:036205, 2002.

[56] E Colomés, Z Zhan, and X Oriols. Comparing wigner, husimi and bohmian distributions: which one is a true probability distribution in phase space? *Journal of Computational Electronics*, 14:894–906, 2015.